

Fall 2009

Landslide susceptibility mapping through enhanced dynamic slope stability analysis using earth observing satellite measurements

Ram Lakhan Ray

University of New Hampshire, Durham

Follow this and additional works at: <https://scholars.unh.edu/dissertation>

Recommended Citation

Ray, Ram Lakhan, "Landslide susceptibility mapping through enhanced dynamic slope stability analysis using earth observing satellite measurements" (2009). *Doctoral Dissertations*. 502.
<https://scholars.unh.edu/dissertation/502>

This Dissertation is brought to you for free and open access by the Student Scholarship at University of New Hampshire Scholars' Repository. It has been accepted for inclusion in Doctoral Dissertations by an authorized administrator of University of New Hampshire Scholars' Repository. For more information, please contact nicole.hentz@unh.edu.

LANDSLIDE SUSCEPTIBILITY MAPPING THROUGH ENHANCED
DYNAMIC SLOPE STABILITY ANALYSIS USING EARTH
OBSERVING SATELLITE MEASUREMENTS

BY

RAM LAKHAN RAY

B.S., Tribhuvan University, Kathmandu, Nepal, 1992
M.S., Vrije Universiteit, Brussel and Universiteit, Gent, Belgium, 2004

DISSERTATION

Submitted to the University of New Hampshire
In Partial Fulfillment of
The Requirements for the Degree of

Doctor of Philosophy
in
Civil Engineering

September, 2009

UMI Number: 3383325

Copyright 2009 by
Ray, Ram Lakhan

INFORMATION TO USERS

The quality of this reproduction is dependent upon the quality of the copy submitted. Broken or indistinct print, colored or poor quality illustrations and photographs, print bleed-through, substandard margins, and improper alignment can adversely affect reproduction.

In the unlikely event that the author did not send a complete manuscript and there are missing pages, these will be noted. Also, if unauthorized copyright material had to be removed, a note will indicate the deletion.

UMI[®]

UMI Microform 3383325
Copyright 2009 by ProQuest LLC
All rights reserved. This microform edition is protected against
unauthorized copying under Title 17, United States Code.

ProQuest LLC
789 East Eisenhower Parkway
P.O. Box 1346
Ann Arbor, MI 48106-1346

ALL RIGHTS RESERVED

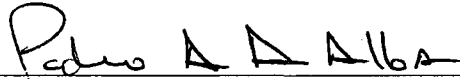
© 2009

Ram L Ray

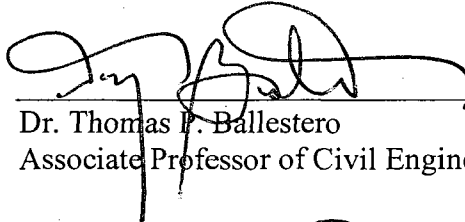
This dissertation has been examined and approved.



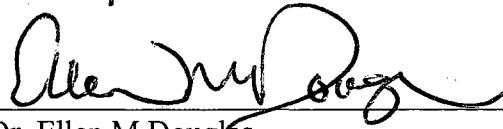
Dissertation Director, Dr. Jennifer M. Jacobs
Associate Professor of Civil Engineering



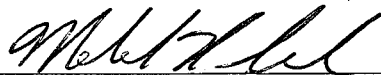
Dr. Pedro A. de Alba
Professor of Civil Engineering



Dr. Thomas P. Ballestero
Associate Professor of Civil Engineering



Dr. Ellen M. Douglas
Assistant Professor
Environmental, Earth and Ocean Sciences
University of Massachusetts, Boston, MA



Dr. Michael H. Cosh
Research Hydrologist
USDA-ARS-Hydrology and Remote Sensing Laboratory
Beltsville, MD

07-16-2009

Date

DEDICATION

This dissertation is dedicated to my family: my father, mother, wife, daughter and son.

ACKNOWLEDGMENTS

I would like to express my sincere appreciation and thanks to my advisor, Prof. Jennifer M. Jacobs for her encouragement, suggestions and constant support throughout my PhD study. Under her guidance, I had the opportunity to expand my skills and knowledge in many directions. I am extremely grateful to my committee: Prof. Pedro de Alba, Prof. Thomas P. Ballestero, Prof. Ellen M. Douglas and Dr. Michael H. Cosh for their guidance and comments in this research work.

I would like to acknowledge NASA for research funding through Earth System Science Fellowship, Grant No: NNG05GP66H, for this research. I would also like to thank Dr. M.E. Reid for providing information about Cleveland Corral Landslide area and in-situ groundwater measurements. I would like to thank Prof. Venkat Lakshmi and Dr. Ujjwal Narayan from University of South Carolina for their help in obtaining AMSR-E data. I am also thankful to my Environmental Research Group colleagues including Dr. Minha Choi, Carrie Vuyovich, Danna Truslow, Gary Lemay and James Sherrard for their support in many ways. I also want to thank Madeleine Wasiewski and Thomas Kurshinsky for their support.

I would like to express my special gratitude to my parents Mr. Bahuru Ray and Mrs. Raswati Devi for their encouragement and support in my chosen career path. I would also like to extend my special thanks to my father-in-law Prof. Dr. Gouri Shankar Roy and mother-in-law Dr. Mrs. Krishna Roy including all family members for their

outstanding love, encouragement and support. All my loves goes to my daughter Samiksha and my son Shawn for their innocent and charming smiles and understanding that encouraged me to work hard to complete this endeavor. Finally, I am extremely grateful to my wife and only one forever life friend Alpana Lakshmi for her encouragement, understanding, support and patience throughout this study.

TABLE OF CONTENTS

DEDICATION	iv
ACKNOWLEDGEMENTS	v
LIST OF TABLES	x
LIST OF FIGURES	xii
ABSTRACT	xvi
CHAPTERS	PAGE
CHAPTER 1.	1
INTRODUCTION	1
CHAPTER 2.	9
RELATIONSHIPS AMONG REMOTELY SENSED SOIL MOISTURE, PRECIPITATION AND LANDSLIDE EVENTS	9
Abstract	9
Introduction.....	10
Relationship between water and slope failure	14
Remote Sensing Products	16
Study Areas.....	19
Results and Discussion	22
Conclusion	26
CHAPTER 3.	33
IMPACTS OF VADOSE ZONE SOIL MOISTURE AND GROUNDWATER TABLE ON SLOPE INSTABILITY.....	33
Abstract	33
Introduction.....	34
Slope Stability Model	38

Material and Methods	42
Model Results	46
Conclusion	56
CHAPTER 4.	71
MODELING LANDSLIDE SUSCEPTIBILITY USING DYNAMIC SOIL MOISTURE PROFILES.....	71
Abstract.....	71
Introduction.....	72
Models.....	75
Study Areas.....	79
Methods and Database	81
Results and Discussion	86
Conclusion	93
CHAPTER 5.	109
REGIONAL LANDSLIDE SUSCEPTIBILITY: STATISTICAL DISTRIBUTION IN SPACE AND TIME.....	109
Abstract.....	109
Introduction.....	110
Theory.....	113
Application.....	115
Results and Discussion	118
Conclusion	123
CHAPTER 6.	140
LANDSLIDE SUSCEPTIBILITY MAPPING USING DOWNSCALED AMSR-E SOIL MOISTURE: A CASE STUDY FROM CLEVELAND CORRAL, CALIFORNIA, US	140
Abstract.....	140
Introduction.....	141
Theoretical Approach.....	145
Downscaling	148
Remotely Sensed Data	150

Study Region.....	152
Results and Discussion	154
Conclusion	162
CHAPTER 7.....	178
CONCLUSION.....	178
FUTURE STUDY.....	181
LIST OF REFERENCES.....	183
APPENDICES	
APPENDIX A.....	198
APPENDIX B	200

LIST OF TABLES

Table 2-1: Statistical Analysis of AMSR-E soil moisture from January 2005 to May 2006 in three study regions	27
Table 3-1: List of model parameters and sources	57
Table 3-2: Predicted susceptible area (%) for the Cleveland Corral region during the wet season.....	57
Table 4-1: Soil, vegetation and slope characteristics of the California and Nepal study regions.....	94
Table 4-2: Soil parameters used in VIC-3L and slope stability model.....	95
Table 4-3: Vegetation parameters used in VIC-3L and slope stability model.....	95
Table 4-4: Physical characteristics and estimated safety factor (FS) of the mapped landslide’s region in California. FS values were calculated under maximum modeled saturation on May 8, 2005 and assumed full saturation.....	96
Table 4-5: Physical characteristics and estimated safety factor (FS) of the mapped landslide’s region in Nepal. FS values were calculated under maximum modeled saturation on August 18, 2004 and assumed full saturation	97
Table 4-6: Groundwater model performance in California	98
Table 4-7: Predicted GW and VIC-3L soil moisture statistics in California and Nepal...	98
Table 4-8: Safety factors, SM and rainfall values in 2004 and 2005 at landslide active pixels.....	99
Table 4-9: Distribution of susceptibility (%) for various scenarios at California, US and Dhading, Nepal study sites	100
Table 5-1: Soil, vegetation and slope characteristics of the California and Nepal study regions.....	125
Table 5-2: Safety factor statistics for the 2003-2006 study period and wet season (Jan to May) for California and (Jun to Sep) for Nepal. Parentheses indicate standard deviation. Classifications are based on maximum modeled susceptibility on May 8, 2005 for California and August, 18, 2004 for Nepal	126

Table 6-1: Soil, vegetation, slope and climate characteristics for the Cleveland Corral, California, US study area.....	164
Table 6-2: The portion of the study area (%) for each landslide susceptibility classification using VIC-3L, AMSR-E 25 km and downscaled soil moisture at Cleveland Corral, California, US. Three wetness scenarios are presented.....	165
Table 6-3: Physical characteristics and estimated safety factor (FS) of the mapped landslide's region. FS values were calculated under maximum modeled saturation conditions (May 8, 2005) and full saturation.....	166

LIST OF FIGURES

Figure 2-1: Locations of the three study regions	28
Figure 2-2: A comparison of soil moisture and rainfall in the three study regions (January 2005 to May 2006).....	29
Figure 2-3: Slope movement/landslides, one week moving average AMSR-E soil moisture and daily TRMM rainfall in California, US from January 2005 to May 2006.....	30
Figure 2-4: Landslides, one week moving average AMSR-E soil moisture and daily TRMM rainfall in.....	31
Figure 2-5: Landslide, one week moving average AMSR-E soil moisture and daily TRMM rainfall in Dhading,.....	32
Figure 3-1: Schematic diagram for the slope angle, saturated and total soil thickness, surcharge, saturated and moist unit soil weights (Adapted and modified from Skempton and Delory, 1957)	58
Figure 3-2: Location of the study region in El Dorado County, California.....	59
Figure 3-3: Rates of change in the safety factor with varying vadose zone soil moisture values and depth to groundwater for total soil depths of (a) 1 m (b) 1.4 m (c) 2 m and (d) 3.0 m. Site characteristics are sandy loam, wooded grassland and 32.5° slope	63
Figure 3-4: Safety factor change with varying vadose zone soil moisture value (0-100%) and a fixed depth to groundwater (0.75 m) for a range of total soil depths from 1 to 3 m	64
Figure 3-5: Highly susceptible area % as a function of GW and soil saturation (Dark: greater highly susceptible area, white: less highly susceptible area). Depth to GW table (1 m @ 10% decrease up to 0 m or surface) and eleven soil saturations (0% @ 10% increments up to 100%) were used to calculate FS. The contour lines show equal percentage of highly susceptible area with 0.01% intervals.	65

Figure 3-6: The depth to GW, VIC-3L model average (layers 1 and 2) vadose zone SM and rainfall at Cleveland Corral region, California from January, 2004 to September 2006. $R^2 = 0.63$ and $p\text{-value} < 0.0001$ 66

Figure 3-7: Four susceptibility classes with varying SM (0 to 100%), three GW positions measured from the surface and observed SM at Cleveland Corral region, California in 2005. A solid line that intersects susceptible classes' line represents observed vadose zone SM and GW tables..... 68

Figure 3-8: Variation of susceptibility area with increase of soil thickness with equal increase in depth to GW table (0.25 m for 1 m thick soil with 0.5 m increment to 2.25 m for 3 m thick soil or constant GW table thickness from the failure plane) and constant vadose zone SM (50%) at Cleveland Corral region, California in 2005..... 69

Figure 3-9: Susceptibility area with increase of soil thickness with equal increase in depth to GW table (0.25 m for 1 m thick soil with 0.5 m increment to 2.25 m for 3 m thick soil or constant GW table thickness from the failure plane) and varying vadose zone SM (as shown in Figure) at Cleveland Corral region, California in 2005..... 70

Figure 4-1: The simulated and observed groundwater (GW) at Cleveland Corral, California for wet season 101

Figure 4-2a: In-situ, predicted GW and VIC-3L average SM at Cleveland Corral, California, US 102

Figure 4-2b: Soil moisture versus GW depth for Nepal 102

Figure 4-3: Simulated GW depth and average surface soil moisture for the wet season in California and Nepal 104

Figure 4-4a: Dynamic safety factors for two monitored landslide pixels in Cleveland Corral, California, US 105

Figure 4-4b: Dynamic safety factors for two monitored landslide pixels in Dhading, Nepal 102

Figure 4-5: Susceptibility map on May 08, 2005 with mapped landslides in California, US 107

Figure 4-6: Susceptibility map on August 18, 2004 with mapped landslides in Dhading, Nepal (Inset picture was taken in August 2003).....	108
Figure 5-1: (a) Mapped landslide (top) and slope movement (bottom) locations at Cleveland Corral, California in 2006 and (b) a major catastrophic landslide along Prithvi Highway, Nepal (Picture was taken in August, 2003).....	127
Figure 5-2a: Average safety factors and rainfall distribution by susceptibility class at the Cleveland Corral, California, US study region	128
Figure 5-2b: Average safety factors and rainfall distribution by susceptibility class at the Dhading, Nepal study region	102
Figure 5-3: The quantile box-plots of daily annual safety factors for both study regions. HS = Highly susceptible, MS = Moderately susceptible, SS = Slightly susceptible, CA = California, NP = Nepal.....	130
Figure 5-4: The coefficient of variance (CV) for all susceptible classes during the wet season, in Cleveland Corral, California, US. Zero represents stable class	131
Figure 5-5: The coefficient of variance (CV) for all susceptible classes during the wet season in Dhading, Nepal. Zero represents stable class.....	132
Figure 5-6: L-moment diagrams for each highly susceptible location by region and potential probability distribution functions during the wet season.....	133
Figure 5-7: The cumulative distribution function (CDF) of daily safety factors at each region during the wet season. HS = Highly susceptible, MS = Moderately susceptible, SS = Slightly susceptible, CA = California, NP = Nepal.....	134
Figure 5-8: The quantile box plots of number of transitions (crossings) below the safety factor threshold value and the average duration that the safety factor stayed below by threshold at each region (Complete year)	135
Figure 5-9: Average duration versus the number of annual crossings for each highly susceptible pixel and mapped landslides at California, US and Dhading, Nepal.....	136
Figure 5-10: (a) Number of annual crossings below the threshold safety factor and (b) average duration (days) below threshold for highly susceptible location from Oct. 2003 to Sep. 2006 in California, US	138

Figure 5-11: (a) Number of annual crossings below the threshold safety factor and (b) average duration (days) below threshold for highly susceptible location from Oct. 2003 to Sep. 2006 in Dhading, Nepal	139
Figure 6-1: The study region in El Dorado County in California with the mapped landslide	167
Figure 6-2: Daily observed AMSR-E (25 km spatial resolution) and downscaled AMSR-E 1 km spatial resolution aggregated to 25 km spatial resolution in 2005 at Cleveland Corral, California, US. $R^2 = 0.58$, $RMSE = 0.017 \text{ cm}^3/\text{cm}^3$	168
Figure 6-3: Observed AMSR-E soil moisture, VIC-3L soil moisture layer (1 and 2), snow and groundwater measurements at Cleveland Corral, California, US. Groundwater thickness is measured from the bottom of piezometer installed at 1.82 m below the surface	169
Figure 6-4: Observed scaled ($0.05\text{-}0.48 \text{ cm}^3/\text{cm}^3$) AMSR-E soil moisture, VIC-3L soil moisture layer (1 and 2) and snow values at Cleveland Corral, California, US.	170
Figure 6-5: AMSR-E (1 km) soil moisture on maximum modeled soil moisture day (May 8, 2005)	171
Figure 6-6: VIC-3L (1 km) soil moisture on maximum modeled soil moisture day (May 8, 2005)	172
Figure 6-7a: The observed albedo (1 km) on maximum modeled soil moisture day (May 8, 2005)	173
Figure 6-7b: The observed NDVI (1 km) on maximum modeled soil moisture day (May 8, 2005)	102
Figure 6-8: Landslide susceptibility map for maximum modeled saturation day (May 8, 2005) using VIC-3L soil moisture	175
Figure 6-9: Landslide susceptibility map for maximum modeled saturation day (May 8, 2005) using downscaled AMSR-E soil moisture.....	176
Figure 6-10: Comparison of highly susceptible area predicted using VIC-3L and AMSR-E on maximum modeled soil moisture day (May 8, 2005). Green square indicates identical predictions. Red squares are location identified by VIC-3L highly susceptible, but not by AMSR-E	177

ABSTRACT

LANDSLIDE SUSCEPTIBILITY MAPPING THROUGH ENHANCED DYNAMIC SLOPE STABILITY ANALYSIS USING EARTH OBSERVING SATELLITE MEASUREMENTS

by

Ram Lakhan Ray

University of New Hampshire, September, 2009

Landslides are common throughout the world and can be triggered by earthquakes, volcanoes, floods, and heavy continuous rainfall in mountainous regions. For most types of slope failure, soil moisture plays a critical role because increased pore water pressure reduces the soil strength and increases stress. The combined effect of soil moisture in unsaturated soil layers and pore water pressure in saturated soil layers is critical to accurately predict landslides. However, dynamic in-situ soil moisture profiles are rarely measured on regional or global scales.

The dynamic soil moisture can be estimated by a soil vegetation atmosphere transfer (SVAT) model or satellite. While a SVAT model can estimate soil moisture profile, satellite estimates are limited to the upper thin surface (0-5 cm). However, considering the complex database needed for a SVAT model, satellite data can be obtained quickly and may produce promising results in less data-rich regions at the global scale. While no previous landslide studies have used remotely-sensed soil moisture data,

Advanced Microwave Scanning Radiometer (AMSR-E) has the potential to be useful in characterizing soil moisture profiles.

First this study investigated relationships among landslides, AMSR-E soil moisture and Tropical Rainfall Measuring Mission (TRMM) in landslide prone regions of California, U.S., Leyte, Philippines and Dhading, Nepal. Then, a modified infinite slope stability model was developed and applied at Cleveland Corral, California, US and Dhading Nepal, using variable infiltration capacity (VIC-3L) soil moisture and AMSR-E soil moisture to develop dynamic landslide susceptibility maps at regional scale.

Results show a strong relationship among remotely sensed soil moisture, rainfall and landslide events. Results also show a modified infinite slope stability model that directly includes vadose zone soil moisture can produce promising landslide susceptibility maps at regional scale using either VIC-3L or AMSR-E soil moisture. Vadose zone soil moisture has a significant role in shallow slope failure. Results show promising agreement between the susceptible area predicted by the model and the actual slope movements and slope failures observed in the study region. This model is quite reasonable to use in shallow slope stability analysis at a regional or global scale.

CHAPTER 1.

INTRODUCTION

Natural disasters, like landslides, tsunamis, and floods, cost billions of dollars and result in numerous deaths and injuries throughout the world in mountainous regions (Metternicht et al., 2005). Both developed countries (e.g., U.S., Australia, Japan and U.K.) and developing countries (e.g., China, India, Indonesia, Philippines and Nepal) routinely have catastrophic landslides, especially during rainy seasons. Furthermore, inventories conducted between 1964 and 1999 show a steady increase in the number of landslide disasters worldwide (Kjekstad, 2002; Metternicht et al., 2005). In the U.S. alone, landslides cause \$3.5 billion in damage and between 25 and 50 fatalities annually (USGS, 2004).

Landslides can be triggered by earthquakes, volcanoes, and floods. However, most of the slope failures are preceded by intense rainfall. Slope failures ultimately are caused by processes that increase shear stresses or decrease shear strengths of soil mass (Abramson et al., 1996). Various natural factors (e.g., earthquake, concentrated rainfall, undercutting of banks by flood) and anthropogenic factors (e.g., deforestation, cuts and fills on slopes) contribute to slope failures by decreasing shear strength or increasing shear stress. Human infrastructure development, such as roads and deforestation that change the topography and remove the vegetation cover, respectively, can decrease slope stability (Sidle et al., 2004).

Slope failure is strongly related to slope, soil moisture/water content, vegetation, and soil types. Weather and climate factors that increase soil water content and hence the pore water pressures serve to enhance slope instability. The mechanism for most of the shallow slope failures is the rapid build up of pore water pressure in the soil mantle above the impervious soil layer or bedrock.

For slope stability analysis, several approaches have been used (Ermini et al., 2005; Abella and Van Westen, 2008; Ray and de Smedt, 2009) including heuristic approaches (Gorsevski et al., 2006^a; Ruff and Czurda, 2008; Abella and Van Westen, 2008), statistical techniques (Skirikar et al., 1998; Suzen and Doyuran 2004; Lee, 2004, 2005; Saha et al., 2005; Ayalew and Yamagishi, 2005), landslide risk assessment (Petley et al., 2004; Saldivar-Sali and Einstein, 2007) and deterministic techniques (Soeters and Van Westen, 1996; Joshi et al., 2000). In heuristic approaches, survey and observed maps as well as individual experience are necessary, but geotechnical parameters are not required (Gulla et al., 2008; Abella and Van Westen, 2008). In statistical approaches, bivariate and multivariate statistics, the spatial correlation is established by linking environmental variables. The qualitative and quantitative probability of loss of life and property technique is used in landslide risk assessment. Of these methods only the deterministic approach is physically-based.

A factor of safety can be computed deterministically using the infinite slope stability model based on the limit equilibrium approach. In this method, a slope can be divided into a number of slices and the factor of safety is computed by solving the static equilibrium equations based on a set of assumptions. The parameters required to perform this type of analysis generally include the soil type, friction angle, cohesive intercept,

shear strength, location of the water table and slope geometry as well as the soil moisture in unsaturated soil layer. Numerous studies have analyzed shallow landslides using a one dimensional infinite slope stability model (e.g., Montgomery and Dietrich, 1994; Van Western and Terlien, 1996; Cho and Lee, 2002; D'Odorico and Fagherazzi, 2003; Onda et al., 2004; Borga et al., 2005; Muntohar and Liao, 2009). These studies typically use wetness indices to estimate the water table position, but neglect the soil moisture in the upper soil layer above the groundwater table (Rosso et al., 2006). Because landslides are triggered by the combined effect of surface and subsurface saturation, it is necessary to be able to link the surface soil moisture to the subsurface layer.

Vadose zone soil moisture can be obtained by in-situ measurements. However, such measurements are time consuming and require complex data collection efforts even for local scales. As a result, there are very few in-situ observing systems to measure soil moisture at regional or continental scale (Gao et al., 2006). At these scales, either remote sensing or soil-vegetation-atmosphere-transfer (SVAT) models are useful methods to estimate soil moisture values. Because SVAT models require significant data and computational resources, they may not be appropriate for a region with limited data such as developing countries.

An alternative is to use remotely sensed soil moisture. While these data have not been used previously for landslide studies, remote sensing can be used to predict catastrophic events and hazardous areas (Ostir et al., 2003). Landslide inventory maps have been developed using aerial photography with photo interpretation technique (Oka, 1998; Brardinoni et al., 2003; van Western and Getahun, 2003) as well as using remotely sensed data with image analysis technique. Over the past decade, the Earth Observing

System (EOS) platforms have deployed a suite of instruments that monitor land conditions relevant to landslide hazard characterization such as Light Detection and Ranging (Lidar), Interferometric Synthetic Aperture Radar (InSAR), Differential SAR Interferometry (DInSAR) data.

The use of multi-temporal satellite imagery is increasingly applied to monitor, classify and detect landslides (Mantovani et al., 1996; Hervas et al., 2003; Cheng et al., 2004). For regional scale landslide analyses, Landsat TM and Advanced Spaceborne Thermal Emission and Reflection Radiometer (ASTER) have been used to derive landcover in regions including the Himalayas range (Zomer et al., 2002; Saha et al., 2002; Sarkar and Kanungo, 2004). Kaab (2005) showed that recent Shuttle Radar Topography Mission (SRTM) results are promising for characterizing topography in regions having landslides. Climate data including precipitation and convection pattern characterization using Tropical Rainfall Measuring Mission (TRMM) and Meteosat-5 have been valuable additions to complement sparse data in the Himalayas (Barros and Lang, 2003; Barros et al., 2004).

Satellite instruments produce imagery with different spatial resolutions. High resolution (10 m) data can isolate critical areas, while lower resolution (10^4 m) data can track the evolution of regional conditions. For example, InSAR has been used to locate and characterize landslides (e.g., Canuti et al., 2004; Singhroy and Molch, 2004). SRTM DEM is available at 30 m spatial resolution for US and 90 m resolution for rest of the world. Even though high resolution DEM (10 m) is more appropriate for landslide studies, one has to use low resolution DEM for regional and global scales research work. Moreover, Advanced Microwave Scanning Radiometer (AMSR-E) soil moisture and

TRMM rainfall are available at 25 and 27.5 km (approx.) spatial resolutions, respectively. The landslide study based on such a low resolution remotely sensed data requires downscaling. Downscaling requires many types of complex specific high resolution data that has demonstrated relationships with surface soil moisture at low resolution. There are also limitations to which scale the coarse resolution data can be downscaled. For example, AMSR-E data can be downscaled to 1 km resolution using normalized vegetation index (NDVI), albedo and land surface temperature (LST) with 1 km spatial resolution. Therefore, it can be appropriate to use comparatively coarse resolution remotely sensed data for landslide studies at regional or global scales.

Pelletier et al. (1997) indicated that continuous remote-sensing of soil moisture coupled with a digital elevation model is a necessary component of a successful landslide hazard mitigation program. While no landslide studies exist using remotely-sensed soil moisture data, global data are available from AMSR-E that may be useful to obtain surface soil moisture. Clearly AMSR-E's 25 km spatial resolution makes it well suited to examine landslide conditions at a regional scale, but not to locate and characterize specific failure zones.

Remote sensing products measure soil moisture for the upper 2 to 5 cm of the Earth's surface. This thin layer soil moisture information does not represent the complete unsaturated soil moisture profile underneath thick soil layer (subsurface) above the bedrock. However, it does provide valuable information on moisture conditions and how they evolve over time. For regional scales, this may be adequate to identify when zones reach potential hazard conditions.

If it is critical to obtain soil moisture profile of the whole soil layer above the bedrock or impermeable layer and to predict the position of the ground water table then remote sensing soil moisture products can not be used directly to identify landslide prone regions. A potential approach is to rely on a hydrologic model that can estimate soil moisture in the subsurface layer and to use the remotely sensed soil moisture product for validation or assimilation. Regardless, preliminary analyses are required to determine the potential of dynamic soil moisture to be used in landslide prone regions and to examine approaches to provide regional scale moisture.

In addition, ancillary remote sensing measurements are a critical aspect of the proposed research. These measurements complement existing physical databases by characterizing dynamic terrestrial systems and hydrologic fluxes. For less data-rich regions, remote sensing measurements may provide the only high resolution data source available for the Earth's surface.

The overall research goal was to develop a regional-scale, physically-based slope stability model that directly includes vadose zone soil moisture derived from satellite measurements or SVAT model to develop dynamic landslide susceptibility maps. The proposed enhanced model was applied to case studies in Dhading, Nepal, a data-poor region, and Cleveland Corral, California, US a data-rich region.

The first objective of this research was to determine if a relationship exists among remotely sensed soil moisture, precipitation and landslide. Specific research questions are: (1) Can remotely sensed soil moisture provide information in landslide prone regions? (2) Is there a qualitative relationship among landslides, TRMM rainfall and AMSR-E soil moisture?

The second objective of this research was to develop a dynamic, infinite slope stability model that directly includes vadose zone soil moisture. To address this objective, research issues were: (1) How the infinite slope stability model can be modified to directly include vadose zone soil moisture? (2) How the unsaturated soil moisture and the saturated zone can jointly be estimated to include in the slope stability model, and (3) Under what conditions is vadose zone soil moisture critical for determining slope failure?

The third research objective was to validate the VIC-3L model soil moisture profile and the wetness based groundwater model. Specific research questions include: (1) Does the Ray and de Smedt (2009) wetness index model provide reasonable groundwater table estimates? (2) Are SVAT derived soil moisture profiles reasonable? (3) What are the regional characteristics of landslide susceptibility maps using dynamic soil moisture and groundwater and how do they compare with traditional susceptibility maps?

The fourth objective of this research was to characterize spatiotemporal landslide susceptibility. The primary goal was to determine: (1) the statistical characteristics of safety factors and differences by region, hazard category, and physical characteristics and (2) the frequency and duration with which potential failure regions fall below critical safety factors.

This study's fifth objective was to evaluate dynamic landslide susceptibility maps that use remotely sensed soil moisture (AMSR-E). Towards this end, a downscaling method was examined to modify the AMSR-E soil moisture from 25 to 1 km spatial resolution. These remote sensing data were used to (1) identify unstable regions and (2) evaluate downscaling impacts on slope stability.

These five research objectives were addressed as a series of individual papers. Each research paper is presented in a separate chapter. The dissertation is organized with Chapter 1 Introduction, Chapters 2 to 6 for the five research papers, and Chapter 7 Concluding Remarks.

CHAPTER 2.

RELATIONSHIPS AMONG REMOTELY SENSED SOIL MOISTURE, PRECIPITATION AND LANDSLIDE EVENTS

Abstract

Landslides are triggered by earthquakes, volcanoes, floods and heavy continuous rainfall. For most types of slope failure, soil moisture plays a critical role because increased pore water pressure reduces the soil strength and increases stress. However, in-situ soil moisture profiles are rarely measured. To establish the soil moisture and landslide relationship, a qualitative comparison among soil moisture derived from AMSR-E, precipitation from TRMM and major landslide events was conducted. This study shows that it is possible to estimate antecedent soil moisture conditions using AMSR-E and TRMM satellite data in landslide prone areas. AMSR-E data show distinct annual patterns of soil moisture that reflect observed rainfall patterns from TRMM. Results also show enhanced AMSR-E soil moisture and TRMM rainfall prior to major landslide events in landslide prone regions of California, U.S., Leyte, Philippines and, Dhading, Nepal.

Introduction

Numerous natural factors, earthquakes, concentrated rainfall events, and undercutting of banks by flood, as well as anthropogenic factors, including deforestation and slope excavation, contribute to slope failures by decreasing shear strength or increasing shear stress of the soil mass (Abramson et al., 1996). However, most of the slope failures coincide with intensive rainfall (Anderson and Sitar, 1995; Iverson, 2000). Landslides are frequently a combined effect of intense rainfall and wet antecedent soil moisture conditions that cause landslides. For these slope failures, soil moisture plays a vital role because water both reduces the soil strength and increases the stress (Ray, 2004).

Soil moisture surrogates have been used extensively in slope stability analyses. Montgomery and Dietrich (1994), Van Westen and Terlien (1996), de Vleeschauwer and De Smedt (2002), and Acharya et al. (2006) analyzed slope stability using wetness indices calculated by the TOPOG model (O'Loughlin, 1986). As pointed out by Rosso et al. (2006), Montgomery and Dietrich's (1994) model neglects the presence of soil moisture in the upper soil layer above the groundwater table. They presented a modified model in order to consider soil moisture in the upper soil layer. Anderson and Sitar (1995), Iverson (2000), D'Odorico and Fagherazzi (2003), and Collins and Znidarcic (2004) showed that slope failures are primarily caused by infiltration of rainfall into the subsurface layer resulting in increased pore water pressure.

These studies focus on saturation level soil moisture contents as they relate to landslides. However, these studies have indirectly estimated the soil moisture or pore water pressure based on rainfall and do not directly account for the highly variable soil moisture prior to and during rainfall events.

Antecedent soil moisture can be obtained by in-situ measurements. However, such measurements are time consuming and require complex data collection efforts even for local scales. As a result, there are very few in-situ observing systems to measure soil moisture at regional or continental scales (Gao et al., 2006). An alternative approach is to obtain surface soil moisture from satellite remote sensing at national and global scales.

Surface soil moisture can be observed (measured) using microwave remote sensing (Jackson, 1982; Teng et al., 1993; Schmugge and Jackson, 1994; Kerr et al., 2001; Jackson, 2002; Moran et al., 2004; Loew et al., 2006; de Rosney et al., 2006). Typically remote sensing instruments can only provide the soil moisture information from the surface soil depth down to one to five cm. Numerous studies (e.g., Njoku et al., 2003; Walker et al., 2004; Lacava et al., 2005; Njoku and Chan, 2006; Gao et al., 2006) point out that microwave remote sensing measurements are affected by surface roughness, topographic features, dense vegetation and soil texture. This indicates that soil moisture data may have limited value on steep topography (Njoku et al., 2000). The few validation experiments, such as Soil Moisture Experiments 2004 (SMEX04) in northern Sonora, Mexico (Vivoni et al., 2008; Jackson et al., 2008), that have been conducted on such terrain show that rocky slopes can mask the moisture signal. As landslides mainly occur on steep slopes, a preliminary challenge is to determine if satellites can provide a signal in landslide prone areas.

Landslides are not triggered only due to surface layer saturation; rather, it is the combined effect of surface and subsurface saturation that is critical. Therefore, it is necessary to be able to link the surface soil moisture to the subsurface layer. A series of studies have established a link between surface soil moisture and groundwater. Choi and Jacobs (2007) soil moisture patterns on the surface were strongly related to those in the root zone. With an assumption of hydraulic potential equilibrium, Jackson (1980) developed a complete soil moisture profile based on surface soil moisture measurements. Arya et al. (1983) developed two approaches, regression and water budget, to establish the correlation between surface and subsurface soil moisture. Reutov and Shutko (1991, 1992) explored a technique to measure the depth of a shallow groundwater table based on microwave remote sensing data that uses the capillary rise above the water table to estimate the water table depth.

This study seeks to determine: (1) can remotely sensed soil moisture provide information in landslide prone regions? and (2) is there a qualitative relationship among landslides, TRMM rainfall and AMSR-E soil moisture? To answer these questions, the daily and seasonal variations of remotely sensed soil moisture from the Advanced Microwave Scanning Radiometer (AMSR-E) on the Earth Observing System (EOS) and rainfall from the Tropical Rainfall Measuring Mission (TRMM) are quantified in three landslide prone regions; Cleveland Corral, El Dorado County, CA, U.S., Guinsaigon, Southern Leyte, Philippines and Krishnabhir, Dhading, Nepal.

The paper presents an overview of the remote sensing technologies available to measure soil moisture and a brief review of the TRMM rainfall measurements. The soil moisture retrieval algorithm is also discussed. Details on the study sites as well as the

rainfall and soil moisture data used in this study are provided. This paper compares and analyzes the AMSR-E soil moisture and TRMM rainfall daily data from January, 2005 to May, 2006 at the three landslide prone regions.

Relationship between Water and Slope Failure

A landslide is a sudden failure of slope with or without the influence of water. Landslides that result in disasters are more commonly known as landslide disasters. Prior to slope failure, there is a slope movement. Sometimes slope movement results in a landslide and sometimes it does not. Many slope failures are caused by soil moisture or groundwater that increases pore water pressure and shear stress and decreases shear strength.

Safety factors (FS) are used to characterize slope stability. Slopes having safety factors less than one are considered unstable. A relationship can be established between soil moisture and slope failure for cohesive or cohesionless soil. Sidle and Ochiai (2006) developed a safety factor equation for any combination of soil and soil moisture, as

$$FS = \frac{c_s}{W \sin \theta} + \frac{\tan \phi}{\tan \theta} - \frac{u \tan \phi}{W \sin \theta} \quad (2-1)$$

$$W = [\gamma_t(H - h) + \gamma_{sat}h] \cos \theta \quad (2-2)$$

$$u = \gamma_w h \cos^2 \theta \quad (2-3)$$

where FS is the safety factor, W is the weight acting on the slope [KN/m²], C_s is the effective soil cohesion [KN/m²], u is the pore water pressure [KN/m²], H and h are the depth of the soil and water above failure plane, respectively [m], φ is the angle of internal friction and θ is slope angle [°], γ_t is the unit moist (but not saturated) weight of the soil [KN/m³], γ_{sat} the saturated unit weight of the soil [KN/m³], and γ_w the unit weight of water [KN/m³].

Equation 2-1 shows that increasing the soil slope decreases the safety factor. Similarly, increasing the soil moisture/water increases pore water pressure (u), effectively decreases the safety factor. Landslides occur when the safety factor becomes less than one.

Remote Sensing Products

Remotely Sensed Soil Moisture

Soil moisture can be measured with passive or active microwave sensors. Although the active and passive sensors observe different parameters, brightness temperatures and backscattering coefficients, respectively, (Jackson, 2002), both sensors provide information about surface reflectivity. Based on surface reflectivity, the dielectric constant necessary to derive surface soil moisture is estimated (Jackson, 2002). However, vegetation and roughness reduce the sensitivity of the microwave observations to soil moisture (Njoku et al., 2003).

Lower frequencies, L band (1-2 GHz), are more sensitive to soil moisture, but they are more susceptible to dense vegetation and radio frequency interference (RFI). The higher frequency C (6.9 GHz) and X (10.65 GHz) bands can be used to retrieve soil moisture (Jackson et al., 2005) because these higher frequency bands are comparatively less susceptible to RFI. At present, there are several satellite systems that are capable of observing surface soil moisture (Cashion et al., 2005). The systems include the Tropical Rainfall Measuring Mission (TRMM) Microwave Imager (TMI) at 10.65 GHz, (Jackson and Hsu, 2001), and the Advanced Microwave Scanning Radiometer (AMSR) on the Earth Observing System (Njoku et al., 2003). Soil Moisture and Ocean Salinity (SMOS) (Kerr et al., 2001) is scheduled to launch in 2009 (Hoffmann, 2005, Scipal et al., 2005).

The soil moisture active passive (SMAP) is expected to launch by 2013 (Drinkwater et al., 2009). This study uses the AMSR-E satellite data.

AMSR-E was developed by the National Space Development Agency of Japan (NASDA) and launched on Aqua satellite by the National Aeronautics and Space Administration (NASA) on May 4, 2002 (Njoku et al., 2003, Li et al., 2004). AMSR-E measures brightness temperature at six frequencies in the range 6.9-89 GHz (Njoku et al., 2003). Soil moisture is retrieved using a microwave radiative transfer (RT) model that links surface geophysical variables to the observed brightness temperature (Jackson, 1993, Njoku et al., 2003). AMSR-E produces soil moisture (product level 3) at 56 km spatial resolution and provides re-sampled products at a 25 km grid scale. AMSR-E data are available from June 18, 2002 to present on a daily basis. However, data are missing on a number of days.

Remotely Sensed Rainfall

The Tropical Rainfall Measuring Mission (TRMM) instrument was launched on November 27, 1997 as joint effort by NASA and the Japanese Space Agency (JAXA) (Kummerow et al., 1998, Gao et al., 2006). TRMM provides precipitation data from 1997 to present (<http://trmm.gsfc.nasa.gov>). The primary instruments are the Precipitation Radar (PR), the first rain radar in space (13.8 GHz), and the TRMM Microwave Imager (TMI), a multi-channel (5 bands from 10.7 GHz to 85.5 GHz) passive microwave radiometer. In addition, the Visible Infrared Scanner (VIRS) instrument is used to image clouds to determine precipitation structure. TRMM provides data from 50° S and 180° W to 50° N and 180° E. This study uses the TRMM precipitation 3B42 3-hr product at a 0.25° x 0.25° (27.5 km²) resolution.

Study Data Sets

For this study, AMSR-E soil moisture data were obtained from the NASA Earth Observing System Data Gateway through National Snow and Ice Data Center (NSIDC). The TRMM rainfall 3B42 3-hr product was obtained from Goddard Distributed Active Archive Center (DAAC). Both TRMM rainfall and AMSR-E soil moisture data are for the period January 1, 2005 to May 31, 2006. Daily rainfall totals were calculated from the TRMM 3-hr product. AMSR-E soil moisture and TRMM rainfall values were analyzed and compared with landslide events to establish relationships among them.

In order to consider the response of soil moisture and rainfall, active landslide locations were selected for the three regions. These landslide areas are on the order of 1 km². Compared to the study areas, both the TRMM and the AMSR-E pixels are much larger. Therefore, one satellite pixel was obtained and analyzed for each site's soil moisture and rainfall.

Study Areas

Three study regions, which are highly prone to landslides, were selected for analysis. The study regions are Highway 50 at Cleveland Corral, El Dorado County, CA, US, Guinsaigon, Southern Leyte, Philippines, and Prithivi highway at Krishnabhir, Dhading, Nepal (Fig. 2-1). Since 1996, landslides and slope movements are very common in the Highway 50 corridor (Reid et al., 2003). In Guinsaigon, Southern Leyte, Philippines, a major landslide disaster occurred on February 17, 2006. This rainfall induced landslide crushed a village where 122 people were confirmed dead, hundreds of people were still missing as of 2006, and thousands of people were left homeless (Lagmay et al., 2006). In Krishnabhir, Dhading, Nepal, landslides have continuously occurred for four consecutive years starting from 2000 (Ray, 2004). Along the Prithivi highway corridor, landslides are very common during every monsoon.

Cleveland Corral, CA, USA

The Cleveland Corral landslide study region in Highway 50 corridor is located in the Sierra Mountains, California, USA (Reid et al., 2003). Highway 50 is a major road located between Sacramento and South Lake Tahoe in California (Spittler and Wagner, 1998). The study area is located between $120^{\circ} 17' 42''\text{W}$ to $120^{\circ} 32' 42''\text{W}$ and $38^{\circ} 39' 12''\text{N}$ to $38^{\circ} 54' 12''\text{N}$. Altitudes range from about 902 to 2379 m. Since 1996, slope

movement and landslides occur infrequently during the winter season. Additionally, one major catastrophic landslide occurred in 1983 in this region (Spittler and Wagner, 1998). Since 1997, the USGS has monitored this region using real time data acquisition systems (Reid et al., 2003). They found elevated pore-water pressures and abundant soil moisture during periods with slope movement and landslides in the winter (rainy) season.

Guinsaugon, Leyte, Philippines

The Philippines is an island country located in South East Asia between latitude 4° 23'N and 21° 25'N and longitude 116°E and 127°E with a 1850 km length and a 965 km width. The country's topography is characterized by alluvial plains to high mountains with an elevation to 3144 m. The Guinsaugon study region, municipality of St. Bernard, is located in Southern Leyte Province, Philippines. The Guinsaugon village, the site of the 2006 landslide disaster, is located at the foot of the slope (Lagmay et al., 2006). The study area is centered at 10° 21' 3"N, 125° 6' 33" E latitude and longitude, respectively, with a maximum elevation of 675 m (Lagmay et al., 2006). The authors indicate that the February, 2006 landslide's cause was a week long intensive rainfall in the Southern Leyte region.

Krishnabhir, Dhading, Nepal

Nepal consists of about 83% mountainous terrain and the remaining 17% in the southern alluvial plains. The country extends from 80° 04' to 88° 12'E longitude and 26°

22' to 30° 27'N latitude and spans approximately 885 km in the east-west direction and varies from 130 to 255 km in north-south direction. The altitude ranges from 70 m at Kanchan Kalan to 8850 m at the top of the Mount Everest within a very short distance. The relatively high landslide frequency in Nepal, as compared with mountain ranges of other countries, may be because Nepalese Mountains are geologically younger (Ray, 2004).

The Krishnabhir study region lies in the Dhusa Village Development Committee (VDC) in Dhading district, Nepal along the Prithvi Highway. The highway connects the Western and Eastern parts of the country to Kathmandu, the national capital. The area is situated between 27° 45' to 27° 52' 30 N latitude and 84° 37' 30" to 84° 52' 30"E longitude. Altitudes range from about 242 to 1922 m above the sea level. One of the major landslide areas is located at Krishnabhir of Dhusa village development committee (VDC) along the Prithivi Highway. Since 2000, landslides occur annually during the rainy season along the Prithivi Highway.

Results and Discussion

Intercomparison

Figure 2-2 shows daily and weekly moving average values of AMSR-E soil moisture for one and half years (January 1, 2005 to May 31, 2006). As daily soil moisture values are highly variable, a weekly moving average soil moisture was calculated for each date by averaging that day's soil moisture with that of the six preceding days. This plot clearly shows daily and seasonal variations for each study region. The period having the wettest soil moisture differs by region. For example, California's highest soil moisture occurs in the spring season. Nepal's soils are very wet shortly before and after the monsoon. The Philippines has the highest soil moisture value in the winter and late summer. Weekly moving average soil moisture values vary gradually in CA, USA, and Dhading, Nepal, but oscillate in Leyte, Philippines.

Table 2-1 presents summary statistics that characterize soil moisture variations by study region. The highest soil moisture values, observed in California, US, are twice those reported for Leyte, Philippines because California study region may have less well-drained soils and a colder climate. Based on the standard deviation of daily values, Nepal has much lower variability than either California or Leyte. Soil moisture ranges are smaller than expected, particularly for Nepal. Overall, these results indicate that, even in steep terrain or landslide prone regions, AMSR-E soil moisture can provide relevant information by capturing mean values and the timing and duration of wet periods.

Cleveland Corral, CA, USA

Figure 2-3 shows the weekly moving average AMSR-E volumetric soil moisture values from January 2005 to May 2006 as well as the daily TRMM rainfall data in the Cleveland Corral, California study region. While the results show only a 12% range in the soil moisture variations annually, the observed variations are adequate to identify the timing of relatively high soil moisture. Seasonal trends show that soil moisture increases from March to late May each year. This rising trend in soil moisture corresponds to a period of high rainfall. Soil moisture peaks occurred in April and May for both 2005 and 2006. However, peaks on 10th May, 2005 (24.9%) and on 14th April, 2006 (28.7%) do not coincide with rainfall peak events on 1st May, 2005 (31 mm) and on 5th April, 2006 (47.8 mm), respectively. This may reflect the lag time between the rainfall event and the satellite measurement. The lag time is not consistent because the rainfall frequency and duration are not consistent with the TRMM and the AMSR-E satellites passing time to that particular region. Thus, soil moisture may better characterize using total accumulated rainfall rather than brief intense rainfall events.

Soil moisture and rainfall trends were compared to slope movements and landslide events. Reported slope movement began in late February, 2005. Also, slope movements were observed throughout May, 2005 (<http://landslides.usgs.gov/monitoring/hwy50>). Two landslides were observed in 2006, one on April 3rd near Whitehall and another on May 7th near Kyburz. All of the slope movements and landslides coincide with periods of enhanced surface soil moisture and rainfall in this region. Interestingly, the peak precipitation days did not necessarily match the dates of observed movements and landslides.

Guinsaugon, Leyte, Philippines

Figure 2-4 depicts the weekly moving average AMSR-E volumetric soil moisture values and daily TRMM rainfall values from January 2005 to May 2006 in Guinsaugon, Leyte, Philippines. This study region has a completely different daily and seasonal soil moisture and rainfall temporal pattern than the California site. In this region, frequent rainfall events were observed throughout the year. Figures 2-2 and 2-4 show higher daily soil moisture variations than seasonal soil moisture variations. Due to the fairly uniform yearly rainfall distribution, no distinct seasonal soil moisture variations were observed. The seasonal evolution of soil moisture appears to somewhat correspond to the rainfall observations, but a clear relationship is not readily evident.

The soil on the day of the landslide disaster, February 17, 2006, was not as wet as that in January, 2006. As shown in Figure 2-4, this region had received high rainfall (375 mm) from 22 to 26 December in 2005. This rainfall causes a gradual increase of soil moisture until mid-January. Without rainfall, gradually decreased soil moisture can be observed from mid-January to mid-February in 2006. A week long continuous heavy rainfall (> 400 mm) that increased soil moisture/pore water pressure in the subsurface layer likely caused the landslide disaster. That the landslide occurred during lower than peak soil moisture indicates the importance of rainfall characteristics in addition to antecedent conditions. This site suggests that additional research is needed to estimate soil moisture for landslide hazard prediction that uses both soil moisture and rainfall.

Krishnabhir, Dhading, Nepal

The one and half year (January 2005 to May 2006) moving average AMSR-E soil moisture and daily TRMM rainfall plot for Dhading, Nepal produces a comparatively uniform distribution pattern than the other two study regions (Fig. 2-5). This is mainly due to Nepal's monsoonal (June to September) climate. In this study region, off monsoonal (October to May) season receives very little rainfall. Dry soil conditions persist until late July. Figures 2-2 and 2-5 show higher seasonal soil moisture variations than daily soil moisture variations. Interestingly, the soil moisture values are nearly constant from September to February and appear to be insensitive to rainfall. This may indicate a measurement problem. As this period coincides with Nepal's typical late August planting, the potential cause is dense vegetation.

From 2000 to present, landslides were observed annually during the monsoon (Mid August) (Ray, 2004) in the Prithivi highway corridor. During the monsoonal rainfall, enhanced soil moisture is shown in Figure 2-5. These wetter conditions increase pore water pressures to levels that are sufficient to cause slope failure. Hence in Nepal, the steady rainfall, measured by TRMM that causes a continuous increase in soil moisture is closely linked with this region's landslides.

Conclusion

Soil moisture is an important parameter for landslide studies. As the soil mass's soil moisture increases, pore water pressure rises. Pore water pressure, which increases shear stress and decreases shear strength, is the main cause for many landslides. This soil moisture can be estimated by in-situ measurements, but such measurements are time consuming and cost prohibitive at national and global scale. In contrast, this study shows that AMSR-E can provide surface soil moisture for global scale at a daily temporal resolution.

Each of the three study regions had landslides or slope movements when soil moisture and rainfall showed higher values. These landslide occurrences clearly indicate a good relationship among landslide events, AMSR-E surface soil moisture and TRMM rainfall. Results show that AMSR-E soil moisture data can be used for landslide studies. However, more intensive research still is necessary to validate soil moisture patterns and to include AMSR-E soil moisture in slope stability analysis.

Table 2-1: Statistical Analysis of AMSR-E soil moisture from January 2005 to May 2006 in three study regions

2005						
California, USA			Leyte, Philippines		Dhading, Nepal	
Descriptions	Soil Moisture (cm³/cm³)	Date	Soil Moisture (cm³/cm³)	Date	Soil Moisture (cm³/cm³)	Date
Mean	0.175		0.084		0.145	
Range	0.117		0.139		0.068	
Std. Dev	0.023		0.025		0.013	
Min	0.132	November, 15	0.015	December, 17	0.109	July, 17
Max	0.249	May, 10	0.154	August, 19	0.177	May, 7
Count (Days)	271		225		232	

2006 (Jan to May)						
California, USA			Leyte, Philippines		Dhading, Nepal	
Descriptions	Soil Moisture (cm³/cm³)	Date	Soil Moisture (cm³/cm³)	Date	Soil Moisture (cm³/cm³)	Date
Mean	0.191		0.079		0.153	
Range	0.147		0.112		0.035	
Std. Dev	0.027		0.023		0.008	
Min	0.14	January, 2	0.013	February, 11	0.141	February, 7
Max	0.287	April, 14	0.125	January, 25	0.176	April, 19
Count (Days)	113		92		101	

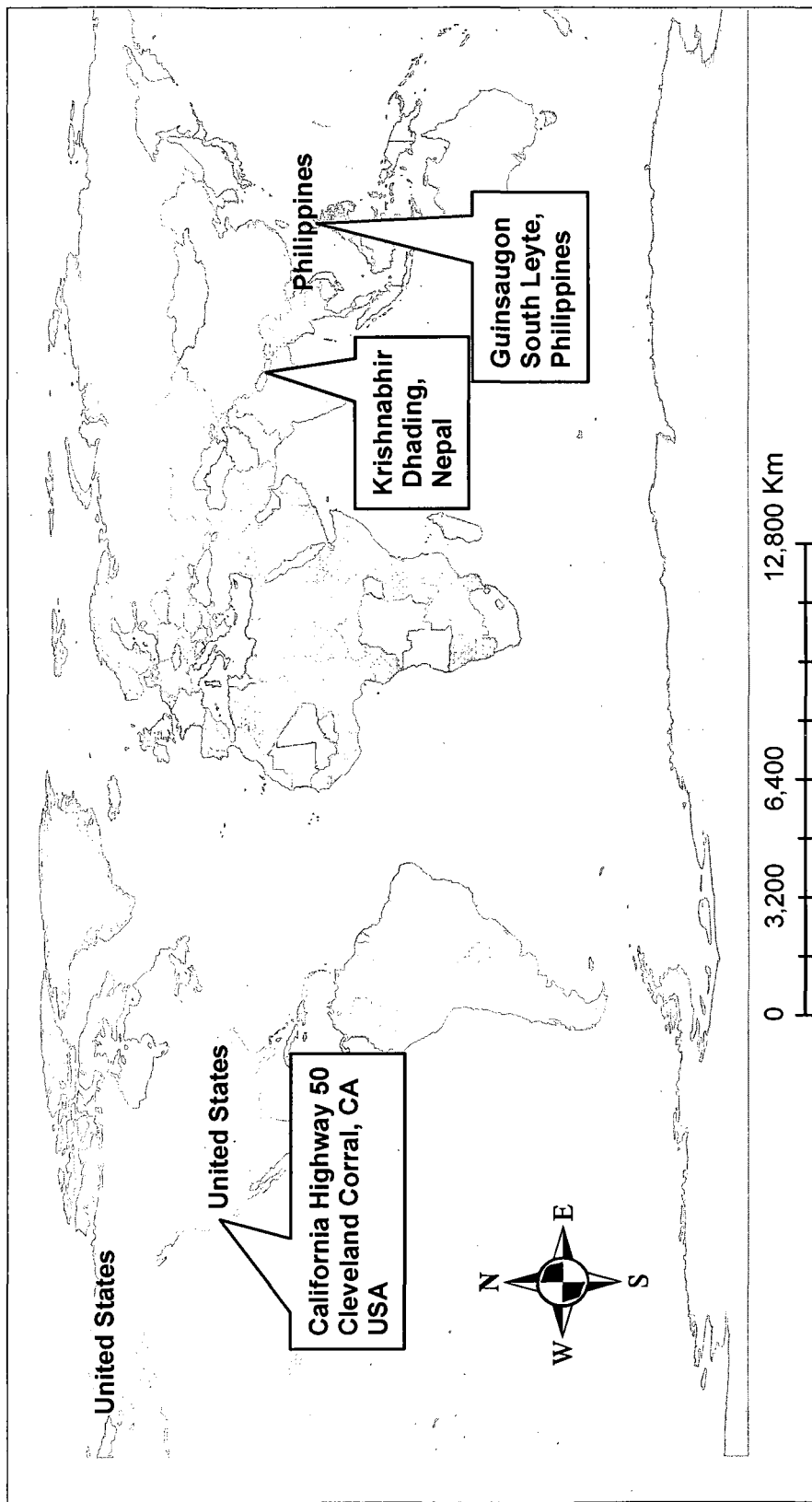


Figure 2-1: Locations of the three study regions

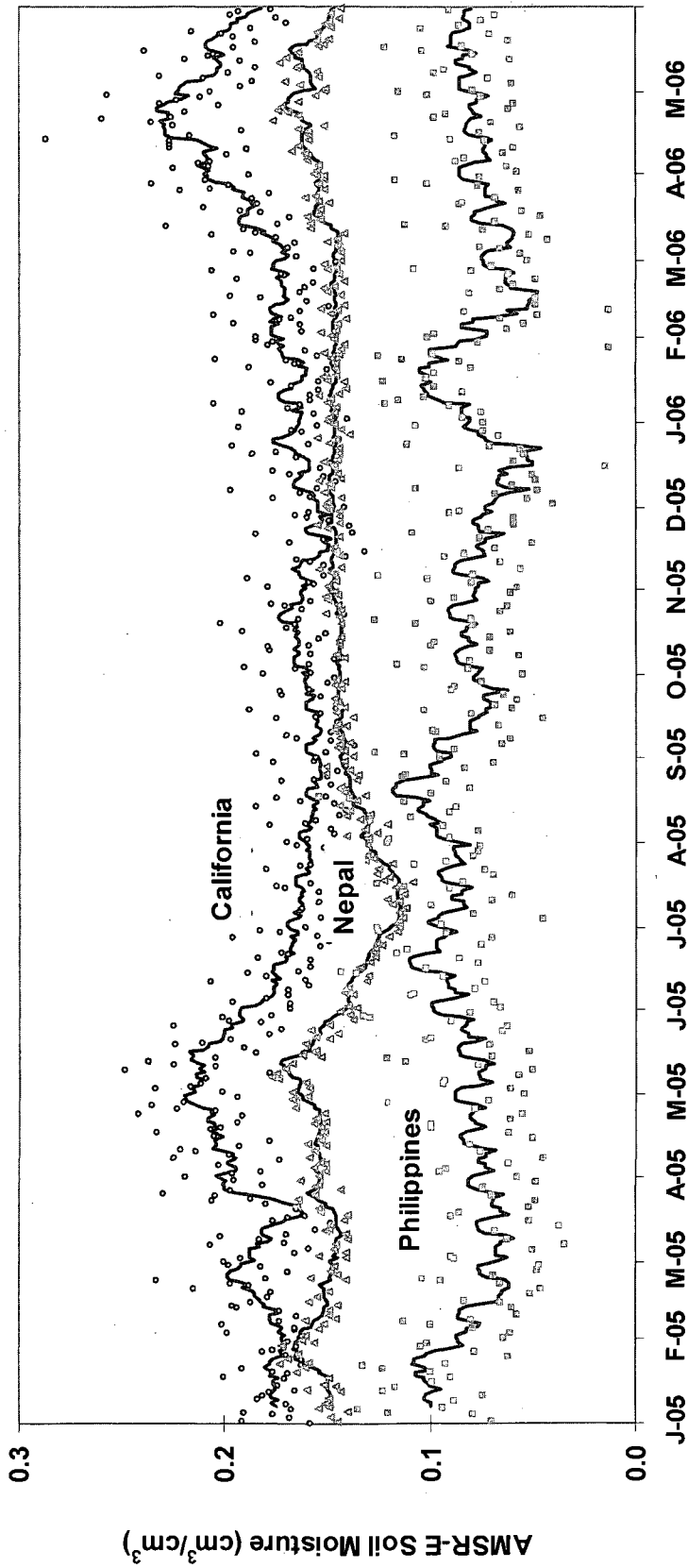


Figure 2-2: A comparison of soil moisture and rainfall in the three study regions (January 2005 to May 2006). Daily values are indicated with circles, triangles, and squares for California, Nepal, and Philippines, respectively. Solid lines correspond to the one week moving average

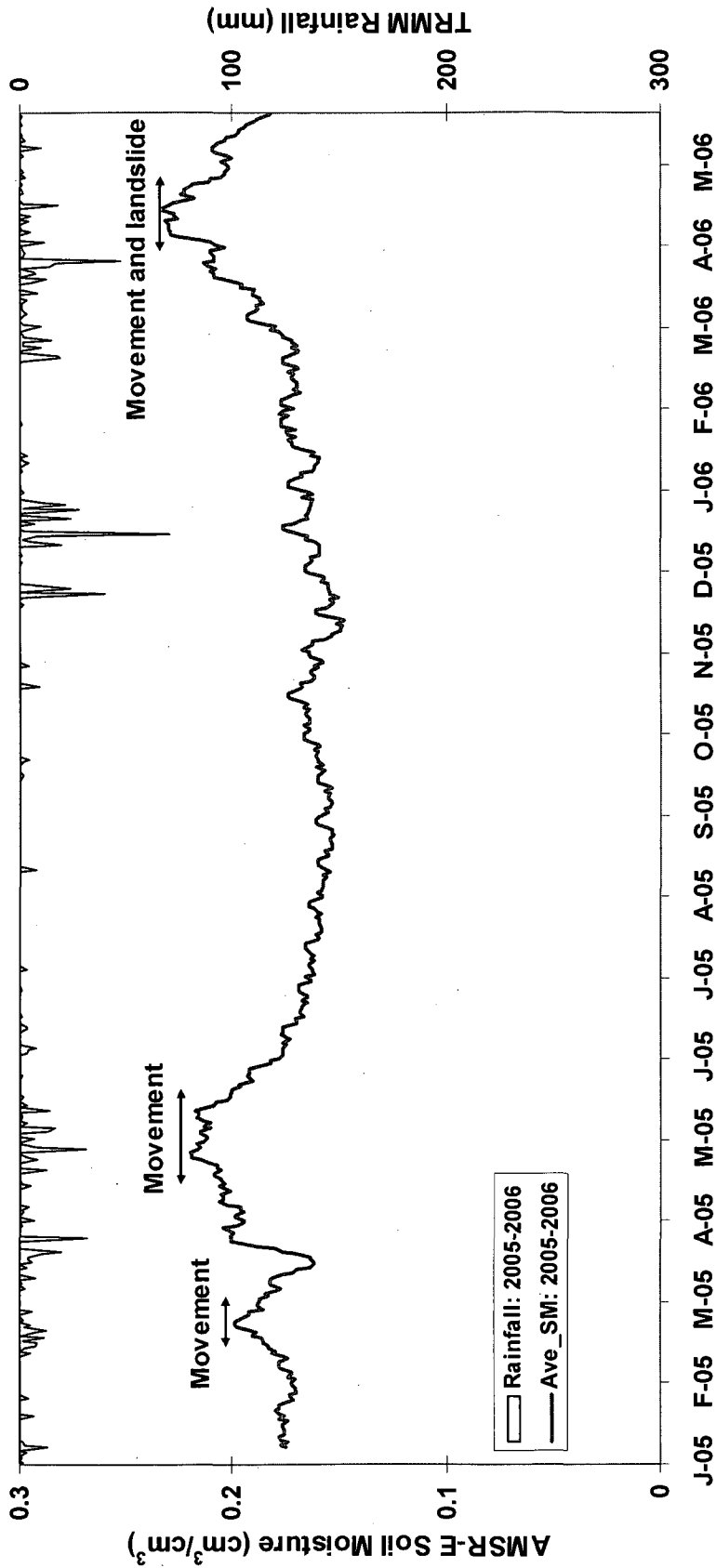


Figure 2-3: Slope movement/landslides, one week moving average AMSR-E soil moisture and daily TRMM rainfall in California, US from January 2005 to May 2006

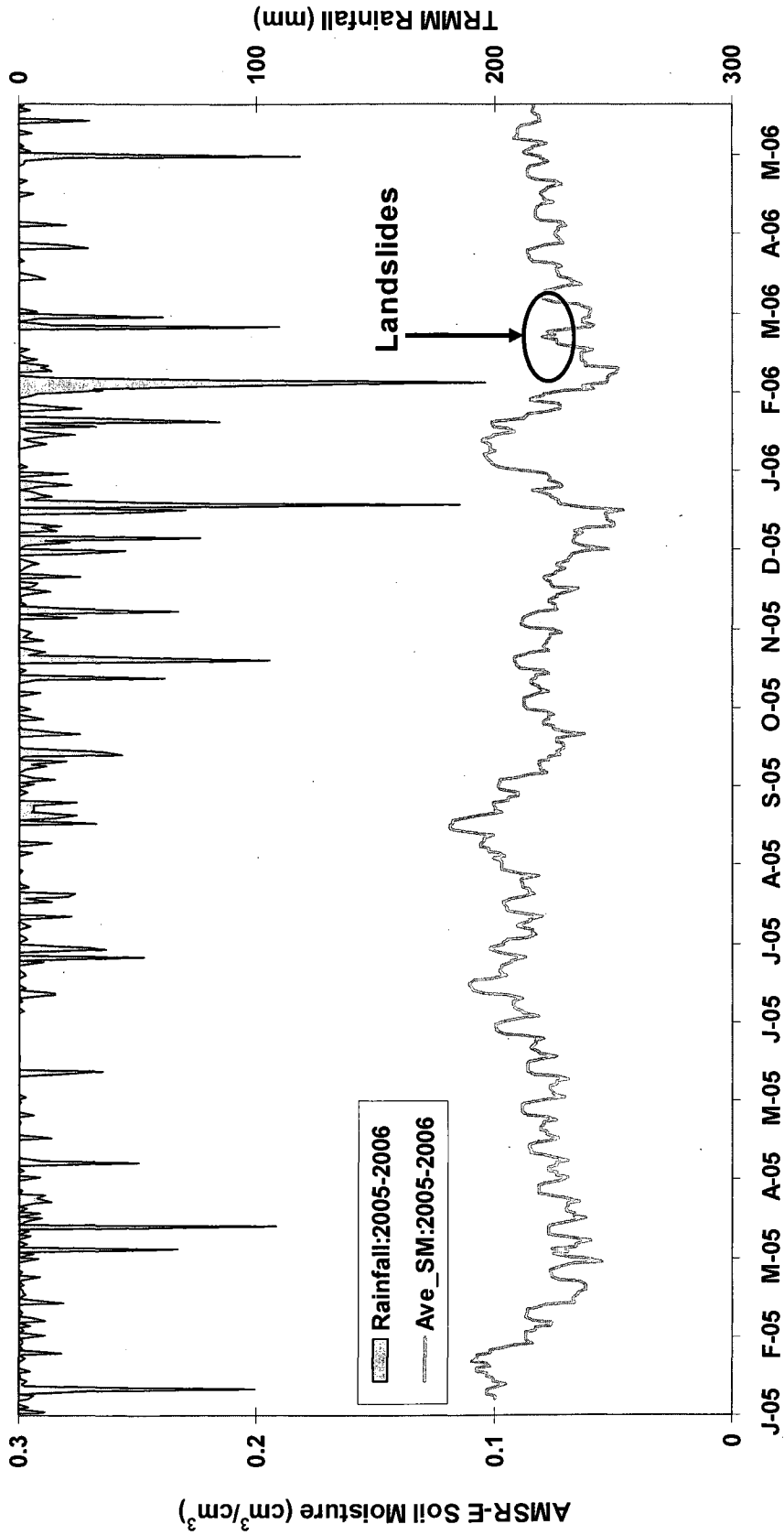


Figure 2-4: Landslides, one week moving average AMSR-E soil moisture and daily TRMM rainfall in Leyte, Philippines from January 2005 to May 2006.

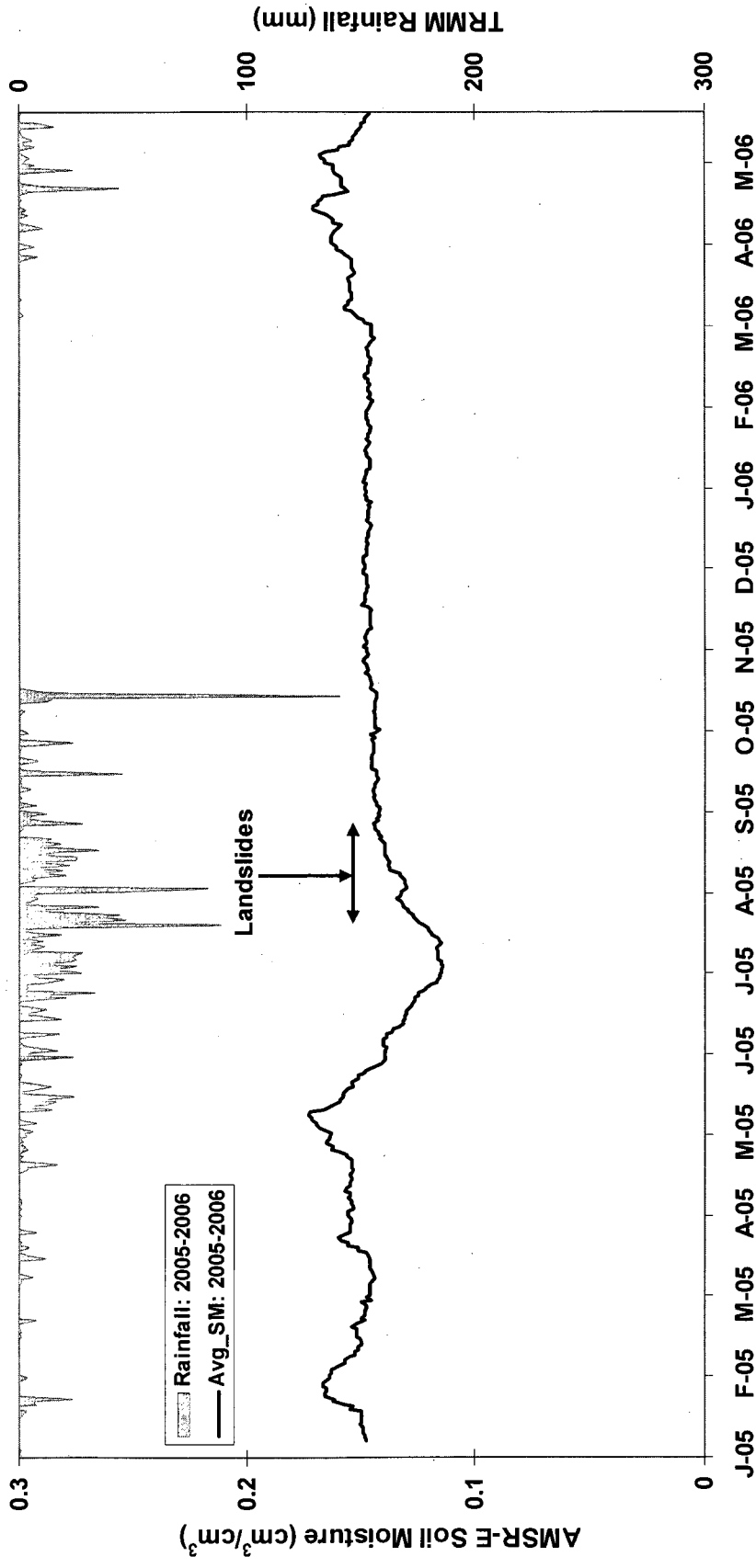


Figure 2-5: Landslide, one week moving average AMSR-E soil moisture and daily TRMM rainfall in Dhading, Nepal from January 2005 to May 2006.

CHAPTER 3.

IMPACTS OF VADOSE ZONE SOIL MOISTURE AND GROUNDWATER TABLE ON SLOPE INSTABILITY

Abstract

The combined effect of soil moisture in unsaturated soil layers and pore water pressure in saturated soil layers is critical to predict landslides. An improved infinite slope stability model, that directly includes vadose zone soil moisture and groundwater, was used to analyze sensitivity of safety factors/susceptibility to vadose zone soil moisture. First, the sensitivity of safety factors to vadose zone soil moisture was studied on pixels that exhibited active landslides at Cleveland Corral, California and later the method was applied to entire study region at regional scale. Results show a significant impact of vadose zone soil moisture in the sensitivity of the safety factor for a shallow soil layers (< 2 m) with comparatively deeper groundwater (1 m). For a shallow soil mantle (1 m), the change in safety factor was 59%, while it was only 13% for the thick soil mantle (3 m) for the 1 m groundwater position. The unstable area increases nonlinearly with increasing vadose zone soil moisture. Vadose zone soil moisture most strongly impacts shallow slope stability when soil mantles are less than 2 m thick.

Introduction

Slope failures ultimately are caused by processes that increase shear stresses or decrease shear strengths between the soil layers (Cernica, 1982; Abramson et al., 1996). An increase in the pore water pressure reduces the effective normal stresses (σ') and, consequently, the shear strength of the soil layers as defined by the Coulomb equation $\tau = c + \sigma' \tan\phi$. Weather and climate factors that increase soil moisture/water content and hence pore water pressure serve to enhance slope instability (Ray and Jacobs, 2007).

Generally, a shallow landslide is assumed when the slope length is greater than the soil mantle thickness (Skempton and DeLory 1957); and ranges from 1 to 2 m (Meisina and Scarabelli, 2007) seldom exceeding 3 m (Au, 1998). Based on the limit equilibrium approach, the one dimensional infinite slope model is frequently used to study shallow landslides (e.g., Montgomery and Dietrich, 1994; Van Western and Terlien, 1996; Cho and Lee, 2002; D'Odorico and Fagherazzi, 2003; Onda et al., 2004; Borga et al, 2005; Muntohar and Liao, 2009). An infinite slope stability model equates resisting and driving forces in order to estimate a safety factor (FS). Soil cohesion and angle of internal friction control the resisting forces. Increasing slope angle enhances the driving force. The unit soil weight, whether it is dry, moist or saturated, affects the resisting force through σ' applied to a potential failure surface and also the driving force along the potential failure surface on a slope. For shallow landslides, effects of soil cohesion are

large (Sidle and Ochiai, 2006). The weight on the slope and thus the driving force increases, when water fills previously empty pore space.

Moreover, in the presence of groundwater or a saturated soil layer, the driving force caused by unit soil weight, can be greater still than the resisting force for any given slope angle because pore water pressure reduces the effective stress, and consequently, the resisting force. According to Ray and Jacobs (2007), landslides are not triggered only due to surface layer saturation; rather, it is the combined effect of surface and subsurface saturation that is critical. During rainfall, water infiltrates into the substratum, which increases soil moisture in the unsaturated zone and also raises the water table. Therefore, the vadose zone soil moisture (SM), which increases the unit soil weight, may play a vital role in shallow slope instability. It is essential to consider vadose SM when estimating moist unit soil weight above the saturated soil layer.

Many authors have studied the unsaturated zone and slope instability by including matric suction or negative pore water pressure in the infinite slope stability model (e.g., Cho and Lee, 2002; Rahardjo et al., 2007; Muntohar and Liao, 2009). These studies show that the infiltrated rainfall water dissipates the soil suction or negative pore water pressure in the vadose zone and, in turn, reduces the shear strength and triggers slope failure. Lu and Godt (2008) modified the infinite slope stability model to include a skeletal stress that varies with the soil moisture variations in the unsaturated zone. They noted that most landslide studies that include unsaturated zone soil suction in an infinite slope stability model are just modifying the shear strength due to soil suction and do not account for the moist unit soil weight of the unsaturated layer or saturated layer weight in the slope stability model.

The two-layer concept, unsaturated and saturated soil layers, is frequently used in the infinite slope stability model to represent different unit soil weights. Some studies use a saturated unit soil weight to represent both layers (e.g., Montgomery and Dietrich, 1994; D'Odorico et al., 2005; Chiang and Chang, 2009). They assume constant saturated unit soil weight for their whole study area. De Vleeschauwer and De Smedt (2002) and Acharya et al. (2006) use dry and saturated unit soil weight, respectively, for the layer above and below the saturated soil layer. Collins and Znidarcic (2004) use effective and total unit soil weight for the saturated and unsaturated soil layers, respectively. Vanacker et al. (2003) and Gabet et al. (2004) use total unit soil weight for both layers. A more physically sound representation uses a moist unit soil weight for the unsaturated soil layer and saturated unit soil weight for a saturated soil layer (e.g., Burton and Bathurst, 1998; Sidle and Ochiai, 2006). The two-layer approaches use static values of moist unit soil weight and saturated unit soil weight, and do not take into account the impact of dynamic moisture condition for slope stability analysis.

The vadose zone SM can be combined with groundwater for calculating wetness indices. The wetness indices are derived in various ways. One widely used wetness index approach is O' Loughlin's 1986 TOPOG model (e.g., Dietrich et al., 1993; Montgomery and Dietrich, 1994; Van Westen and Terlien, 1996; Pack et al., 1998; de Vleeschauwer and De Smedt, 2002; Acharya et al., 2006). The TOPOG model is based on the topographic wetness index developed by Beven and Kirkby (1979) within the runoff model TOPMODEL. These approaches are based on the assumption that all the infiltrating water in the upgradient contributing area contributes to the groundwater flow at the downstream convergence point. This assumption does not account for the time

duration for flow accumulation or the water storage and delay in the upgradient area (Barling et al., 1994). Van Westen and Terlien (1996) and Acharya et al. (2006) calculate wetness indices by taking the ratio of the saturated soil layer thickness to the total soil thickness.

According to Rosso et al. (2006), wetness indices calculated by the TOPOG model neglect the presence of soil moisture in the upper soil layer above the groundwater table. The TOPMODEL approach, for calculating wetness indices, does not take into account the unsaturated soil thickness or vadose zone SM. This is a problem because the ground does not have to be saturated for failure (Dietrich et al., 1993) and slope failures can occur above the groundwater table in the unsaturated zone under the steady infiltration conditions (Lu and Godt, 2008). It is necessary to estimate a wetness index that includes the combined effects of vadose zone SM, pore water pressure or groundwater level.

This paper proposes to directly include vadose zone SM in the slope stability model to estimate safety factors. The approach is to develop a wetness index model that takes into account both saturated zone and vadose zone SM. Moreover, this paper also uses an approach to calculate moist soil unit weight that takes into account the temporal dynamics of vadose SM. The main objectives of this study are: (1) to modify the infinite slope stability model to directly include vadose zone SM and (2) to analyze the combined impacts of vadose zone SM, groundwater table position and soil mantle thickness on instability.

Slope Stability Model

This study uses the infinite slope method (Skempton and DeLory, 1957) to calculate safety factors that express the ratio of resisting forces to driving forces. Figure 3-1 shows a schematic representation of a typical slope. The infinite slope stability model as adapted from the several studies (e.g., Montgomery and Dietrich 1994; van Westen and Terlien 1996; Acharya et al., 2006; Ray and De Smedt 2009) is

$$FS = \frac{C_s + C_r}{\gamma_e H \sin \theta} + \left(1 - m \frac{\gamma_w}{\gamma_e} \right) \frac{\tan \phi}{\tan \theta} \quad (3-1)$$

where C_s and C_r are the effective soil and root cohesion [kN/m^2], γ_e is the effective unit soil weight [kN/m^3], H is the total depth of the soil above the failure plane [m], θ is the slope angle [$^\circ$], m is the wetness index [adimensional], ϕ is the angle of internal friction of the soil [$^\circ$], and γ_w is the unit weight of water [kN/m^3]. Originally, Skempton and DeLory (1957) used the saturated unit soil weight (γ_s) instead of the effective unit soil weight (γ_e) and the vertical soil depth above the potential failure plane. However, Acharya et al. (2006) and Ray and De Smedt (2009) used the soil depth perpendicular to the potential failure plane (Fig. 3-1). The effective unit soil weight as defined by de Vleeschauwer and De Smedt (2002) is:

$$\gamma_e = \frac{q \cos \theta}{H} + (1 - m) \gamma_m + m \gamma_s \quad (3-2)$$

where q is any additional load on the soil surface [kN/m^2]. De Vleeschauwer and De Smedt (2002) used dry unit soil weight instead of moist unit soil weight (γ_m) [kN/m^2] for

the unsaturated soil layer. Hence we define the moist unit soil weight of the unsaturated soil layer above the saturated soil layer [kN/m^3] is defined as:

$$\gamma_m = \frac{G + S_w e}{1 + e} \gamma_w \quad (3-3)$$

where G is the specific gravity of soil [adimensional], S_w is the degree of soil saturation [cm^3/cm^3] or vadose zone soil moisture and e is the void ratio [adimensional]. The degree of soil saturation (range from 0 to 1) is replaced by the vadose zone SM when calculating moist unit soil weight for the unsaturated layer.

The traditional approach for calculating the wetness index is based on the TOPMODEL and uses effective rainfall, transmissivity, upslope specific contributing area and slope as well as the ratio of the saturated soil layer thickness to the total soil thickness. These approaches do not take into account the impact of vadose zone SM in the wetness index model. Here, a wetness index model is proposed that directly links vadose zone SM with the saturated soil layer thickness and the total soil thickness (Eq. 3-4).

$$m = \frac{h + (H - h) * S_w}{H} \quad (3-4)$$

where h is the saturated thickness of the soil above the failure plane [m].

To study the impact of vadose zone SM on slope instability, Eqs. 3-1 to 3-4 are combined. The combined safety factor equation is

$$\begin{aligned}
 FS = & \frac{C_s + C_r}{S_w^2 E \gamma_w \sin \theta (h - H) + S_w \sin \theta (E \gamma_w H - E \gamma_w h + \gamma_s H - \gamma_s h + \gamma_d H) + \sin \theta (q \cos \theta + \gamma_s h + \gamma_d H - \gamma_d h)} \\
 & + T - \frac{S_w \gamma_w T \left(1 - \frac{h}{H}\right) + \gamma_w T \frac{h}{H}}{S_w^2 E \gamma_w \left(\frac{h}{H} - 1\right) + S_w (E \gamma_w - E \gamma_w) \frac{h}{H} + \gamma_s - \gamma_d + \frac{h}{H} \frac{q \cos \theta}{H} + \gamma_s \frac{h}{H} + \gamma_d - \gamma_d \frac{h}{H}}
 \end{aligned} \quad (3-5)$$

where $E = \frac{e}{1+e}$, $T = \frac{\text{Tan}\phi}{\text{Tan}\theta}$, and dry unit soil weight $(\gamma_d) = \frac{G}{1+e} \gamma_w$

The Eq. 3-5 can be differentiated with respect to vadose zone SM, S_w , to develop a general relationship for the safety factor's rate of change with respect to vadose zone SM. The differentiated equation is

$$\begin{aligned}
 \frac{dFS}{dS_w} = & - \frac{(C_s + C_r)(2 S_w E \gamma_w \sin \theta (E \gamma_w H - E \gamma_w h + \gamma_s H - \gamma_s h + \gamma_d H))}{[S_w^2 E \gamma_w \sin \theta (h - H) + S_w \sin \theta (E \gamma_w H - E \gamma_w h + \gamma_s H - \gamma_s h + \gamma_d H) + \sin \theta (q \cos \theta + \gamma_s h + \gamma_d H - \gamma_d h)]^2} \\
 & - \frac{D_2 \left[\gamma_w T \left(1 - \frac{h}{H}\right) - N \left[2 S_w E \gamma_w \left(\frac{h}{H} - 1\right) + (E \gamma_w - E \gamma_w) \frac{h}{H} + \gamma_s - \gamma_d \frac{h}{H} \right] \right]}{[S_w^2 E \gamma_w \left(\frac{h}{H} - 1\right) + S_w (E \gamma_w - E \gamma_w) \frac{h}{H} + \gamma_s - \gamma_d + \frac{h}{H} \frac{q \cos \theta}{H} + \gamma_s \frac{h}{H} + \gamma_d - \gamma_d \frac{h}{H}]^2}
 \end{aligned} \quad (3-6)$$

where $N = S_w \gamma_w T \left(1 - \frac{h}{H}\right) + \gamma_w T \frac{h}{H}$ and

$$D_2 = S_w^2 E \gamma_w \left(\frac{h}{H} - 1\right) + S_w \left(E \gamma_w - E \gamma_w \frac{h}{H} + \gamma_s - \frac{h}{H} \gamma_s + \gamma_d \frac{h}{H} - \gamma_d\right) + \frac{q \cos \theta}{H} + \gamma_s \frac{h}{H} + \gamma_d - \gamma_d \frac{h}{H}$$

The calculated FS values are used to categorize slopes into stability classes using Pack et al. (1998) and Acharya et al.'s (2006) stability classification system. The proposed four susceptibility classes are highly susceptible ($FS \leq 1$), moderately susceptible ($1 < FS < 1.25$), slightly susceptible ($1.25 < FS < 1.5$) and not susceptible ($FS \geq 1.5$).

Material and Methods

Study Area

The sensitivity of slope stability to soil moisture was considered using the physical characteristics at Cleveland Corral, CA. This landslide prone area is located on the slope of the Sierra Nevada Mountains along the Highway 50 corridor (Reid et al., 2003). Highway 50 is a major road located between Sacramento and South Lake Tahoe in California (Spittler and Wagner, 1998). Since 1996, slope movements and landslides occurred infrequently during the winter season with a catastrophic landslide in 1983. A mapped landslide at the most active landslide zone is shown in Figure 3-2.

The study domain is a 28 x 22 km area in El Dorado County, California, USA (Fig. 3-2). As derived from a 90 m Digital Elevation Model (DEM), elevations range from about 902 to 2,379 m and slopes range from 0 to 48°. This study region has considerable variability in soil texture ranging from clay loam to sandy loam. The majority of the observed soil is sandy loam (72%). On this rugged topography, conifers and wooded grassland are the dominant land covers: 80% and 14% of the study region, respectively. Some rock outcrops are also observed along the Highway 50 corridor.

Since 1997, the USGS has monitored this active landslide region using real time data acquisition systems that measure rainfall, pore water pressure, slope movements, ground vibrations and landslides (Reid et al., 2003). The daily groundwater measurements for water years 2004 to 2006 were obtained from the USGS (Mark Reid, USGS).

Piezometers were used to measure the hydraulic head at the active landslide grid. High groundwater tables were observed during the periods with slope movement and landslides in the winter (rainy) season (Reid et al., 2003).

Methods

To study the impact of vadose zone SM in slope instability, an active landslide pixel was selected from this study region. The Eq. 3-6 was used to estimate the rate of change of the safety factors for a time series of groundwater (GW) levels and total soil depth with varying vadose zone SM. To obtain spatial distributions of susceptibility, the model was also applied to the entire study region with modeled vadose zone SM and in-situ GW measurements.

The Three-Layer Variable Infiltration Capacity (VIC-3L) model (Liang et al., 1994) was used to estimate soil moisture in the unsaturated zone. VIC-3L is a macroscale land surface model that simulates water and energy budgets and includes spatial variations of soil properties, soil topography, precipitation, and vegetation (Maurer et al., 2002; Huang and Liang, 2006). The model's soil column has three layers (Parada and Liang, 2004). The top, thin soil layer and the middle soil layer characterize the dynamic response of the soil to weather and rainfall events. The lowest layer captures the seasonal soil moisture behavior (Liang et al., 1996; Huang and Liang, 2006). Based on the climatic parameter and soil and vegetation characteristics, this model can estimate soil moisture storage, evapotranspiration, runoff and snow water equivalent at hourly to daily time-steps.

For this study region, the VIC-3L model was run using a daily time-step from 2004 to 2006 with layers of 0.05, 0.35, 0.4 to 1.0 m thickness at a 0.0083° (approximately 1 km) resolution. This study region has a total of 900, 0.7 km² pixels.

Model Data

The data required for the VIC-3L hydrologic model and the slope stability model are summarized in Table 3-1. Rainfall, temperature and wind speed measurements were obtained from the National Climatic Data Center (NCDC) from 2000 to 2006. Soil layers, soil thickness and soil texture information were obtained from the States Soil Geographic (STATSGO) soil database (NRCS, USDA). There are a total of eleven soil layers in STATSGO. However, many layers have similar soil texture classes. To coincide with the VIC-3L model, the eleven soil layers were regrouped into three soil layers by merging similar soil textures from many layers to one layer. The first, second to fifth and sixth to eleventh soil layers of the STATSGO soil database were regrouped into three soil layers; respectively, first, second and third soil layers for the VIC-3L model. Consequently, the first and second layers have similar soil textures. About 72 and 28% of study area is covered with sandy loam and loam, respectively in both layers. The third (lower) layer consists of four soil types, loam, sandy loam, clay loam and sandy clay, and covers, respectively, 72, 16, 3 and 9%, of the study area. Soil types were identified from the STATSGO soil database. Each pixel was assigned a soil texture for each of the three soil layers based on majority type. For verification purposes, four soil samples were collected from the active landslide grid and tested in a laboratory using sieve analysis and

Atterberg Limits tests. The tests showed similar soil texture to the STATSGO soil database classification. The total soil depth ranged from 0.6 m to 1.4 m. The assumed potential failure plane underneath the soil layer is bedrock. The unit soil weight (saturated and moist) was calculated based on the soil moisture, soil porosity, and specific gravity of the soil samples using Eq. 3-3. Each soil type was assigned soil cohesion and friction angle values that were adapted from Deoja et al. (1991)

Advanced Very High Resolution Radiometer (AVHRR) land cover data (1 km spatial resolution) were obtained from University of Maryland (UMD) (Hansen et al., 2000). There are four land cover classes (types) in this study region. Each land cover class was assigned a root cohesion values that was adapted from Sidle and Ochiai (2006). The Land Data Assimilation System (LDAS) project has produced a gridded vegetation database for the USA. Root fraction, root depth, vegetation roughness, and vegetation height required for the VIC-3L model parameterization were obtained from the LDAS (Mitchell et al., 2004). The Shuttle Radar Topography Mission (SRTM) DEM (90 m spatial resolution) was used to derive slope angle in this study.

Model Results

Soil Moisture and Groundwater Impact Analysis

Theoretical safety factors and susceptible areas were calculated with Eqs. 3-5 and 3-6. First, a safety factor sensitivity analysis was conducted at an active landslide location in the study area. Then, the impact of vadose zone SM and GW was considered with respect to susceptible areas in the study region.

Figures 3-3a, b, c and d show the rate of change in safety factors with varying vadose zone SM for a series of GW table positions, respectively for varying soil thicknesses. This analysis used characteristics obtained for the most active landslide grid in the California study region. The selected active landslide grid has a 1.4 m soil depth with sandy loam soil and wooded grassland land cover. This grid has a 32.5° slope.

Using Eq. 3-6, the rates of change in safety factors were calculated with varying vadose zone SM (0-100%, using 5% increments). This analysis was repeated for a series of GW table positions (depth to groundwater) from 0.1 to 1 m below the surface (0.1 m increment). The 0.1 m GW table is the wettest scenario. The 1 m GW table is the driest scenario. The maximum saturation scenario was limited to 0.1 m depth to GW table because there is no impact of vadose zone SM under full saturation.

Figure 3-3 shows a significant impact of vadose zone SM when the depth to GW is deep. For a thick soil layer (soil thickness ≥ 2 m), the FS sensitivity is constant for all GW table positions. A constant FS sensitivity is also observed for a thin soil layer (soil thickness < 2 m) when the GW table is shallow (depth to GW table ≤ 0.5 m).

The observed FS is less sensitive with increasing vadose zone SM (true until 70% SM) for a thin soil layer with a deeper GW table. When the vadose zone SM is greater than 70%, the FS values are equally sensitive to increases SM even with deep GW table.

For all of the soil thicknesses (1 to 3 m in this analysis), the FS sensitivity decreases when the GW approaches the surface. The decrease has a nearly constant rate near the surface. For example, when the depth to GW is 0.5 m, the observed rates of changes for safety factors are 27, 15, 10 and 6% for soil thicknesses of 1, 1.4, 2 and 3 m, respectively. When the GW table is shallow, 0.1 m (0.4 m change), the safety factors' sensitivity declines to 4, 2, 2 and 1% for the 1, 1.4, 2 and 3 m thicknesses, respectively. Thus, a 0.4 m GW table rise significantly changes the FS sensitivity; by 20, 13, 8 and 5%. When the same 0.4 m GW table change occurs for deeper GW positions, 1 m rising to 0.6 m, an even larger change in the FS occurs with differences of 29, 17, 9 and 6% for the 1, 1.4, 2 and 3 m, soil thicknesses, respectively.

Figure 3-4 shows the safety factors' sensitivity to soil depth with a controlled GW positions and varying vadose zone SM. These results show small rates of safety factor change (less than 15%) when the total soil depth is greater than 2 m. These changes increase nonlinearly with decreasing soil thickness. For example, when the soil thickness changes from 1 to 1.5 m, the difference in the rate of change in safety factor was 18%, but it was only 7% when the soil thickness was changed from 1.5 to 2 m.

At a regional scale, variations in SM and GW differentially effect individual locations. Figure 3-5 shows how the vadose zone SM and the GW table jointly influence regional susceptibility. Using Eq. 3-5, safety factors (FS) were calculated for a series of GW depths below the surface (0 to 1 m, 0.1 m increment) with varying vadose zone SM

(0-100%) for the entire Cleveland Corral study region. This study uses the 90 m spatial resolution for a total of 75988 grid cells.

The results show that 0.58% of the study region is highly susceptible under the completely saturated scenario (lower right). No area is highly susceptible under the dry scenario (upper left). The contour lines of equal % susceptible area, 0.01% interval, become closer as the GW table approaches the ground surface and the vadose zone SM approaches the saturation level. Figure 3-5 shows that wetter unsaturated soils can be more vulnerable to landslides than the less wet unsaturated layer, even if the GW table is deeper for the former.

Not surprisingly, as the GW thickness increases, the highly susceptible area increases. However, Figure 3-5 shows that regardless of soil saturation, the marginal increase in susceptible area increases as the GW table nears the surface. A 10% increase in soil saturation will cause more of the region to become unstable if the hillside is already wet than if the slopes were initially dry. It should also be noted that the marginal increases decrease somewhat for very wet slopes, 80 to 100% saturation, as compared to more moderately wet slopes, 30 to 80%. Overall this analysis shows that the vadose zone SM can have a significant role in slope instability.

Application

VIC-3L Model Results

The VIC-3L model was run at a 0.0083° (approximately 1 km) spatial resolution from 2004 to 2006 to obtain vadose zone soil moisture at Cleveland Corral. Figure 3-6 shows the daily average modeled vadose zone soil moisture, rainfall and in-situ GW measurements at one active landslide grid (1 x 1 km) in this study region. Average daily soil moisture was calculated by weighted average of daily soil moisture obtained from the VIC-3L model in the top two layers. The GW measurements from the USGS station were used to validate the VIC-3L model results. Since no in-situ soil moisture measurements were available, soil wetness variations captured by the VIC-3L model were compared with GW fluctuations during the wet season. During the wet season, the GW was very close to the surface in this region. The near surface GW fluctuations are strongly indicative of the soil moisture storage in the unsaturated zone above the saturated zone. VIC-3L vadose zone SM values and the in-situ GW measurements show similar daily and seasonal variations throughout the year.

Spring is the wettest season because relatively high amounts of rainfall (Fig. 3-6) and snow melt occur during this period. This period has the highest vadose zone SM and also has a GW level that is very close to the surface. During the 2005 wet season, January to May, the highest and the lowest vadose zone SM values estimated by the model were 82 and 49%, respectively, when the shallowest and the deepest GW positions were 28 and 137 cm below the surface, respectively. During the 2006 wet season, January-April,

the model predicted 83 and 52% vadose zone SM when the GW table was 35 and 75 cm below the ground surface, respectively. The highest vadose zone SM predicted by the model in 2004, 2005 and 2006 were 84, 84.5 and 82.9%, respectively, when the groundwater levels were 38.5, 40.3 and 45.7 cm below the ground surface.

The dry summer periods have the lowest vadose zone SM and very deep GW levels. There is a good agreement between the dry period predicted by the model and the groundwater measurements from July to November in 2005 and from June to September in 2006. In 2005, vadose zone SM ranged 20 to 27% when the groundwater levels were 181 to 186 cm below the surface. Similarly, in 2006, vadose zone SM was 21% when the groundwater depth was 182 cm below the ground surface.

Overall, the simple linear regression analysis for depth to GW and average vadose zone SM provided a good fit with a R^2 of 0.63 and p-values less than 0.0001. Thus, results show that the vadose zone SM values predicted by the VIC-3L reasonably capture the wetting and drying of the vadose zone. In addition, it is clear that the GW and the SM values are strongly related. The predicted vadose zone SM values in combination with GW levels can be used in the slope stability model to calculate the safety factors.

Regional Slope Stability Analysis

The slope stability model described earlier was used at the Cleveland Corral to determine safety factors. This study used a 90 m spatial resolution to calculate wetness index, moist unit soil weight, effective unit soil weight and FS. Modeled moisture values with a 1 km spatial resolution were reclassified into 90 m spatial resolution using the

nearest-neighbor re-sampling technique. Wetness indices were calculated by using measured depth to GW, total soil thickness and average vadose zone SM values obtained from the VIC-3L model (Eq. 3-4). The vadose zone SM, obtained from the VIC-3L model, was also used to estimate moist unit soil weight in the unsaturated soil layer (above the saturated soil layer) (Eq. 3-3). The effective unit soil weight was calculated using moist unit soil weight, wetness index, total depth of soil, surcharge and slope angle (Eq. 3-2). Finally, Eq. 3-1 was used to calculate safety factors continuously for the region and a range of results are presented to demonstrate varying conditions.

Three typical wet scenarios were identified based on the soil saturation wetness. A very wet scenario, on May 8, 2005, the GW position was 0.28 m below the surface. A wet scenario, on May 23, 2005, the GW position was 0.65 m below the surface, that is, between the failure plane and the ground surface. A slightly wet scenario, on 4th May, 2005, the GW position was 1.12 m below the surface, that is, near to the bottom of the failure plane. These three wetness scenarios were used to estimate the range of safety factors (Table 3-2). A higher vadose zone SM was predicted for a shallow depth to GW as compared to a deeper depth to GW. Table 3-2 shows the proportion of the study area by susceptibility class for the three GW positions. Results show more susceptible area when the GW table is near the surface and has a high vadose zone SM. Interestingly, the susceptible area decreases include both a GW that is farther from the surface as well as a lower vadose zone SM.

Slope stability variations were compared to slope movements and landslide events. All of the slope movements and landslides coincided with periods of enhanced surface soil moisture and high groundwater position in this region (Fig. 3-6). In the Cleveland

Corral region, 2 to 3 cm per day slope movements were frequently observed during the winter of 2005 (<http://landslides.usgs.gov/monitoring/hwy50>). Reported slope movements began in early April, 2005 when the GW table was near the surface and it continued until end of the May.

Safety Factors as a Function of Vadose Zone SM and GW

To understand the relationship among vadose zone SM, GW table depth and soil thickness, safety factors were calculated using Eq. 3-1 for three scenarios at the Cleveland Corral, California study region. First, actual groundwater measurements were used with a varying vadose zone SM (0-100%, 10% increment). In this scenario, the typical wet season GW positions described earlier, 0.28, 0.65 and 1.12 m, were used to estimate the range of safety factors. Second, vadose zone SM and GW position were held constant while the total soil thickness varied. In this scenario, the total soil thickness increased from 1 to 3 m in 0.5 m increments with a constant 0.75 m groundwater saturated thickness and a 50% vadose zone SM. Finally, GW position was held constant while the vadose zone SM and the total soil thickness were varied. In this scenario, GW position was fixed at a 0.75 m saturated thickness and the vadose zone SM and the total soil thickness, respectively changed from 90% and 1 m to 50% and 3 m with 0.5 m increases in soil thickness and 10% decreases in soil moisture. These values reflect the modeled observations of the highest vadose zone SM for the shallowest GW table and lowest vadose zone SM for the deepest GW table.

Influence of Vadose Zone SM in Instability

Figure 3-7 shows plots of percentage susceptible area by susceptibility class for completely dry to saturated vadose zone SM with the observed wet season GW tables. Under completely saturated conditions, 0.58% of the area was highly susceptible to failure. For a completely dry soil, the 0.84 m range in the wet season GW table has a highly susceptible area which ranges from 0.006 to 0.27% of the study area. The same GW table range results in nearly a 1% increase in the moderately susceptible areas. The combined increase in all susceptibility classes is equivalent to the reduction in stable area. For the 1.12 m GW table when vadose zone SM transitions from completely dry to saturation, the stable area was reduced by 5.2%, and the slightly susceptible, moderately susceptible and highly susceptible areas were increased by 2.85, 1.78, and 0.58%, respectively.

The transition from dry to wet depends on the susceptibility class and the GW table. Safety factors for the highly and the moderately susceptible classes have a similar dependence on GW table and SM. In the dry conditions, when the GW table was deep, there is a pronouncedly non-linear increase in instability with increasing vadose zone SM. As the GW table approaches the ground surface, there is a more linear increase in instability with increasing vadose zone SM. On the other hand, the slightly susceptible and the stable classes have fairly constant rates of change in area under all SM conditions. The rate of change in the highly susceptible area is lower than the slightly susceptible area for similar saturation levels. Similarly, the rate of change in the highly susceptible area is lower for the shallowest GW table than for the deepest GW table. This shows that the vadose zone soil moisture has less of an impact on instability when the GW table is

very close to the ground surface. For example, the total highly susceptible area increased by 0.32% for the shallowest GW table and by 0.58% for the deepest GW table when the region went from a completely dry vadose zone to a completely saturated vadose zone.

Influence of the Soil Thickness in Instability at Constant GW Thickness and Vadose Zone SM

The impact of a thick unsaturated soil layer as compared to a thin unsaturated soil layer on stability was assessed by determining the susceptible area with a varying soil thickness for a constant saturated thickness or GW table thickness (0.75 m) and the vadose zone SM (50%). For example, a 1 m thick soil has a GW table 0.25 m below the ground surface where as 3 m thick soil has a GW table that is 2.25 m below the surface.

Figure 3-8 shows that a thick unsaturated soil layer produces more unstable area than a thin unsaturated soil layer for the same GW table thickness. The rate at which the highly susceptible area increases is lower than that for the slightly susceptible area. The estimated highly, moderately, and slightly susceptible area increases from 0.14, 0.54 and 1.57% to 0.82, 2.44 and 4.12%, respectively, as the soil thickness increases from 1 to 3 m. The changes, 0.67, 1.9 and 2.54%, respectively, in highly, moderately, and slightly susceptible areas are quite different with the highly susceptible class's rate of change is fairly constant in comparison to the moderately and slightly susceptible classes. Notably, there is more than a 500% increase in the highly susceptible area.

These results show that accurate knowledge of depth to a potential failure plane, in addition to GW table, is necessary when accounting for a dynamic vadose zone SM. A

thick unsaturated soil layer is more vulnerable to instability than a thin unsaturated soil layer for shallow soil mantles.

Influence of the Soil Thickness and Vadose Zone SM in Instability at Constant GW Thickness

While the previous section maintained a constant vadose zone SM, the observed vadose zone SM varied as a function of the GW position. In this section, the joint relationship between a varying vadose zone SM (90 to 50%, 10% decrease) and soil thickness (1 to 3 m, 0.5 m increase) was examined for a fixed GW table thickness. Wetter and drier conditions were assigned, respectively, for the shallowest and the deepest GW tables.

Figure 3-9 shows the greatest sensitivity for shallow soil layers and less for the thicker, drier unsaturated soil layer. When the total soil thickness above the potential failure plane increased from 2 to 3 m, the estimated change in highly, moderately and slightly susceptible areas were 0.1, 0.16 and 0.35%, respectively. In contrast, when the soil thickness increased from 1 to 2 m, the estimated change was dramatically larger for highly, moderately and slightly susceptible areas, respectively, 0.51, 1.52 and 1.87%.

These results show that including vadose zone SM in an infinite slope stability model is best suited for shallow slope stability analysis. When soil mantles are deep, slope stability is less sensitive to anticipated vadose zone SM variations. These observations clearly support Sidle and Ochiai's (2006) finding that for shallow soils, effects of pore water pressure are large and for deep soil mantles, effects of pore water pressure are small.

Conclusion

The vadose zone soil moisture and pore water pressure are important parameters for slope stability analysis because landslides are not triggered only due to surface layer saturation; rather, it is the combined effect of surface and subsurface saturation that is critical. This study developed methods to estimate wetness indices based on vadose zone soil moisture and saturated soil thickness as well as to calculate dynamic moist unit weight using vadose zone soil moisture. This relationship was used to characterize the sensitivity of safety factors to vadose zone SM for a series of groundwater positions and soil depths. The same infinite slope stability model was applied to the Cleveland Corral region, California in order to examine the sensitivity results within an applied context.

Results show significant impacts of vadose zone soil moisture on slope instability. The susceptibility to slope failure increases with an increase of vadose zone soil moisture as well as groundwater position. For shallow slope soil mantles, a thicker unsaturated soil thickness is more vulnerable to landslides in comparison to a thinner unsaturated soil thickness for the same position of the groundwater level above the potential failure plane. However, when soil mantles are deep, slope stability is less sensitive to anticipated vadose zone SM variations.

Table 3-1: List of model parameters and sources

Parameters	Sources	Model
Soil cohesion	Deoja et al. (1991)	Slope stability
Soil porosity	Dingman (2002)	Slope stability and VIC-3L
Soil texture	STATSGO	Slope stability and VIC-3L
Soil depth	STATSGO	Slope stability and VIC-3L
Hydraulic conductivity	STATSGO	VIC-3L
Soil bulk density	Dingman (2002)	Slope stability and VIC-3L
Angle of internal friction	Deoja et al. (1991)	Slope stability
Additional load (surcharge)	Ray (2004)	Slope stability
Land cover	University of Maryland	Slope stability and VIC-3L
Root cohesion	Sidle and Ochiai (2006)	Slope stability
Root depth	LDAS	VIC-3L
Root fraction	LDAS	VIC-3L
Vegetation roughness	LDAS	VIC-3L
Vegetation height	LDAS	VIC-3L
Leaf Area Index (LAI)	LDAS	VIC-3L
Rainfall	NCDC	VIC-3L
Groundwater	USGS (Mark Ried)	Slope stability
Temperature	NCDC	VIC-3L
Wind speed	NCDC	VIC-3L

Table 3-2: Predicted susceptible area (%) for the Cleveland Corral region during the wet season

Depth to GW (m)	Avg. Vadose Zone SM (%)	Highly Susceptible	Moderately Susceptible	Slightly Susceptible	Not Susceptible
0.28	72	0.49	1.67	2.87	94.96
0.65	60	0.30	1.15	2.44	96.11
1.12	52	0.11	0.55	1.61	97.73

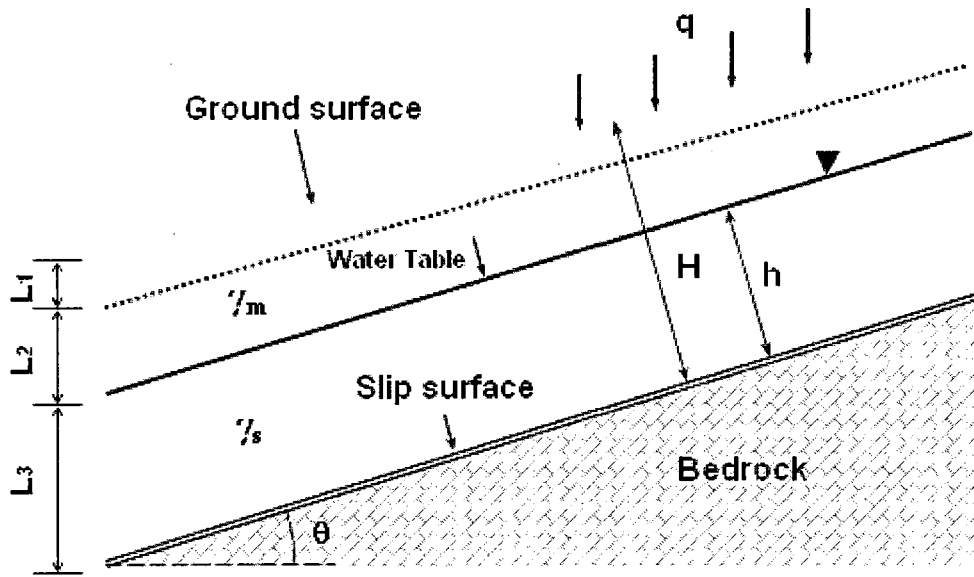


Figure 3-1: Schematic diagram for the slope angle, saturated and total soil thickness, surcharge, saturated and moist unit soil weights (Adapted and modified from Skempton and Delory, 1957)

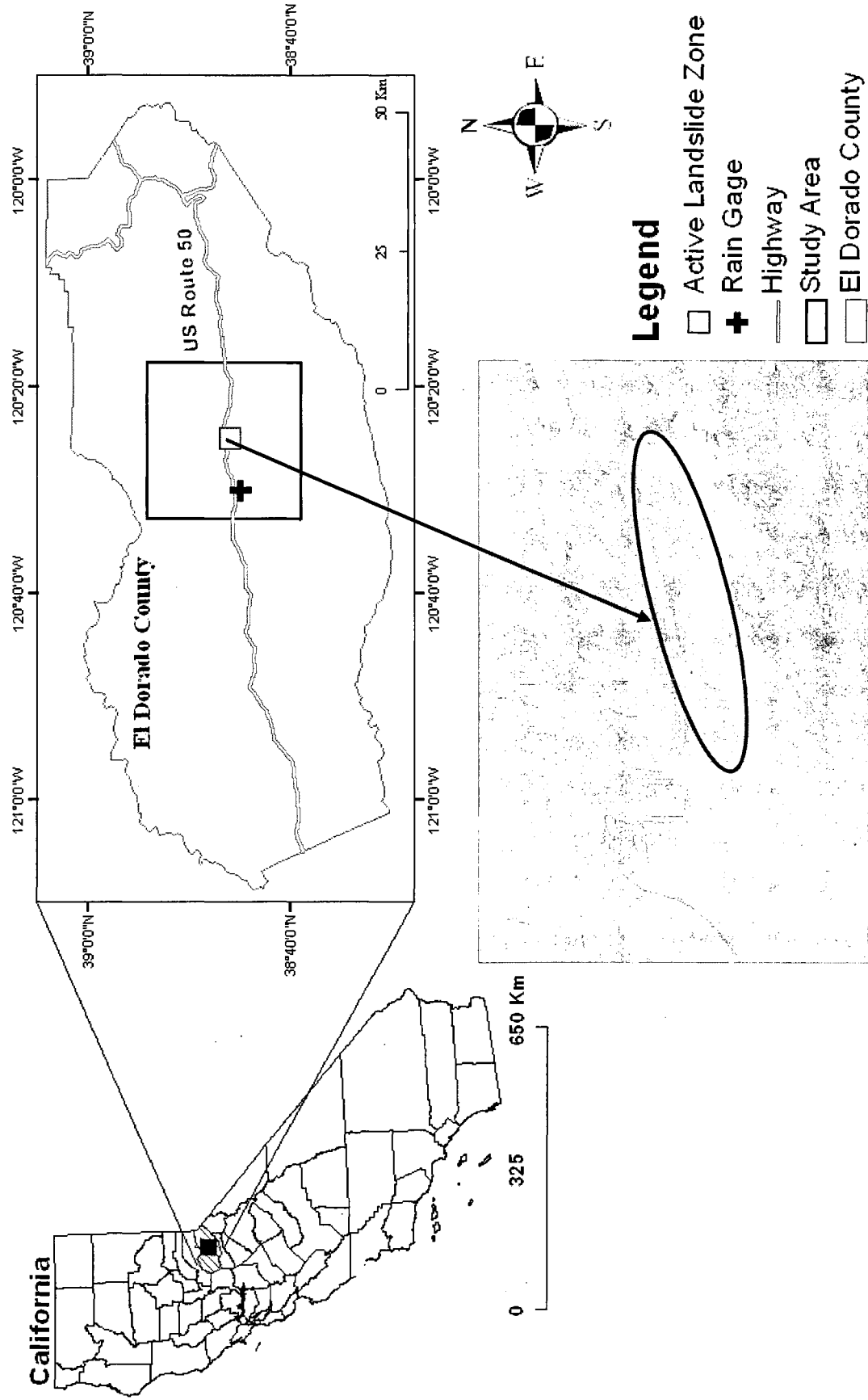
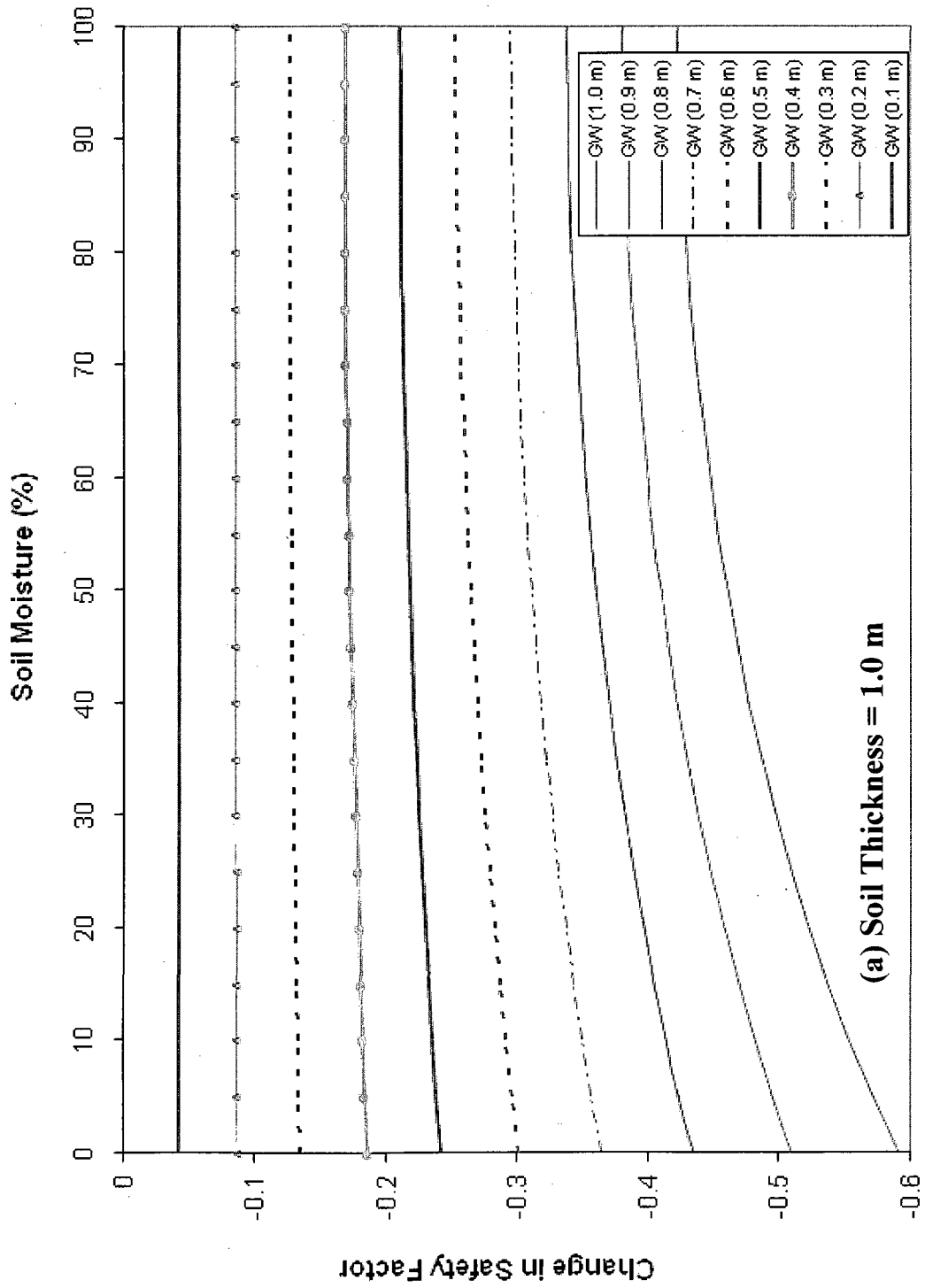
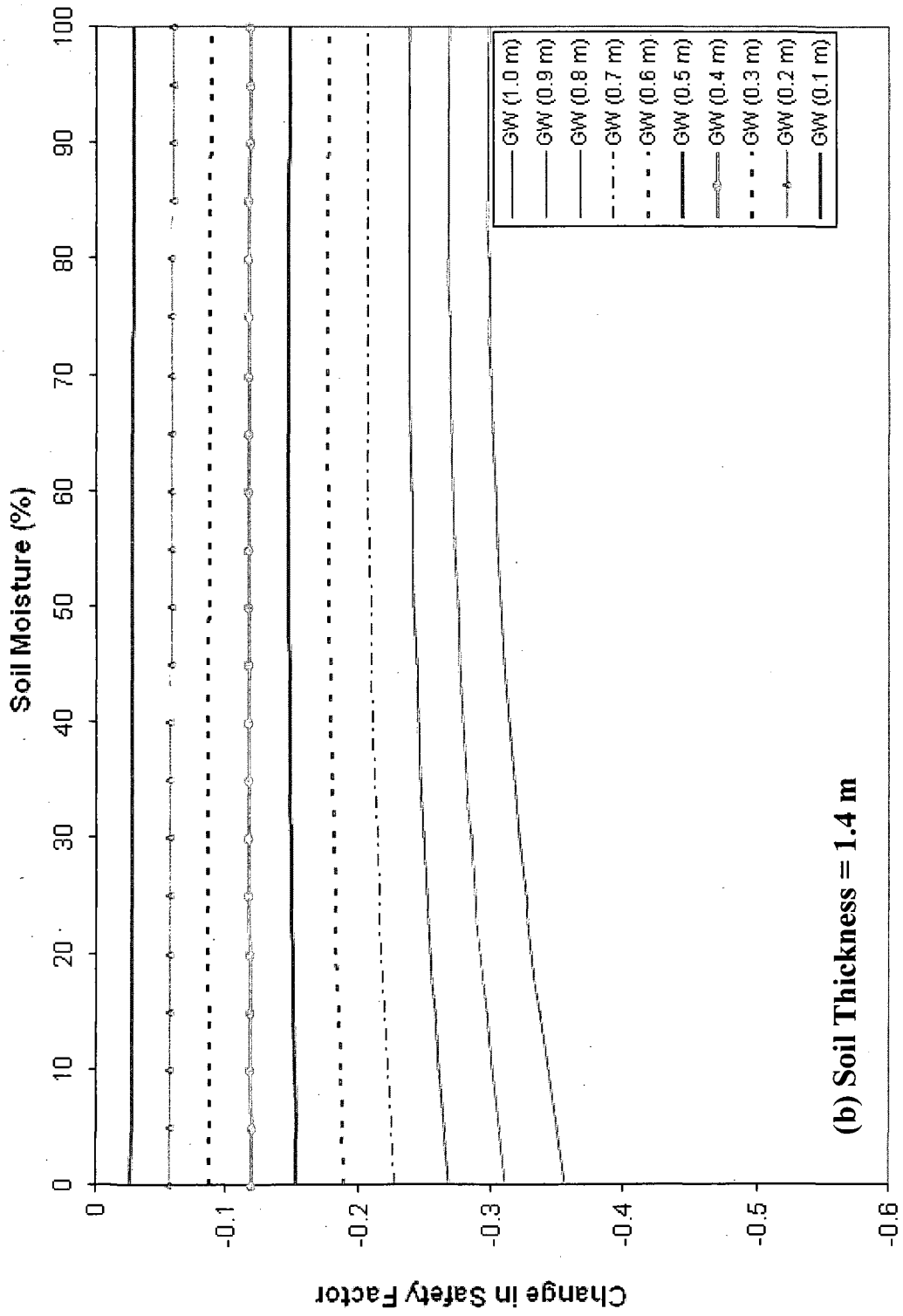
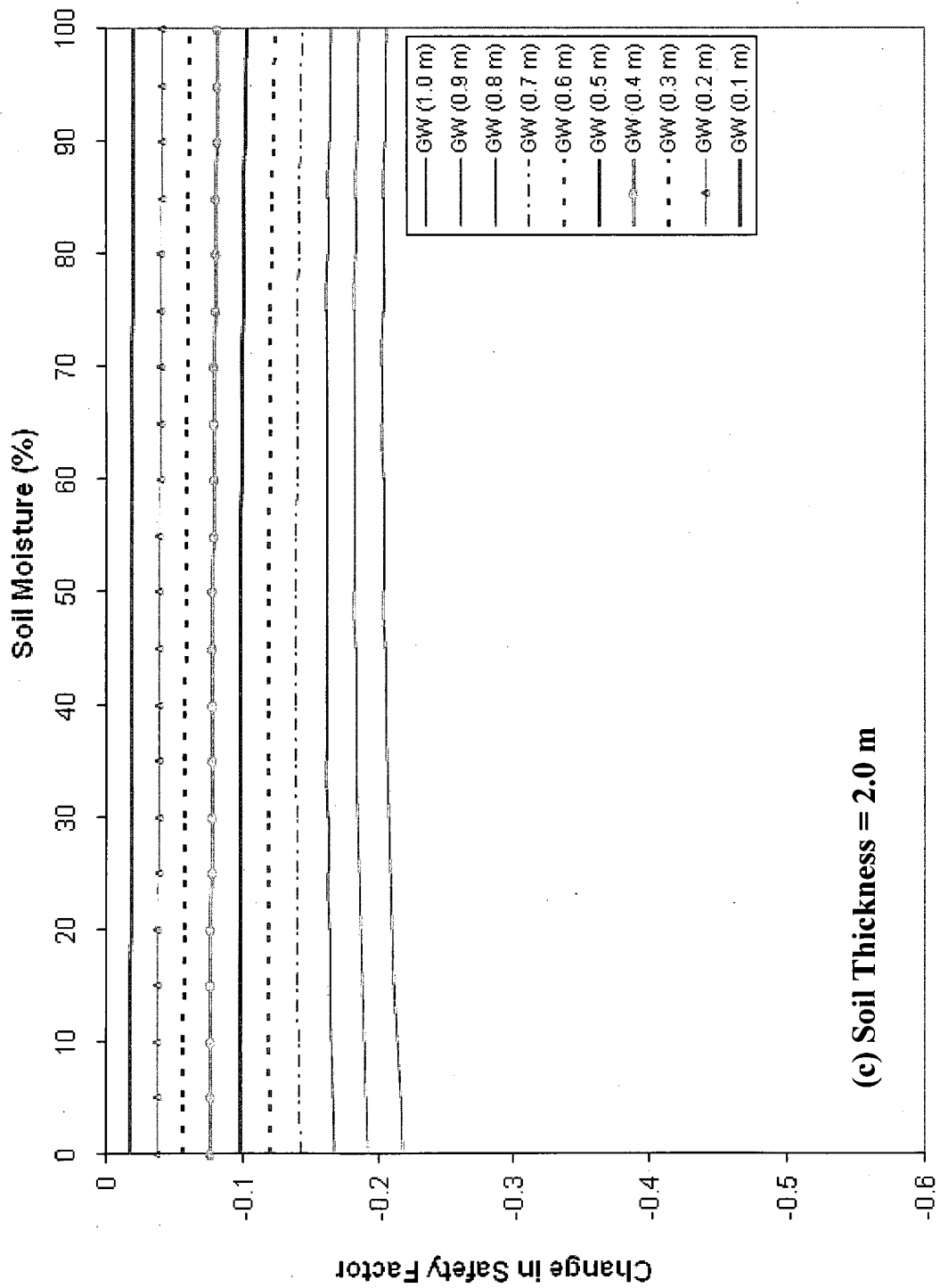


Figure 3-2: Location of the study region in El Dorado County, California





(b) Soil Thickness = 1.4 m



(c) Soil Thickness = 2.0 m

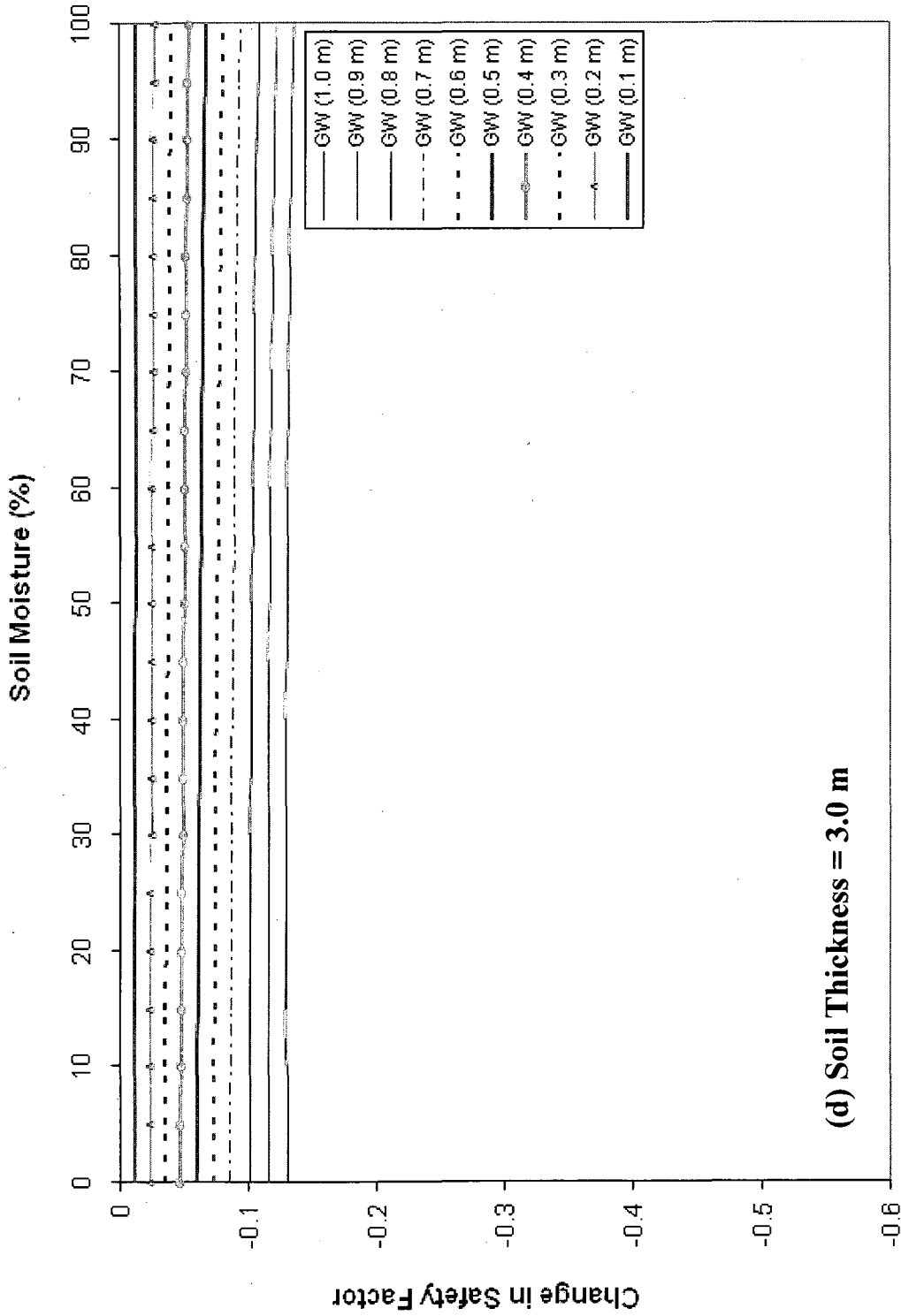


Figure 3-3: Rates of change in the safety factor with varying vadose zone soil moisture values and depth to groundwater for total soil depths of (a) 1 m (b) 1.4 m (c) 2 m and (d) 3.0 m. Site characteristics are sandy loam, wooded grassland and 32.5° slope

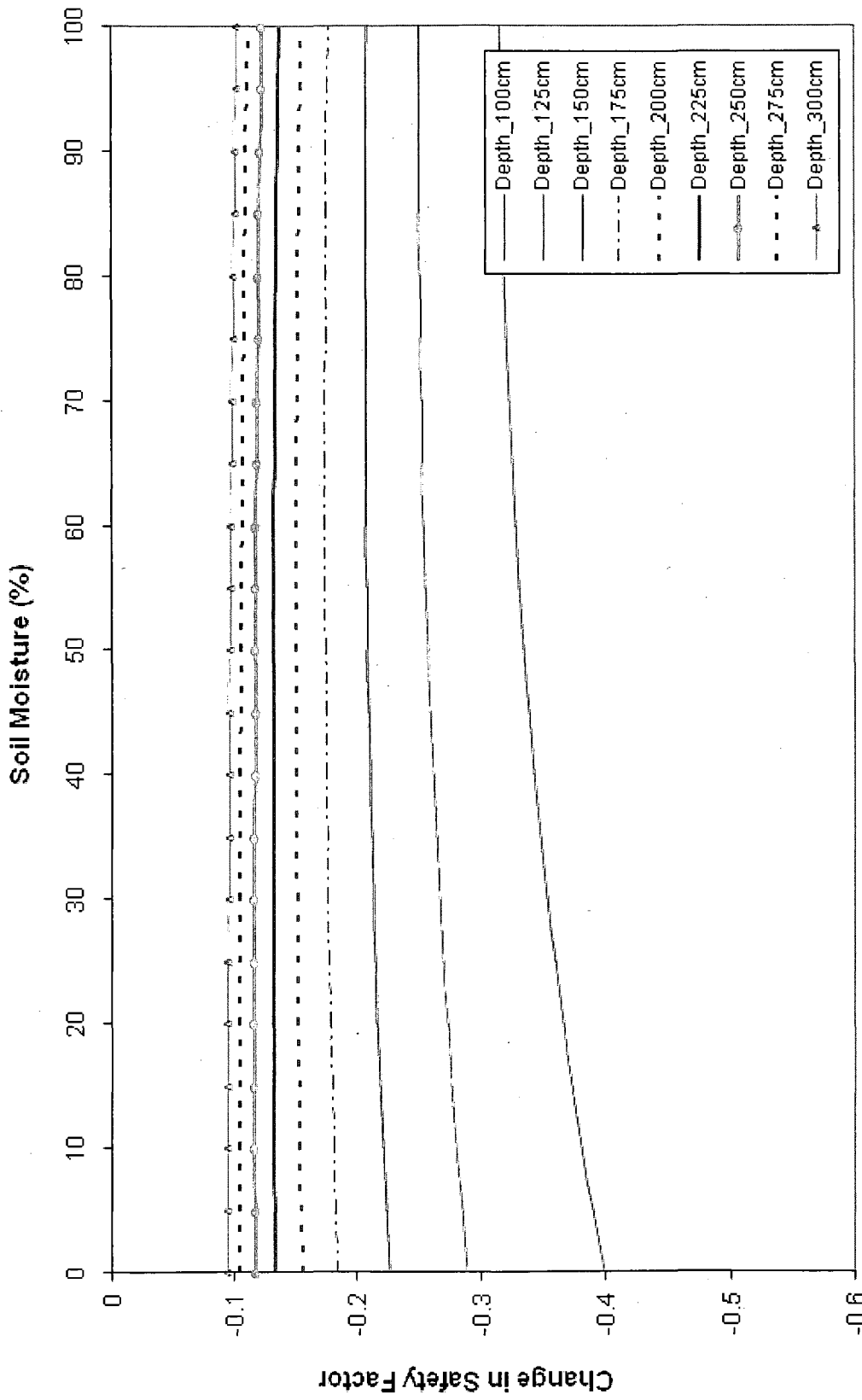


Figure 3-4: Safety factor change with varying vadose zone soil moisture value (0-100%) and a fixed depth to groundwater (0.75 m) for a range of total soil depths from 1 to 3 m

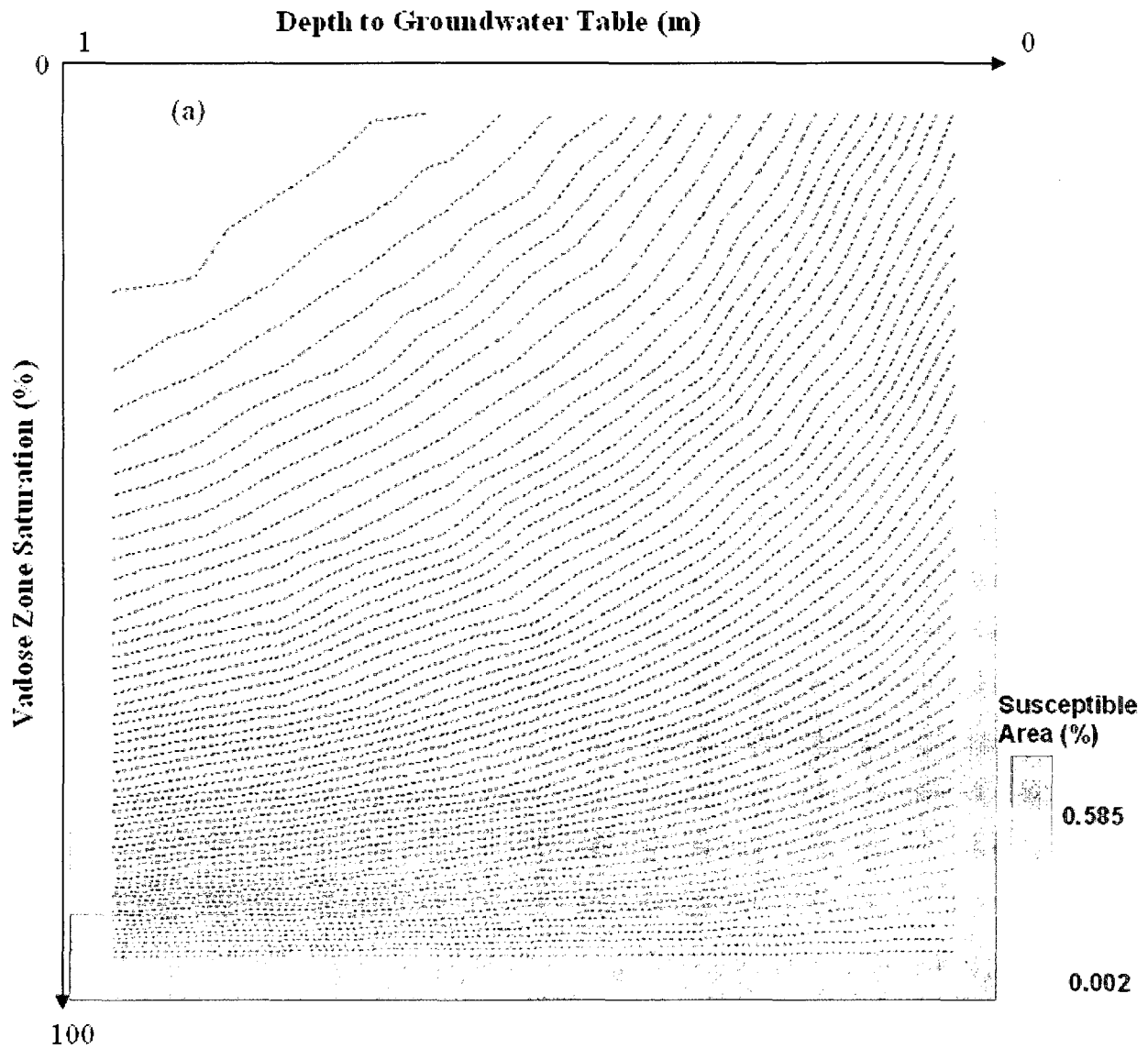


Figure 3-5: Highly susceptible area % as a function of GW and soil saturation (Dark: greater highly susceptible area, white: less highly susceptible area). Depth to GW table (1 m @ 10% decrease up to 0 m or surface) and eleven soil saturations (0% @ 10% increments up to 100%) were used to calculate FS. The contour lines show equal percentage of highly susceptible area with 0.01% intervals.

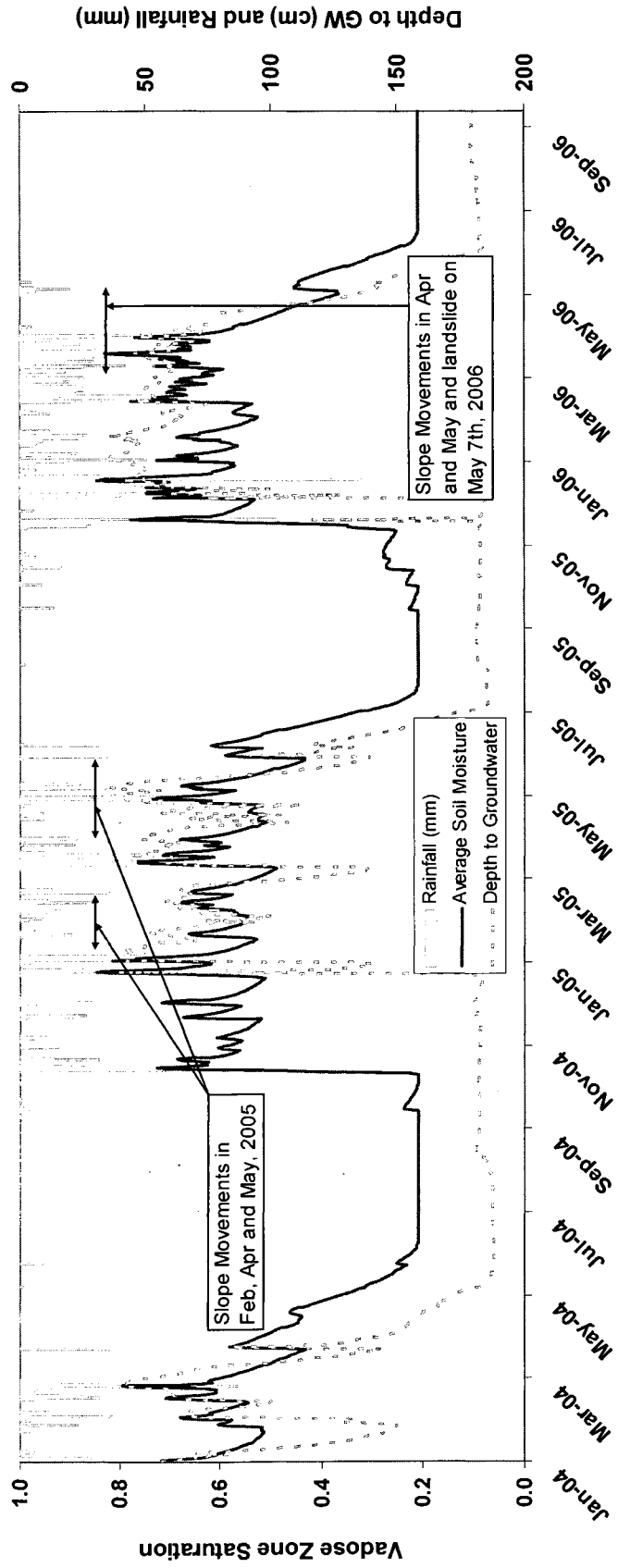
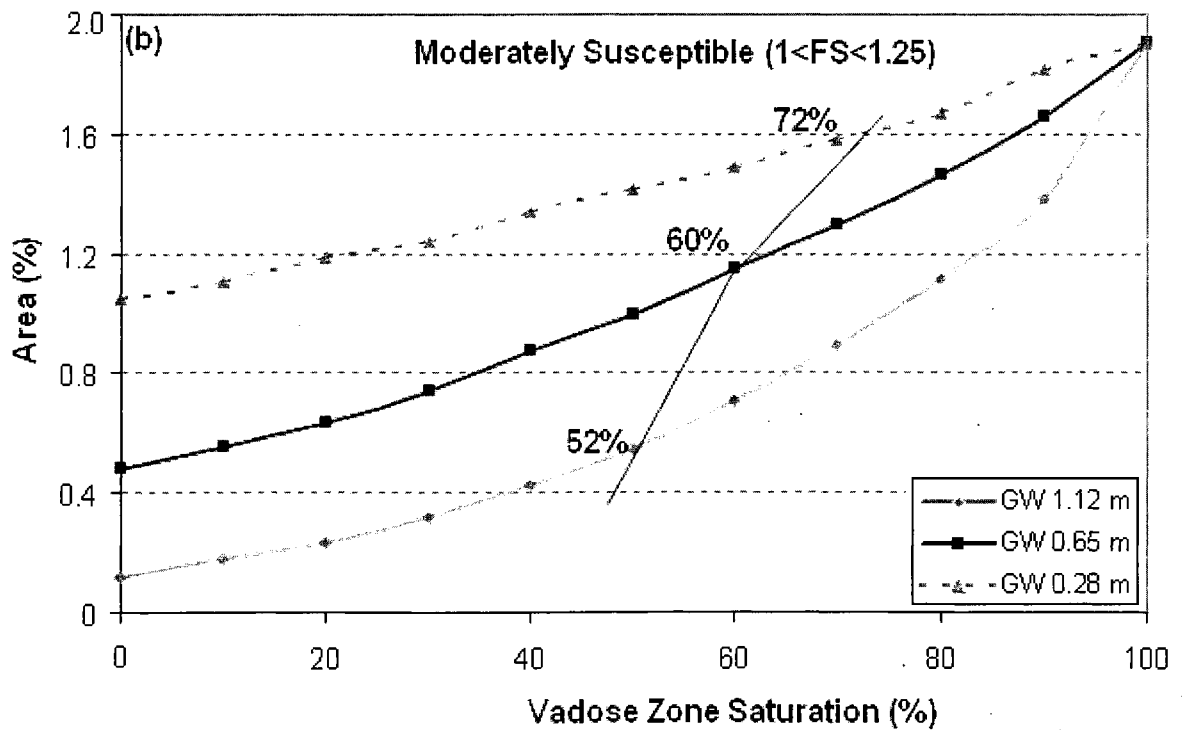
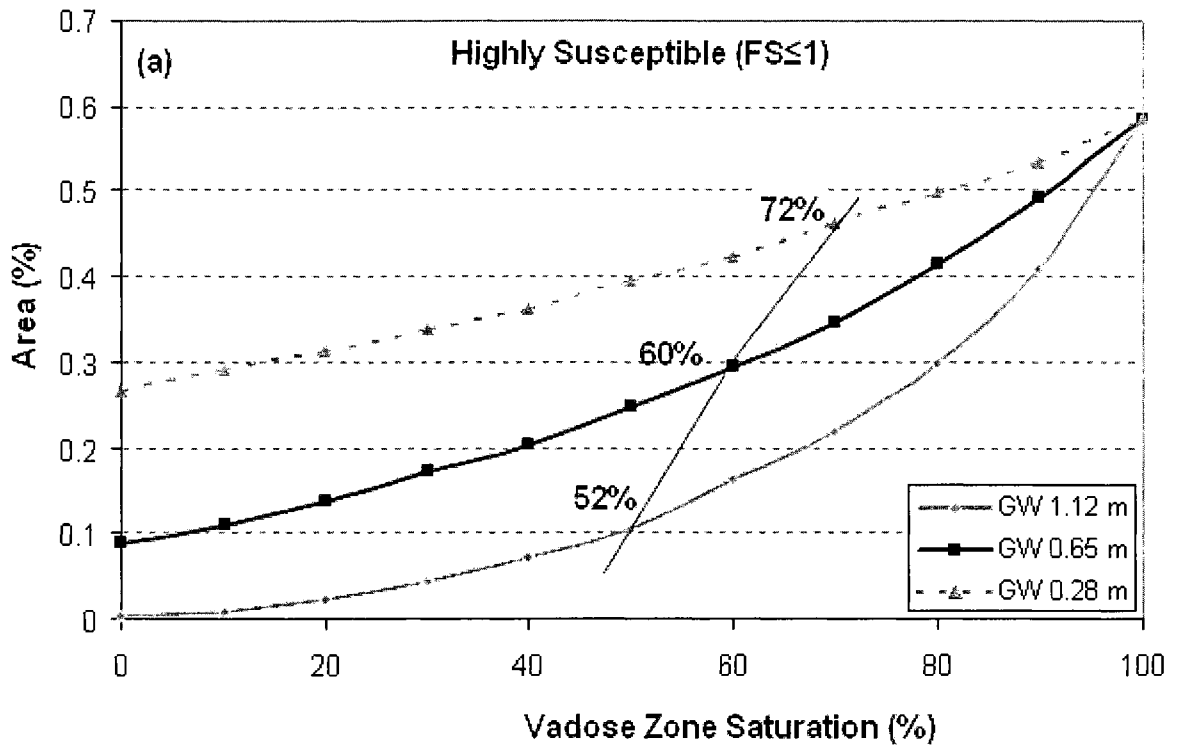


Figure 3-6: The depth to GW, VIC-3L model average (layers 1 and 2) vadose zone SM and rainfall at Cleveland Corral region, California from January, 2004 to September 2006. $R^2 = 0.63$ and $p\text{-value} < 0.0001$



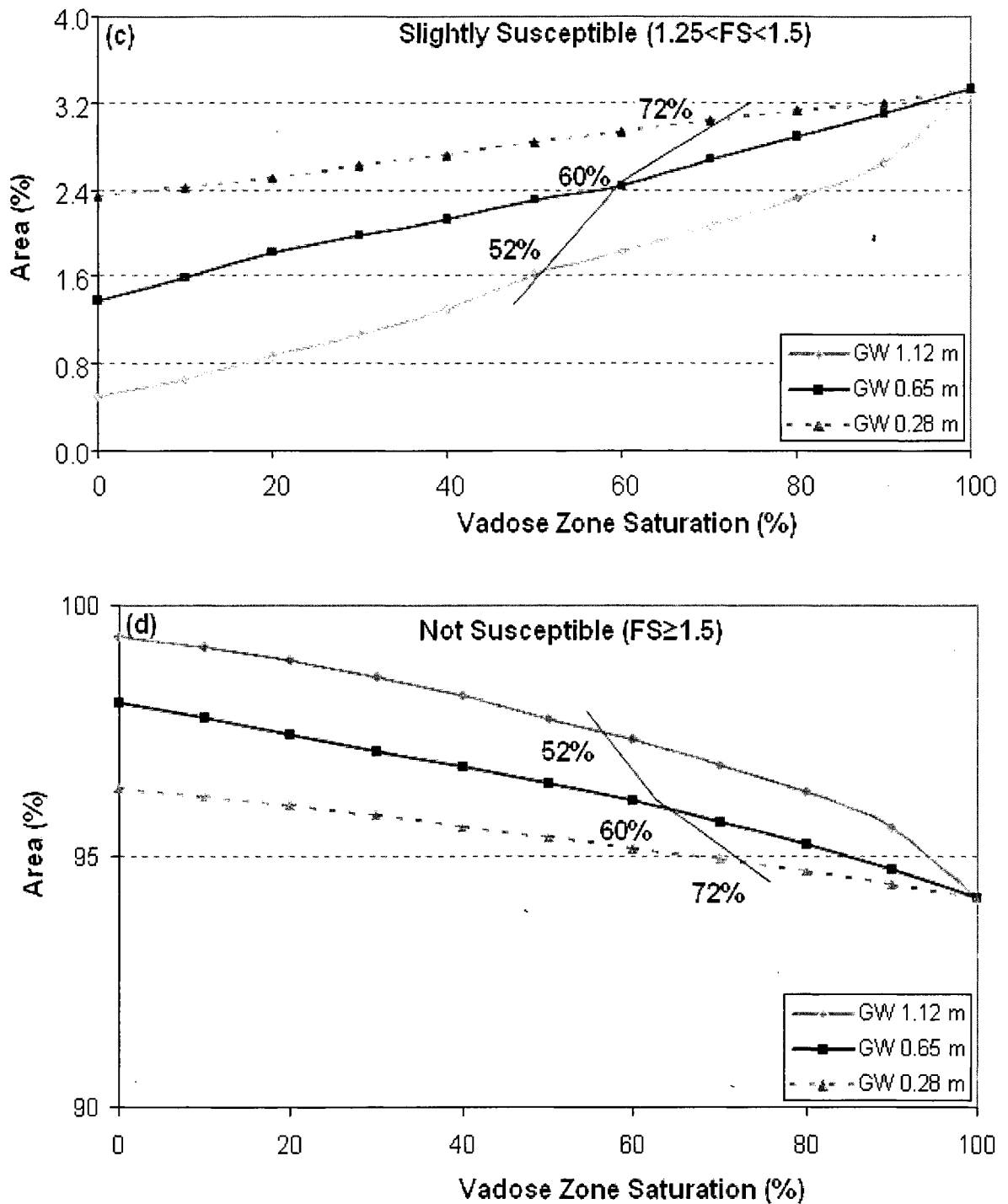


Figure 3-7: Four susceptibility classes with varying SM (0 to 100%), three GW positions measured from the surface and observed SM at Cleveland Corral region, California in 2005. A solid line that intersects susceptible classes' line represents observed vadose zone SM and GW tables

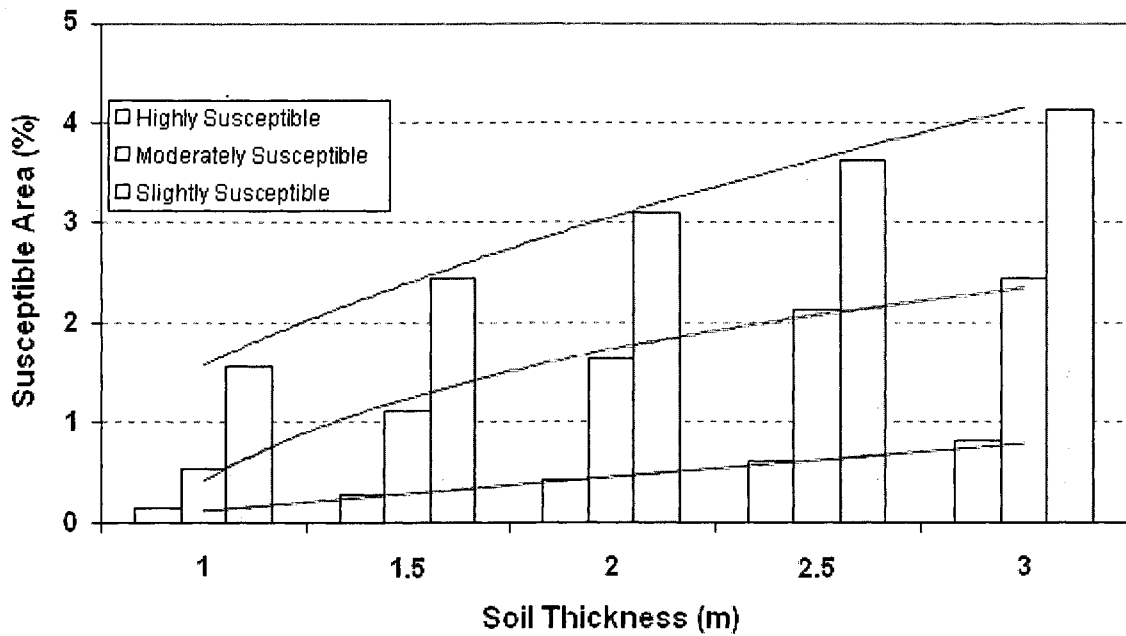


Figure 3-8: Variation of susceptibility area with increase of soil thickness with equal increase in depth to GW table (0.25 m for 1 m thick soil with 0.5 m increment to 2.25 m for 3 m thick soil or constant GW table thickness from the failure plane) and constant vadose zone SM (50%) at Cleveland Corral region, California in 2005

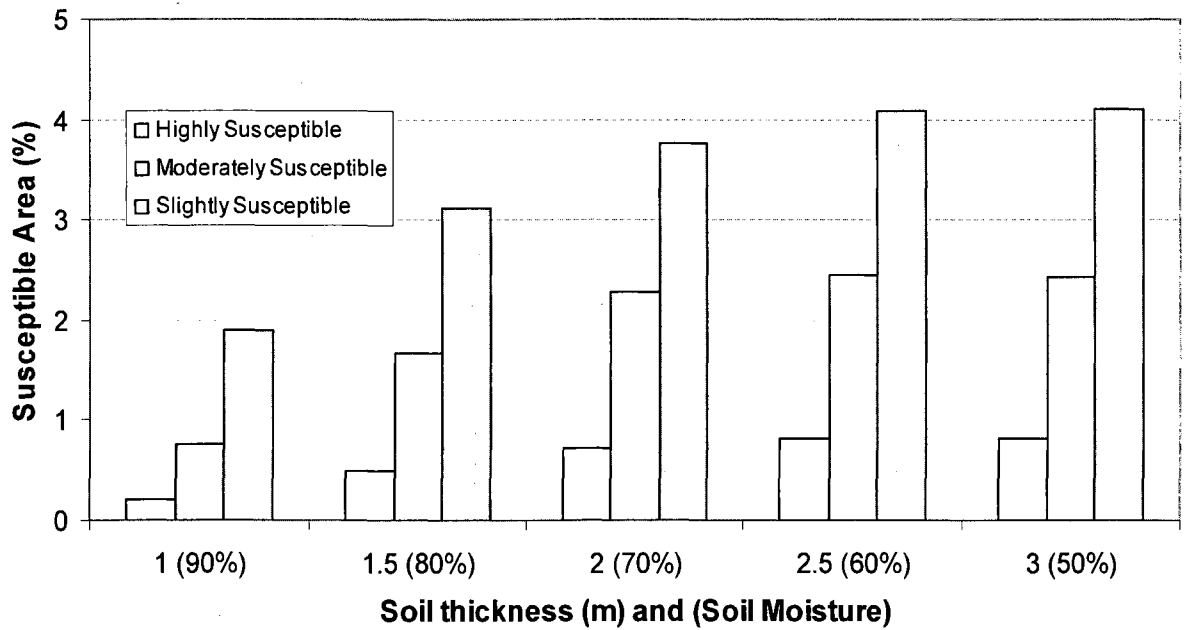


Figure 3-9: Susceptibility area with increase of soil thickness with equal increase in depth to GW table (0.25 m for 1 m thick soil with 0.5 m increment to 2.25 m for 3 m thick soil or constant GW table thickness from the failure plane) and varying vadose zone SM (as shown in Figure) at Cleveland Corral region, California in 2005

CHAPTER 4.

MODELING LANDSLIDE SUSCEPTIBILITY USING DYNAMIC SOIL MOISTURE PROFILES

Abstract

A landslide susceptibility mapping study was performed using dynamic hillslope hydrology. The modified infinite slope stability model that directly includes vadose zone soil moisture (SM) was applied at Cleveland Corral, California, US and Dhading, Nepal. The variable infiltration capacity (VIC-3L) model simulated vadose zone soil moisture and the wetness index hydrologic model simulated groundwater (GW). The GW model predictions had a 75% NASH-Sutcliffe efficiency as compared to California's in-situ GW measurements. The model performed best during the wet season. Using predicted GW and VIC-3L vadose zone SM, the developed landslide susceptibility maps show very good agreement with mapped landslides at each study region.

Introduction

Weather and climate factors that increase soil moisture and pore water pressures enhance slope instability. Slope stability analysis via the limit equilibrium approach can be used to quantify the impact of soil moisture on landslides (e.g., Montgomery and Dietrich, 1994; D'Odorico et al., 2005; Chiang and Chang, 2009). The limit equilibrium approach uses two unsaturated and one saturated soil layers. Some studies use a single saturated unit soil weight to represent both layers (e.g., Montgomery and Dietrich, 1994; D'Odorico et al., 2005; Chiang and Chang, 2009). Others use dry and saturated unit soil weight, respectively, for the layer above and below the saturated soil layer (De Vleeschauwer and De Smedt, 2002; Ray and De Smedt, 2009). An analogous approach uses wetness indices such as O' Loughlin's 1986 TOPOG model (e.g., Dietrich et al., 1993; Montgomery and Dietrich, 1994; Van Westen and Terlien, 1996; Pack et al., 1998; de Vleeschauwer and De Smedt, 2002; Ray and De Smedt, 2009). These wetness indices can provide a dynamic spatially distributed representation of the water table, but neglect soil moisture in the upper soil layer above the groundwater table (Rosso et al., 2006).

Ray and De Smedt (2009) developed landslide susceptibility maps for three steady state and two quasi dynamic scenarios. They assumed dry, half saturation and full saturation as steady state scenarios and 2 year and 25 year return period rainfall as dynamic scenarios. For quasi dynamic scenarios, they used infiltration based model to estimate increase of groundwater over the assumed half saturation. However, these authors pointed out that those results may not be realistic because an initial groundwater

prior to rainfall events was assumed. They recommended to study further based on the real groundwater table and antecedent soil moisture conditions. Although it is more realistic to use in-situ groundwater and soil moisture measurements, it is rather expensive, time consuming and almost impossible to monitor dynamic groundwater and soil moisture for dynamic susceptibility analysis at a regional or global scale. An alternate approach is to use a hydrologic model to characterize groundwater table and vadose zone soil moisture (SM) evolution. Ray et al.'s (2009a) enhanced wetness index model uses vadose zone SM to estimate moist unit soil weight and wetness index. At these scales, soil-vegetation-atmosphere-transfer (SVAT) models offer a useful method to estimate soil moisture values.

Most SVAT models are well suited to predict soil moisture dynamics (Whitfield et al., 2006). Some SVAT models such as Biosphere Atmosphere Transfer Scheme (BATS; Dickinson et al., 1986) and Simple Biosphere Model (SiB; Sellers et al., 1986) are not viable in slope stability analysis because they do not include topographic effects (Ling et al., 1994). Other models, the Common Land Model (CLM; Dai et al., 2003) and Land Surface Process (LSP; Liou et al., 1999), require soil layer characteristics that are not the appropriate model for shallow slope stability analysis. The variable infiltration capacity (VIC-3L) model (Wood et al., 1992; Liang et al., 1994) considers topography and has three soil layers. This model has no vertical flow from the third soil layer, but instead generates baseflow. This agrees well with the infinite shallow slope stability model which assumes no vertical water movement on the impervious soil layer or bedrock.

This paper seeks to improve Ray and De Smedt's (2009) approach by including VIC-3L's soil moisture effects in landslide susceptibility maps. The results are demonstrated for two study regions; Cleveland Corral, California, USA and Dhading, Nepal. This paper also evaluates the Ray and De Smedt (2009) wetness index model by simulating the groundwater table at Cleveland Corral, California. The landslide susceptibility results are compared to mapped landslides and previous studies. The specific research objectives are: (1) to examine the Ray and De Smedt (2009) wetness index model groundwater table simulation, (2) to validate SVAT derived soil moisture profiles, (3) to characterize the regional landslide susceptibility maps using dynamic soil moisture and groundwater and (4) to compare these results with traditional susceptibility maps.

Models

Slope Stability Model

This study uses the infinite slope method (Skempton and DeLory, 1957) to calculate safety factors that expresses the ratio of resisting forces to driving forces. The infinite slope stability model as adapted by the several researchers (e.g., Montgomery and Dietrich 1994; van Westen and Terlien 1996; Acharya et al., 2006; Ray and De Smedt, 2009) is:

$$FS = \frac{C_s + C_r}{\gamma_e H \sin \theta} + \left(1 - m \frac{\gamma_w}{\gamma_e} \right) \frac{\tan \phi}{\tan \theta} \quad (4-1)$$

where C_s and C_r are the effective soil and root cohesion [kN/m^2], γ_e is the effective unit soil weight [kN/m^3], H is the total depth of the soil above the failure plane [m], θ is the slope angle [$^\circ$], m is the wetness index [adimensional], ϕ is the angle of internal friction of the soil [$^\circ$], γ_w is the unit weight of water [kN/m^3]. The effective unit weight is estimated as:

$$\gamma_e = \frac{q \cos \theta}{H} + (1 - m) \gamma_m + m \gamma_s \quad (4-2)$$

where q is any additional load on the soil surface [kN/m^2] and γ_m is moist unit soil weight [kN/m^3] for the unsaturated soil layer.

The wetness index model follows Ray et al. (2009a) given as

$$m = \frac{h + (H - h) * S_w}{H} \quad (4-3)$$

where h is the saturated thickness of the soil above the failure plane [m] and S_w is the degree of soil saturation [cm^3/cm^3] or vadose zone soil moisture.

VIC-3L Model

The vadose zone SM is simulated using the VIC-3L model. The VIC-3L hydrologic model (Liang et al., 1994, 1996, 1999; Cherkauer and Lettenmaier, 1999) is a three-layer SVAT land surface scheme (Lohmann et al., 1998) that has been widely applied for surface runoff generation and soil moisture profile estimation (Liang and Xie, 2003; Yuan et al., 2004; Dengzhong and Wanchang, 2005). This macroscale land surface model that simulates water and energy budgets by including spatial variations of soil properties, soil topography, precipitation, and vegetation (Maurer et al., 2002; Huang and Liang, 2006) and can be run at grids sizes ranging from a fraction of degree to several degrees latitude and longitude (Maurer et al., 2002). Based on the climate data and soil and vegetation characteristics, this model can estimate soil moisture storage, evapotranspiration, runoff and snow water equivalent at hourly to daily time-steps. Moreover, other distinguishing characteristics of this model are the ability to represent sub-grid variability in land surface vegetation classes, soil moisture storage capacity, topography as well as precipitation (Nijssen et al. 2001; Yuan et al., 2004; Zhou et al., 2004; Huwang and Liang, 2006). VIC-3L uses the variable infiltration capacity approach (Nijssen et al. 1997) and varies runoff generation and evapotranspiration based on topography, soil and vegetation (Wood et al., 1992).

The model's soil column has three layers (Parada and Liang, 2004). The top, thin soil layer and the middle soil layer characterize the dynamic response of the soil to weather and rainfall events. The lowest layer captures the seasonal soil moisture behavior (Liang et al., 1996; Huang and Liang, 2006) and only responds to rainfall when the upper layer is wet. The first soil layer receives soil moisture from precipitation and drains it to the second soil layer by gravity using the Brooks and Corey (1988) relationship (Lohmann et al., 1998). The base flow from the third soil layer contributes to runoff based on the ARNO model (Francini and Pacciani, 1991).

The VIC-3L model characterizes $N+1$ land cover types where N is the different land cover types and 1 represents bare soil. There is no restriction in number of model land covers, however, it is more appropriate if they do not exceed 10 (Liang et al., 1994). Each land cover type has a leaf area index (LAI), minimum stomatal resistance, roughness length, displacement length and relative fraction of root (Liang et al., 1994; Nijssen et al., 1997). This model uses the Penman-Monteith equation to calculate evapotranspiration at each grid cell (Nijssen et al., 1997).

The VIC-3L model can be operated in various simulation modes including an energy balance and water balance. The energy balance model is forced by maximum and minimum temperature, precipitation, wind speed, air pressure, vapor pressure, and incoming shortwave and long wave radiation. The energy balance simulates the surface energy flux and solves the complete water balance. The water balance model, applied for this research, only requires maximum and minimum temperature, precipitation and wind speed forcing data (Zhou et al., 2004; Yulin et al., 2008).

Groundwater Model

The GW table fluctuations are simulated using the wetness index model (Ray and De Smedt, 2009) loosely coupled with VIC-3L soil moisture variation in the upper two soil layers. The Ray and De Smedt wetness index model estimates the thickness of saturated soil layer based on effective precipitation, specific yield and soil depth. The amount of water stored, ΔS [m], per increase in water table elevation, Δh , is the specific yield (or effective porosity), $\alpha = \Delta S/\Delta h$ [-], a soil characteristic (De Smedt, 2006). Ray and De Smedt's (2009) wetness index model based on effective precipitation is

$$m_{GW} = \frac{h_0 + \Delta h}{H} = \frac{h_0}{H} + \frac{\Delta S}{\alpha H} = m_0 + \frac{I \Delta t \cos \theta}{\alpha H} \quad (4-4)$$

where m_{GW} is the wetness index due to the GW, $m_0 = h_0/H$ is the initial wetness index before the rainfall event and is user defined saturated soil thickness prior to simulation time, and the amount of infiltrated rainfall stored in the soil is given by $\Delta S = (\cos \theta) I \Delta t$, I is an effective precipitation [m], Δt the duration of the storm [s] and $\cos \theta$ compensates for the fact that rain intensities are equated on a horizontal area basis while the soil surface has a slope angle θ . Given m_{GW} , the thickness of groundwater or saturated soil thickness can be determined by

$$h = m_{GW} * H \quad (4-5)$$

Equations (4-3) and (4-5) are used to estimate the wetness index. Eq. 4-5 estimates a wetness index for a measured or estimated groundwater position and a dry vadose zone.

Equation 4-3 includes the groundwater and the vadose zone SM.

Study Areas

Cleveland Corral, CA, USA

The Cleveland Corral study region in the Highway 50 corridor is located in the Sierra Mountains, California, USA (Reid et al., 2003). Highway 50 is a major road located between Sacramento and South Lake Tahoe in California (Spittler and Wagner, 1998). The study area is about 28 by 22 km or 616 km². Elevations range from about 902 to 2379 m. Based on the 90 m digital elevation model (DEM), slopes in this region range from 0 to 48°. Since 1996, slope movements and landslides occur infrequently during winter. One major catastrophic landslide occurred in 1983 in this region (Spittler and Wagner, 1998). Since 1997, the USGS has monitored this region using real time data acquisition systems (Reid et al., 2003). They found elevated pore-water pressures and abundant soil moisture during periods with slope movement and landslides in the rainy season.

This study region has considerable variability in soil texture ranging from clay loam to sandy loam (Table 4-1). The predominant soil is sandy loam. 72 and 28% of study area is covered with sandy loam and loam, respectively in the first and second soil layers. The third (lowest) layer consists of four soil types, loam, sandy loam, clay loam and sandy clay, and covers, respectively, 72, 16, 3 and 9%, of the study area (Table 4-1). The total soil depth ranges from 0.6 to 1.4 m. Conifer and wooded grassland are the dominant land covers at 80 and 14% of the study region, respectively. Some rock outcrops are also observed along the Highway 50 corridor.

Krishnabhir, Dhading, Nepal

Nepal is about 83% mountainous terrains, the remaining 17% is southern alluvial plains. The country extends from 80° 04' to 88° 12'E longitude and 26° 22' to 30° 27'N latitude and spans approximately 885 km in the east-west direction and varies from 130 to 255 km in north-south direction. The elevation ranges from 70 m at Kanchan Kalan to 8850 m at the top of the Mount Everest within a very short distance.

The study area is situated in Dhading, one of the seventy-five districts of Nepal. The transnational Prithvi highway connecting Kathmandu and Pokhara runs through the southern part of the district. The road parallels the Trishuli River. The study area is about 25 km by 14 km or 350 km² in total. Based on the Shuttle Radar Topography Mission (SRTM) DEM, altitudes in this region range from 256 to 1918 m with slope 0 to 57°. Landslides occur frequently in this area during the monsoon season, July to September, usually leading to interruption of the traffic. One of the major landslides in the district occurred in 2003 along the Prithvi highway at Krishna Bhir. The relatively high landslide frequency in Nepal, as compared with mountain ranges of other countries, may be because Nepalese mountains are geologically younger (Ray, 2004).

Based on the United States Department of Agriculture (USDA) soil classification system, sandy clay loam, sandy clay, sandy loam, loam and sand soil types were identified in this region. The predominant soils are sandy clay loam (36%) and sandy loam (22%). On this steep terrain, woodland and cropland are the dominant land covers, 50 and 29% of the study region, respectively.

Methods and Database

This study uses a 90 m spatial resolution to calculate wetness index, moist unit soil weight, effective unit soil weight and safety factor (FS). Soil moisture, obtained from the VIC-3L model, was used to estimate moist unit weight of soil in the unsaturated layer above the water table. Wetness indices were calculated by using modeled GW depth, total soil thickness and average vadose zone SM values obtained from the VIC-3L model (Eq. 4-3) at both study regions. The effective unit weight of soil was calculated using moist unit weight, wetness index, depth of soil, surcharge and slope angle (Eq. 4-2). However, for Ray and De Smedt (2009) model, Eq. 4-4 was used to estimate wetness index based on the assumed GW position at half of total soil thickness (half saturation) and calculated additional GW using rainfall, specific yield and slope with dry vadose zone.

Theoretically, landslides occur when the safety factor is less than one. Susceptibility maps were developed using four safety factor categories; highly susceptible ($FS \leq 1$), moderately susceptible ($1 < FS < 1.25$), slightly susceptible ($1.25 < FS < 1.5$) and not susceptible ($FS \geq 1.5$).

Since no tools or methods exist to map an entire susceptible area for validation, this study compares observed landslides to the model results. Each study area was surveyed to identify a series of landslide locations for validation (Table 4-4 and 5). Due to the study extent and terrain, the survey was not comprehensive or all inclusive. 10 and 12 landslide sites were observed, respectively, in the California and Nepal study

regions. Most of the sites failed prior to the study period. Several failures occurred during the study period. In California, slope movements and landslides occurred in May 2005 and earlier. In Nepal, landslides occurred in August 2004 and earlier.

California

Methods

For the Cleveland Corral study region, the VIC-3L model was run using a daily time-step from October 1, 2003 to September 30, 2006 with layers of 0.05, 0.35, 0.4 to 1.0 m thickness at a 0.0083° (approximately 1 km) resolution. This duration was selected because this region has in-situ groundwater measurements for the study period. The Cleveland Corral study region has 900 0.7 km^2 pixels.

Model Data

The soil and vegetation parameters required for the VIC-3L hydrologic model and the slope stability model are summarized in Tables 4-2 and 3, respectively. Soil layers, soil thickness and soil texture information were obtained from the States Soil Geographic (STATSGO) soil database (NRCS, USDA). There are eleven soil layers in the STATSGO soil database. To coincide with the VIC-3L model, these layers were regrouped into three soil layers. The first, the second to fifth and the sixth to eleventh soil layers of the STATSGO soil database were combined to parameterize the first, second and third soil layers, respectively, for the VIC-3L model. The assumed potential failure

plane underneath the soil layer is bedrock. The unit soil weight (saturated and moist) was calculated based on the soil moisture, soil porosity, and specific gravity of the soil samples using methods adapted by Ray et al. (2009a). Each soil type was assigned soil cohesion and friction angle values that were adapted from Deoja et al. (1991) and the slope of the retention curve adapted from Clapp and Hornberger (1978). Similarly, soil bulk density, field capacity, wilting point and saturated hydraulic conductivity values were adapted from the VIC-3L model documents and Miller and White (1998).

Advanced Very High Resolution Radiometer (AVHRR) land cover data (1 km spatial resolution) were obtained from University of Maryland (UMD) (Hansen et al., 2000). There are four land cover types excluding water and wetland in this study region. Each land cover class was assigned a root cohesion values that was adapted from Sidle and Ochiai (2006). Architectural resistance, minimal stomatal resistance, minimum incoming shortwave radiation, root fraction, root depth, vegetation roughness and vegetation height required for the VIC-3L model parameterization were obtained from the Land Data Assimilation System (LDAS; Mitchell et al., 2004). The monthly LAI data required for the VIC-3L model were obtained from Moderate Resolution Imaging Spectroradiometer (MODIS). The MOD15A2, 8-day composite LAI values were averaged to monthly values.

Rainfall, temperature and wind speed measurements were obtained from the National Climatic Data Center (NCDC) from 2000 to 2006. The 90 m SRTM DEM was used to derive slope angle in this study. The daily groundwater measurements for water years 2004 to 2006 were obtained from the USGS (Mark Reid, USGS).

There are six model calibration parameters which can not be estimated from vegetation or soil information (Zhou et al., 2004). These six parameters are the infiltration shape parameter $b_{infiltr}$, the maximum subsurface flow D_{max} , the fraction of maximum subsurface flow D_s , the fraction of maximum soil moisture in the third layer W_s and the two soil depths layer second and layer third. The VIC-3L model results were calibrated by comparing VIC-3L soil saturation in the third soil layer to in-situ groundwater measurements. The six determined model parameters were; $b_{infiltr} = 0.2$, $D_{max} = 30$, $D_s = 0.0001$, $W_s = 0.99$, soil depth of layer 1, soil depth of layer 2, $D2 = 0.35$ m, and soil depth of layer 3, $D3 = 0.4 - 1.0$ m.

Nepal

Methods

For this study region, the VIC-3L model was run using a daily time-step from October 1, 2003 to September 30, 2006 with layers of 0.05, 0.35 and 0.6 to 1.1 m thickness at a 0.0083° (approximately 1 km) resolution. This study region has 450, 0.75 km^2 pixels.

This region does not have in-situ groundwater measurements. Groundwater table was simulated using Eq. (4-4) and compared with the VIC-3L model average surface soil moisture. The simulated groundwater table was used for all safety factor related calculations. Geotechnical and hydrologic parameters used in this region are similar to California study region.

Model Data

The soil and vegetation parameters required for the VIC-3L hydrologic model and the slope stability model are summarized in Table 4-2 and 4-3, respectively. Soil layers, soil thickness and soil texture information were obtained from previous research work (Ray, 2004; Ray and De Smedt, 2009). No vertical soil texture separation was observed in this study region. The assumed potential failure plane underneath the soil layer is bedrock. Ray (2004) developed a soil map for this study area using geology map, land cover map, Ariel photograph as well as Food and Agriculture Organization (FAO) digital soil map. All other soil (Ray, 2004) and land cover (UMD, Hansen et al., 2000) parameter estimates are identical to the California study region.

The in-situ measurements of rainfall, temperature and wind speed were obtained from the Department of Hydrology, Nepal from 2003 to 2006. The 90 m SRTM DEM was used to derive slope angle in this study region.

Results and Discussion

Groundwater Simulation in California and Nepal

The modeled soil moisture profiles and GW table depths were compared to in-situ groundwater measurements from October 1, 2003 to September 30, 2006 at Cleveland Corral, California. The wetness based groundwater model performance compares well to the observed GW values (Table 4-6 and Fig. 4-1). The model's average GW depth and its variability are very close to observed GW values. In addition, the model has relatively low errors, strong correlation and high efficiency.

California's rainy or wet season is from January to May. Figure 4-2a shows that the predicted GW results do an excellent job tracking the range and variability of the observed GW, particularly during the wet season. Because landslides occur during the wet season, it is critical for this period to have accurate GW tables and vadose zone SM. Errors are much less critical during the dry season. These results support the wetness model's application in a landslide prone region. The wetness based model's success in the California study region is valuable because this is its first application to a landslide prone region where in-situ dynamic GW measurements were available.

The VIC-3L vadose zone SM values, the predicted GW and the in-situ GW measurements show similar daily, seasonal and annual variations in both study regions (Fig. 4-2a and 2b). There is also a strong correlation between SM and GW at both study regions (Table 4-7). The R^2 values are 0.47 and 0.76, respectively for the California and the Nepal study regions and p-values are less than 0.0001 for both study regions.

In California, spring is the wettest season because there is relatively high rainfall and snow melt occurs during this period. The modeled SM values are wet during spring and dry in late summer and fall. The dry to wet transition, which shows that soil moisture increases prior to the GW table rising, is physically sound. In Nepal, the VIC-3L vadose zone SM values and predicted GW values also show similar daily, seasonal and annual variations (Fig. 4-2b). Nepal's rainy or wet season is from June to September. In contrast to California, the wet monsoon season begins with both SM and GW increasing simultaneously because intense rainfall occurs during this period. During Nepal's 2005 dry season, there were some significant GW table increases that did not correspond to SM increases. While very good agreement between the VIC-3L SM and the model predicted GW values is found during the monsoon (wet season), the method is not recommended for the dry season.

Figure 4-3 provides further support to the independent GW and VIC-3L SM models' wet season results. The relationship between the GW table depth and SM is analogous to a soil moisture characteristics curve. For both study regions, SM increases as the GW table rises. The relationship differs by region. The predominant soil types are sandy clay loam and sandy loam in Nepal and California, respectively. The coarse California soils drain relatively quickly when the water table lowers as compared to the finer Nepal soils. Figure 4-3 relationships are comparable to classic soil-water pressure versus saturation curve for the sites' soil types.

Overall, the wetness based GW model and the VIC-3L SM demonstrate promising results for landslide studies where no GW measurements are available,

especially during the wet season. Practically, this approach can provide promising results for landslide studies that mainly occur during a wet season.

Safety Factor Variations

The strength of the GW and SM modeling approach is that it makes possible daily safety factor estimates at regional scales. This section first demonstrates the dynamic safety factor results then examines critical saturation states at a regional scale.

Two 90 m pixels that are near observed landslides and slope movements were selected for each study region. Under the maximum modeled saturation, one pixel is highly susceptible and one is moderately susceptible in each region. Using the VIC-3L model soil moisture values and the model predicted GW, dynamic safety factors were calculated. Daily safety factors and rainfall are presented in Figures 4-4a and b for the California and the Nepal study regions, respectively. The lowest FS values were observed during the rainy season in each study region. This wet period is characterized by modest variations in these low FS values. Theoretically, a slope will fail when its FS value is less than or equal to 1. However, the safety factor time series show that FS values for active landslide pixels crossed the threshold many times from 2004 to 2006 in each region but slides did not occur each time.

Clearly these dynamic safety factors are not perfect indicators of slope failure. Rather, they can show how a stable slope changes to unstable when a series of rainfall events raises the GW table, wets the vadose zone and increases the pore water pressure.

These cumulative impacts are often sustained for a period of time during which a slope is primed for failure.

The monthly average VIC-3L surface SM, rainfall and number of days when the FS values went below the threshold are presented in Table 4-8. California had less rainfall in 2004 than in 2005. In contrast, Nepal had more rainfall in 2004 than in 2005. Table 4-8 shows that highly susceptible periods, when safety factor was below the threshold, occurred from January to May in 2005 and May to August in 2004 in California and Nepal, respectively. These periods agree well with Nepal's mapped landslides in 2004 and no landslides in 2005 (Figs. 4-4a and b). Similarly, California had series of slope movements in 2005 but no slope movements in 2004. The current findings suggest a strong potential for quantifying antecedent moisture conditions and applying them to estimate safety factors. While the threshold of one is not a perfect failure indicator, the relative variations among months and across years can enhance predicted susceptibilities, slope movements and landslide events for these regions.

Dynamic safety factors are valuable at specific locations. However, the true value of this method is its ability to provide dynamic hazard risk maps at regional scales. This section presents regional landslide susceptibility results for four scenarios. Two dynamics scenarios were considered. The half-saturated condition has a variable soil moisture in the vadose zone and a GW table at the middle of the soil thickness (May 23, 2005 in California and September 12, 2004 in Nepal). The maximum modeled saturation condition has a variable soil moisture and GW table. For the 3-year study period, the maximum saturation occurred on May 8, 2005 and August 18, 2004 for California and Nepal, respectively. The remaining two scenarios, completely dry and full saturation,

provide lower and upper susceptibility boundaries. The dynamic scenarios are those used by Ray and De Smedt (2009) in Nepal except that their model did not consider vadose zone SM. Their half saturation case had a water table at 50% depth and 0% moisture in vadose zone. Their 2-year return period rainfall, 100 mm, estimated by Ray and De Smedt (2009) using 41 years of historical rainfall data, was used to compare to this study's maximum saturation scenario.

Table 4-9 shows the susceptibility distributions for these four scenarios. These results show strong impacts of soil moisture and groundwater on instability. Both regions have negligible or no susceptible area when the soil is completely dry and comparatively high susceptible area when the soil is completely wet. Practically, no slope fails under dry conditions. For dry conditions in Nepal, the presence of highly susceptible area indicates that either no soils exist on these steep slope or that there are some input data errors. Considering that Nepal is a poor data region with steep terrain this finding is not unreasonable. All scenarios have more highly susceptible area in Nepal than California. Nepal has a steeper terrain and receives higher rainfall in the wet season than California.

When comparing the current results with Ray and De Smedt (2009)'s results, there are some minor differences because they used topography and land cover maps developed in 1992 from aerial photographs and field verifications by the Nepal Government. This paper uses the most recently available remotely sensed land cover data and DEM.

For the half saturation scenario, Ray and De Smedt (2009)'s method gives much less susceptible area than the current results. Their assumption that the vadose zone is dry in the wet season neglects some potentially high risk regions on their landslide hazard

maps. Ray and De Smedt (2009) considered a quasi-dynamic approach for susceptibility prediction. They estimated stability after a 2-year rainfall event using an infiltration approach. Nepal's 2-year design rainfall is 100 mm whereas the modeled maximum saturation conditions for this study had only 50 mm of rainfall. California's 2-year design rainfall is 86 mm whereas the modeled maximum saturation conditions for this study had only 61 mm of rainfall. Table 4-9 shows that the maximum modeled saturation for the 3-year study period agrees extremely well with the 2-year rainfall events using the infiltration approach for both study regions. This result suggests that susceptibility mapping based on quasi-dynamic scenarios may provide reasonable insights. However, the design rainfall only indicates where hazardous regions exist, not when they occur. Since the model is based on estimated or measured groundwater and vadose zone SM, it can produce more reasonable results without any assumption of groundwater or soil moisture unlike Ray and De Smedt (2009). Also, the Ray and De Smedt (2009) model required long historical rainfall data to predict rainfall events but this model does not require any historical rainfall data. Interestingly, locations of the predicted highly susceptible area match each other, but the potential hazard area is not completely captured by the Ray and De Smedt (2009) model (not shown).

Figures 4-5 and 6 show the susceptibility maps distribution for the two observed failures dates; May 8, 2005 for California and August 18, 2004 for Nepal. In California, most of the predicted highly susceptible areas are located along the Highway 50 corridor. This shows a clear anthropogenic impact on slopes that enhanced instability. Most of the mapped landslides were located on the predicted highly susceptible areas. On May 8, 2005, four of the mapped landslides were identified as moderately susceptible (Table 4-4).

Since, the exact dates of mapped landslides are unknown; it is possible that some of the landslides occurred when soil moisture was higher than maximum modeled soil moisture on May 8, 2005. Results show excellent agreement between the predicted susceptible area and the observed landslide events.

In Nepal, the predicted highly susceptible areas are not only located along the Prithvi highway, but are also found throughout the study region on steep slopes. The 11 out of 12 mapped landslides were found on the predicted highly susceptible area along the Prithvi Highway (Table 4-5). There are many other susceptible zones where it was not possible to verify the model prediction because of lack of accessibility and resources during the field survey. Because susceptibility does not always mean slope failure, these results are quite reasonable and appropriate. One mapped landslide was found in a moderately susceptible zone. The exact dates of all the mapped landslides are not known, making it difficult to match the mapped slope failures with the August 18, 2004 susceptibility maps. Moreover, the moderately susceptible area is very close to the highly susceptible area, some slope failures under moderately susceptible may not be uncommon.

Conclusion

This paper developed landslide susceptibility maps, using the VIC-3L model's vadose zone soil moisture coupled with simulated groundwater in two distinct different geographical regions. A simple wetness based groundwater model, based on daily rainfall, specific yield and slope angle, was used to estimate groundwater table. This model requires few inputs and it can be readily applied to data poor regions. This model is best suited for wet season. Thus, it produces promising results for rainfall induced landslides which typically occur only during the wet season.

When comparing the observed landslides and slope movements with the predicted highly susceptible area in both study regions, the results show promising agreement between the modeled and the slope failure ground truth. This modeling approach improves upon susceptible area predictions from the earlier quasi-dynamic model for design rainfall events and also informs the timing of landslide arrivals. Therefore, the approach is very useful for landslide hazard characterization in poorly monitored regions at scales from local and regional to global scale.

While this research suggests the potential of dynamic models, significant improvements are possible. Because not all predicted highly susceptible areas are verified, additional field validation is required. Due to a lack of in-situ soil moisture measurements, the VIC-3L model results were not verified independently. It is recommended that further studies monitor surface soil moisture on landslide prone slopes. Finally, the analysis scales exceed typical slide scales. These differences should be explored further.

Table 4-1: Soil, vegetation and slope characteristics of the California and Nepal study regions

	California	Nepal
Land cover (%)		
Evergreen forest	3.3	1.0
Conifer	79.9	-
Deciduous forest	2.7	-
Woodland	-	50.3
Wooded grassland	14.1	18.2
Grassland	-	1.7
Cropland	-	28.8
Soil texture (%)		
Loamy sand	-	16.2
Sandy loam	72.0	22.5
Loam	16.0	9.8
Sandy clay	3.0	15.0
Sandy clay loam	-	36.5
Clay loam	9.0	-
Slope (°)		
0-15	71.2	19.0
15-30	27.5	53.2
30-45	1.2	27.0
45-60	0.0	0.8

Table 4-2: Soil parameters used in VIC-3L and slope stability model

USDA soil types	Bulk density (g/cm ³)	Field capacity	Wilting point	Saturated hydraulic conductivity (cm/hr)	Slope of retention curve	Internal friction (deg.)	Soil cohesion (KN/m ²)	Study regions
					b			
Loamy sand	1.52	0.15	0.06	10.87	3.99	32	7.00	NP
Sandy loam	1.57	0.21	0.09	5.24	4.84	32	3.43	NP, US
Loam	1.49	0.29	0.14	1.97	5.30	31	3.92	NP, US
Sandy clay	1.57	0.31	0.23	1.19	12.00	28	5.39	NP
Sandy clay loam	1.6	0.27	0.17	2.40	8.66	31	6.00	NP, US
Clay loam	1.43	0.34	0.21	1.77	8.02	30	4.41	US

Note: US = USA, NP = Nepal

Table 4-3: Vegetation parameters used in VIC-3L and slope stability model

Land cover	Overstory	r _{arc} (s/m)	r _{min} (s/m)	Depth of root penetration (m)	Root Cohesion (kN/m ²)	Surcharge (kN/m ²)	R _{GL} (W/m ²)	Study Regions
Evergreen forest	1	60	250	1	6	0.7	30	NP, US
Conifer	1	60	250	1	6	0.7	30	US
Deciduous forest	1	60	125	1	3.3	0.7	30	US
Woodland	1	60	125	1	3.3	0.7	50	NP
Wooded grassland	0	40	125	0.9	1	0	75	NP, US
Grassland	0	25	120	0.75	1	0	100	NP
Cropland	0	25	120	0.75	1	0	100	NP

Note: US = USA, NP = Nepal, r_{arc} = Architectural resistance; r_{min} = Minimal stomatal resistance; R_{GL} = Minimum incoming shortwave radiation

Table 4-4: Physical characteristics and estimated safety factor (FS) of the mapped landslide's region in California. FS values were calculated under maximum modeled saturation on May 8, 2005 and assumed full saturation

S.N.	Longitude	Latitude	Slope ($^{\circ}$)	Land cover	Soil types	FS: Full saturation	FS: Maximum modeled SM
1	-120° 27' 26"	38° 51' 03"	27.4	Evergreen	Loam	0.753	0.770
2	-120° 29' 18"	38° 50' 23"	28.6	Evergreen	Loam	0.875	0.896
3	-120° 24' 22"	38° 46' 46"	32.5	Woodland	Sandy loam	0.815	0.838
4	-120° 23' 34"	38° 46' 37"	27.4	Woodland	Sandy loam	0.987	1.016
5	-120° 23' 23"	38° 46' 33"	24.1	Woodland	Sandy loam	0.997	1.026
6	-120° 22' 53"	38° 46' 23"	36.1	Woodland	Sandy loam	0.988	1.012
7	-120° 21' 34"	38° 46' 05"	31.1	Woodland	Sandy loam	0.856	0.881
8	-120° 20' 28"	38° 46' 04"	29.6	Woodland	Sandy loam	0.939	0.965
9	-120° 16' 33"	38° 46' 58"	36.6	Woodland	Sandy loam	0.988	1.014
10	-120° 16' 47"	38° 46' 20"	34.9	Woodland	Sandy loam	0.751	0.775

Table 4-5: Physical characteristics and estimated safety factor (FS) of the mapped landslide's region in Nepal. FS values were calculated under maximum modeled saturation on August 18, 2004 and assumed full saturation

S.N.	Longitude	Latitude	Slope (°)	Land cover	Soil types	FS: Full saturation	FS: Maximum modeled SM
1	84° 38' 05"	27° 51' 30"	39.0	Woodland	Sandy clay	0.885	0.919
2	84° 38' 45"	27° 51' 46"	36.0	Cropland	Loamy sand	0.580	0.639
3	84° 39' 52"	27° 50' 22"	25.5	Woodland	Sandy clay	0.829	0.860
4	84° 40' 11"	27° 49' 32"	42.1	Wooded grassland	Loam	0.986	1.010
5	84° 40' 22"	27° 48' 52"	38.4	Wooded grassland	Sandy loam	0.879	0.902
6	84° 41' 17"	27° 48' 30"	41.4	Cropland	Loam	0.665	0.707
7	84° 43' 39"	27° 47' 46"	44.4	Cropland	Sandy loam	0.794	0.817
8	84° 44' 11"	27° 47' 48"	44.2	Cropland	Sandy loam	0.606	0.637
9	84° 48' 42"	27° 48' 45"	35.1	Wooded grassland	Sandy clay loam	0.640	0.693
10	84° 49' 28"	27° 48' 28"	36.2	Cropland	Loamy sand	0.586	0.628
11	84° 50' 31"	27° 48' 02"	34.6	Cropland	Loam	0.818	0.877
12	84° 51' 36"	27° 48' 15"	30.9	Cropland	Sandy clay loam	0.700	0.811

Table 4-6: Groundwater model performance in California

Parameter	Value
Mean (O)	1.27
Mean (P)	1.28
Std Dev (O)	0.56
Std Dev (P)	0.42
Number of Data	365
Intercept (a)	0.45
Slope (b)	0.65
Mean Absolute Error (MAE)	0.20
Root Mean Square Error	0.28
Root Mean Square Error, Systematic (RMSEs)	0.20
Root Mean Square Error, Unsystematic (RMSEu)	0.20
Normalized Root Mean Square (NRMSE) %	16
Nash-Sutcliffe Efficiency Coefficient (NS)	0.75
R-square (R ²)	0.76

Note: O = Observed, P = Predicted, the terms N, NS, b, d and R² are dimensionless and other terms have unit m.

Table 4-7: Predicted GW and VIC-3L soil moisture statistics in California and Nepal

	California			Nepal		
	Mean	Std. Dev.	R ²	Mean	Std. Dev.	R ²
Average SM	0.60	0.07	0.47	0.68	0.12	0.76
Simulated GW	0.91	0.16		0.76	0.14	
						p-value
						<0.0001

Table 4-8: Safety factors, SM and rainfall values in 2004 and 2005 at landslide active pixels

Month	California										Nepal				
	2004					2005					2004		2005		
	Rainfall (mm)	Average SM (%)	No. Days SF<1	Rainfall (mm)	Average SM (%)	No. Days SF<1	Rainfall (mm)	Average SM (%)	No. Days SF<1	Rainfall (mm)	Average SM (%)	No. Days SF<1	Rainfall (mm)	Average SM (%)	No. Days SF<1
Jan	121	56	2	355	62	14	42	46	0	46	46	0	46	46	0
Feb	288	61	7	147	59	2	0	46	0	46	47	0	8	47	0
Mar	55	52	3	274	60	9	8	40	0	40	42	0	34	42	0
Apr	19	44	0	97	56	5	186	65	2	65	42	0	34	42	0
May	10	27	0	192	58	15	220	66	18	66	55	0	124	55	0
Jun	0	21	0	73	49	0	311	76	30	76	66	4	180	66	4
Jul	0	21	0	0	28	0	490	78	31	78	79	29	570	79	29
Aug	0	21	0	2	21	0	415	78	29	78	76	30	396	76	30
Sep	11	21	0	14	21	0	259	72	21	72	67	13	128	67	13
Oct	210	40	0	30	22	0	63	64	5	64	64	11	221	64	11
Nov	89	57	0	103	28	0	16	45	0	45	49	0	0	49	0
Dec	242	58	1	603	64	10	0	41	0	41	40	0	0	40	0
Total	1045		13	1890		55	2010		136		1741		136		87

Table 4-9: Distribution of susceptibility (%) for various scenarios at California, US and Dhading, Nepal study sites

	Highly Susceptible	Moderately Susceptible	Slightly Susceptible	Stable
California				
Dry	0.00	0.04	0.22	99.74
Half saturation	0.31	1.15	2.34	96.20
Max. modeled saturation	0.49	1.67	2.87	94.96
Fully saturation	0.58	1.90	3.01	94.51
Nepal				
Dry	0.17	1.73	6.35	91.75
Half saturation	7.39	19.43	22.15	51.03
Max. modeled saturation	11.59	23.30	21.12	43.99
Fully saturation	15.99	25.16	19.90	38.95
Ray and De Smedt (2009) model				
Half saturation				
California	0.09	0.43	1.29	98.19
Nepal	2.66	10.18	20.77	66.39
Max. modeled saturation (2-year return period)				
California	0.47	1.65	2.84	95.04
Nepal	11.77	27.51	20.71	40.00

Maximum modeled saturation occurred on May 08, 2005 for California and August 18, 2004 for Nepal

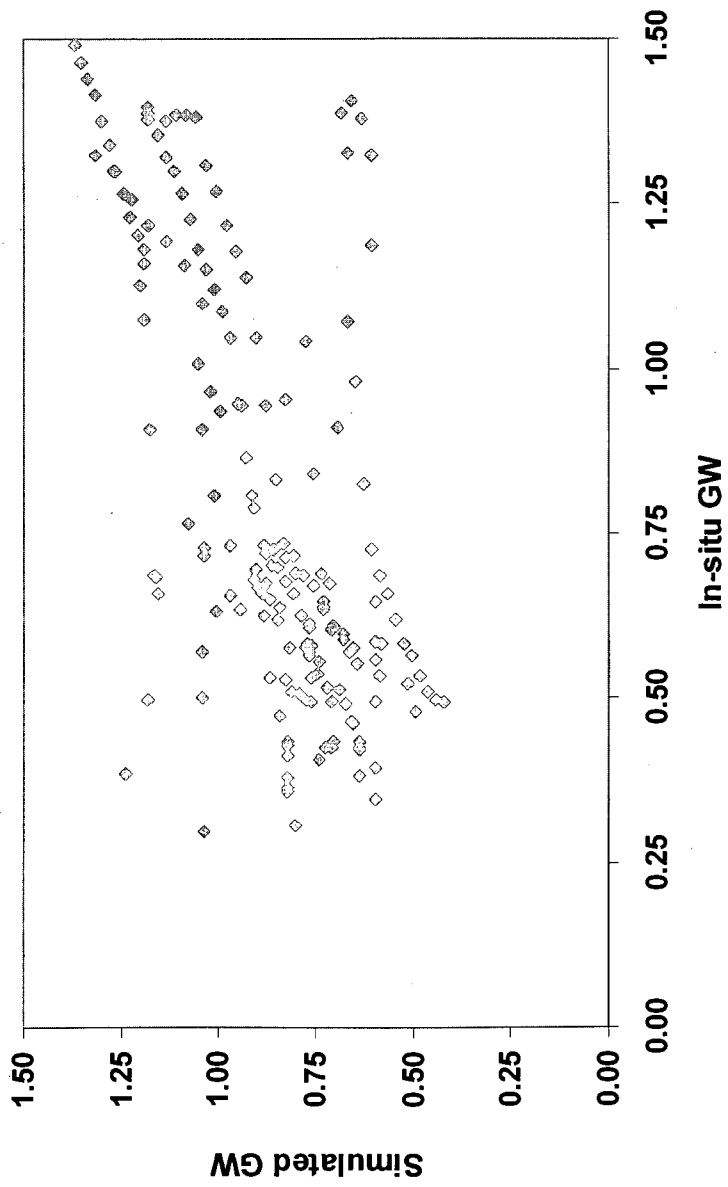


Figure 4-1: The simulated and observed groundwater (GW) at Cleveland Corral, California for wet season

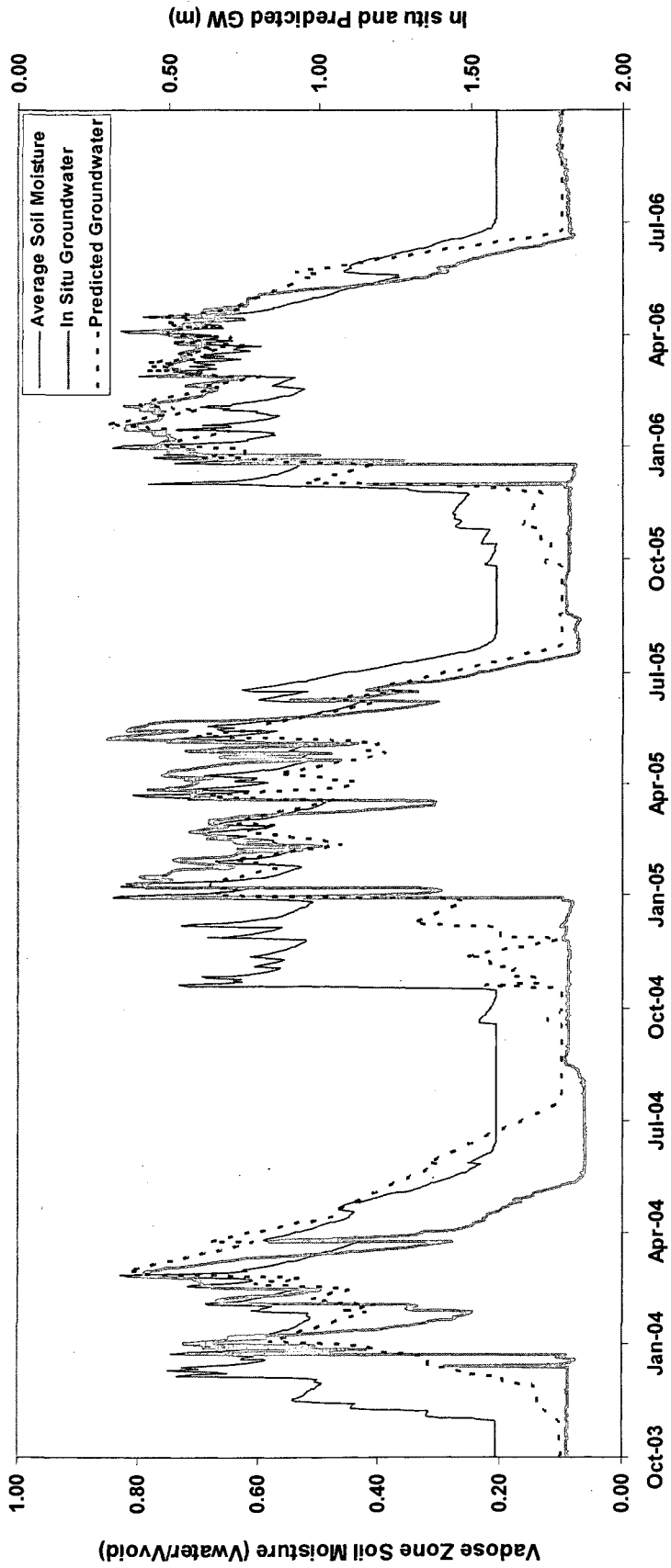


Figure 4-2a: In-situ, predicted GW and VIC-3L average SM at Cleveland Corral, California, US

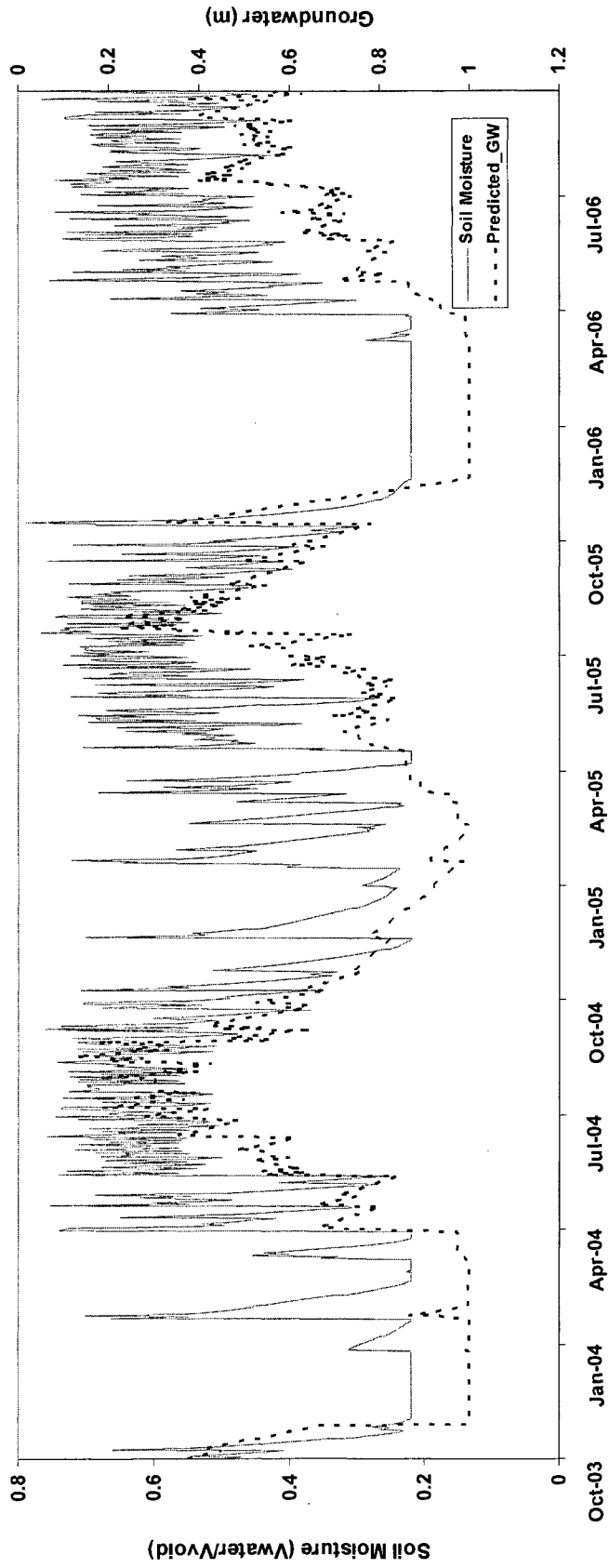


Figure 4-2b: Soil moisture versus simulated GW depth for Nepal

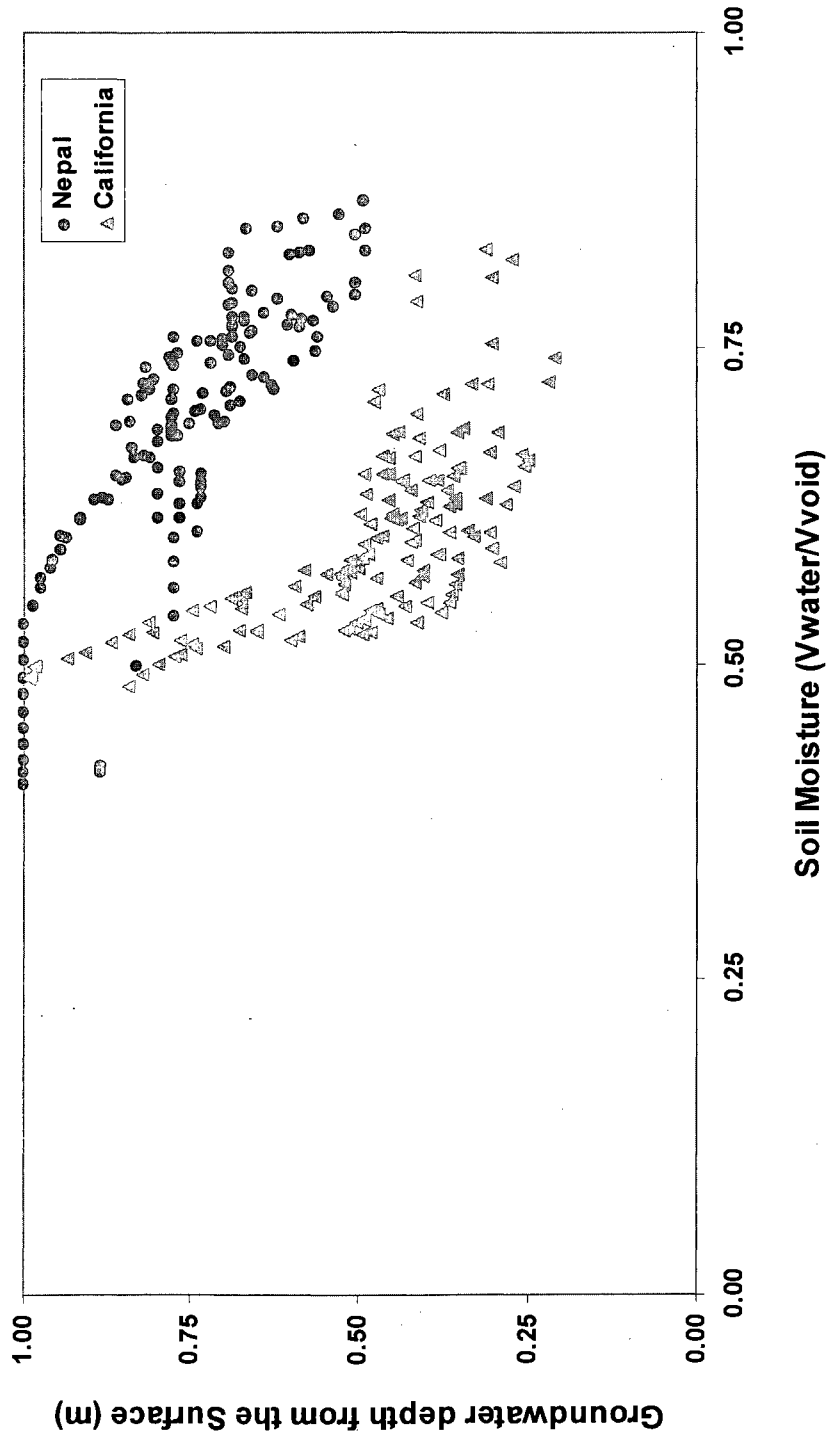


Figure 4-3: Simulated GW depth and average surface soil moisture for the wet season in California and Nepal

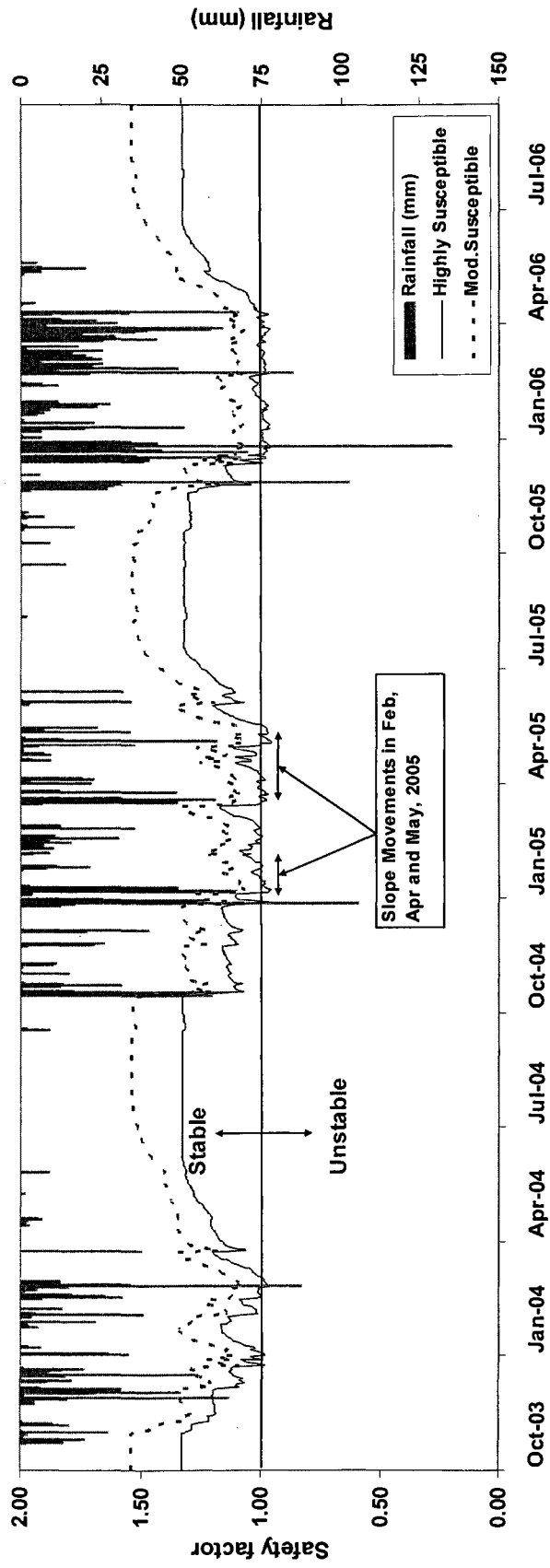


Figure 4-4a: Dynamic safety factors for two monitored landslide pixels in Cleveland Corral, California, US

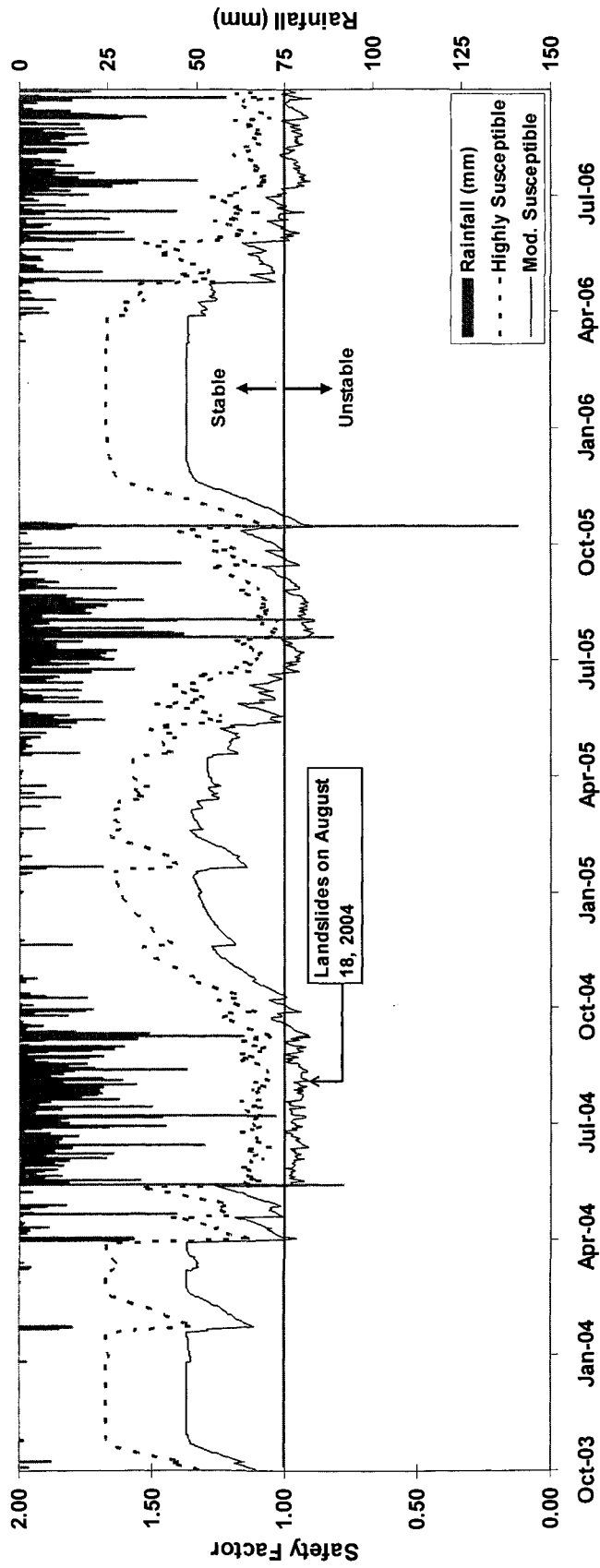


Figure 4-4b: Dynamic safety factors for two monitored landslide pixels in Dhading, Nepal

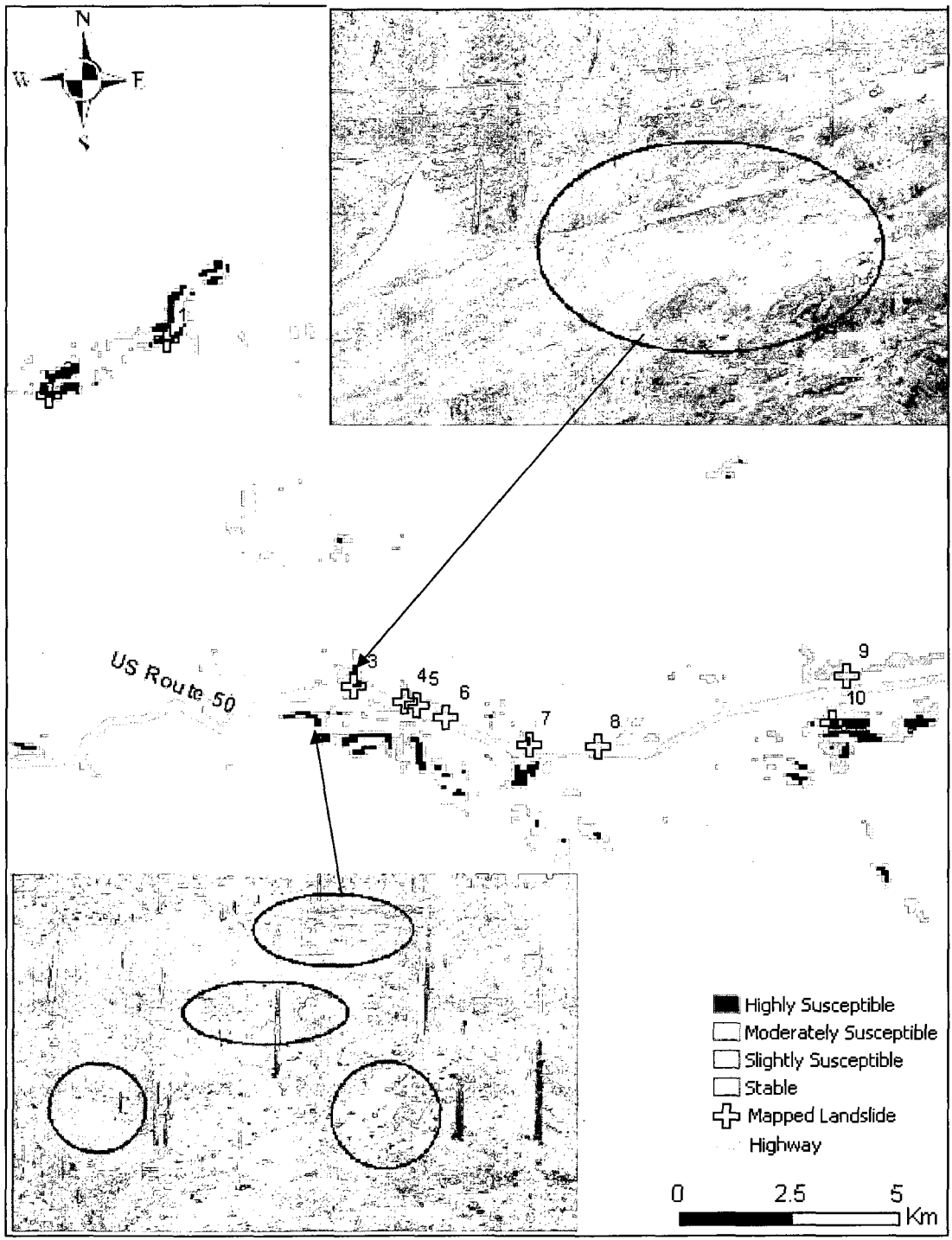


Figure 4-5: Susceptibility map on May 08, 2005 with mapped landslides in California, US

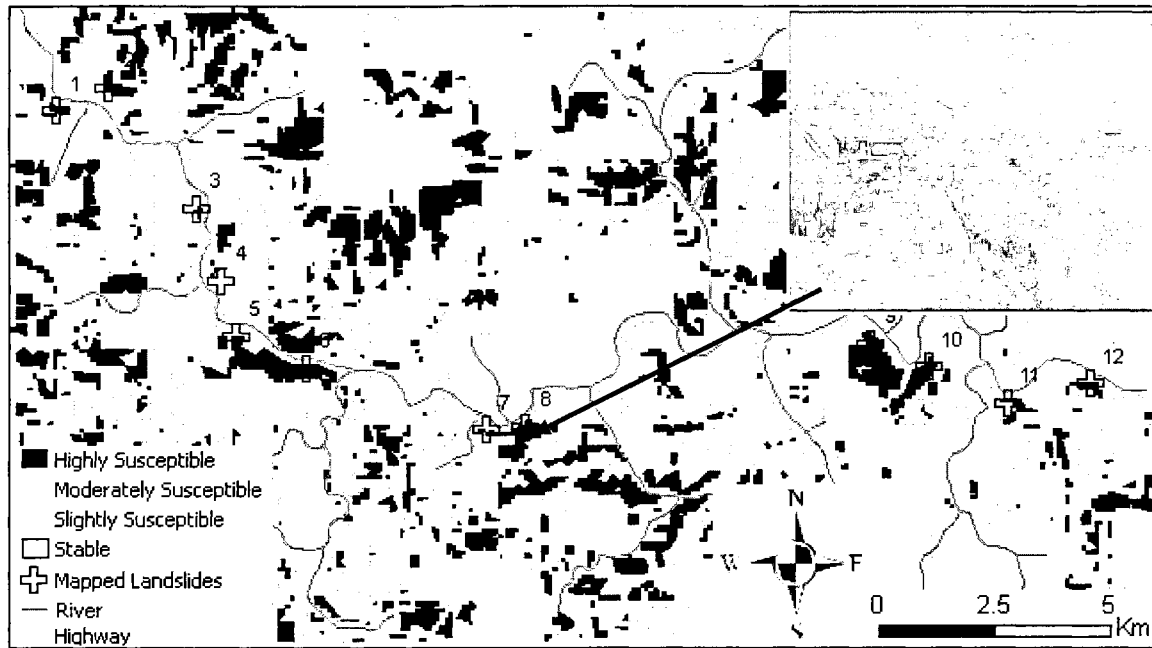


Figure 4-6: Susceptibility map on August 18, 2004 with mapped landslides in Dhading, Nepal (Inset picture was taken in August 2003)

CHAPTER 5.

REGIONAL LANDSLIDE SUSCEPTIBILITY: STATISTICAL DISTRIBUTION IN SPACE AND TIME

Abstract

Landslides can be characterized based on spatial and temporal distribution of susceptibility. This paper presents spatiotemporal susceptibility distributions at two study regions; Cleveland Corral, California, US and Dhading, Nepal. Mean, standard deviation, skewness, L-moments, coefficient of variation and transitional characteristics of safety factors for each pixel were used to characterize landslide susceptibility variations in each study region. The results show that the variability of safety factors is lower during the wet season than the dry season. The relative variability of the safety factor is lower in Nepal, the highly susceptible region. Results also show that Nepal has much higher probability (95%) of being unstable than California (70%) study region. Transitional characteristics of safety factors show a strong power law relationship between the average duration and number of crossings for both regions. Mapped landslide locations typically had frequent crossings with brief unstable conditions suggesting stress relaxation as a possible cause of slope failure.

Introduction

Shallow slope failures are quite common throughout the world in mountainous regions (Borga et al., 1998; Gulla et al., 2008). The soil moisture in an unsaturated zone and pore water pressure in a saturated zone are the controlling parameters that turn a stable slope to being unstable because both parameters reduce the shear strength and increase the shear stress to some extent. The intrinsic variables including topography, geology, soil regolith, engineering properties and extrinsic variables including rainfall, glacier outburst, earthquake, volcano play critical roles in slope stability (Dai and Lee 2002; Dahal, et al., 2008).

Researchers generally agree that wetness is a triggering factor in slope failure for rainfall induced landslides (Caine 1980; Iverson and Major, 1987; Rahardjo, 2000; Lee, 2005; Adler et al., 2006; Meisina and Scarabelli, 2007). These authors mainly studied the role of rainfall spatial distribution, duration and intensity in triggering landslides. Few studies have examined the role of rainfall temporal distribution in landslide susceptibility. Iverson (2000) and Lan et al. (2005), studying short and moderately intense rainfall events, found that landslides and slope movements change in response to rainfall. Slope movements occur in higher permeability soils and rapid slope failures in lower permeability soils.

The pore water pressure and soil moisture in saturated and unsaturated soil layers, respectively, are linked with the rainfall. The timing of soil wetting and drying controls

the landslide trigger and slope failure. Therefore, it is necessary to analyze soil moisture and pore water pressure both in time and space to determine landslide susceptibility.

Landslide susceptibility is characterized by the static variables, slope and soil properties, and the dynamic variables, pore water pressure, soil moisture and human influence. Static variables change very slowly (Gorsevski et al., 2006). However, significant changes are possible in the dynamic variables. Therefore, to understand physical and dynamic processes of instability, it is necessary to develop landslide susceptibility both in time and space (Wu and Sidle, 1995). While Saha et al. (2005) expressed difficulties with predicting susceptibility in space and time, Wu and Sidle (1995) and Gorsevski et al. (2006) presented a dynamic, distributed, physical-based model to develop landslide susceptibility in space and time scales from hours to several years. However, these authors mainly focused on vegetation strength and surcharge changes and did not consider the impact of vadose zone soil moisture on instability. Wu and Sidle (1995) used precipitation as a dynamic input to their model but did not characterize the pore water and soil moisture during the non-rainy periods. Wu and Sidle (1995)'s and Gorsevski et al. (2006)'s results are monthly and annual landslide susceptibility maps which do not provide insight to the frequency or timing of susceptibility.

This paper characterizes daily landslide susceptibility distribution annually and during the wet season. Distributions are derived from safety factors estimated for three years at Cleveland Corral, California, US and Dhading, Nepal. These two study regions, differing in location, terrain, soils and climate, provide insight into the landslide

susceptibility temporal variability and hazard. This research quantifies landslide susceptibility in space and time by (1) statistically characterizing safety factors, (2) describing the distribution and frequency of susceptibility in landslide prone regions, and (3) quantifying the transition properties of landslide prone regions.

Theory

This paper uses the modified infinite slope stability model to develop landslide susceptibility that directly link vadose zone soil moisture and groundwater (Ray et al., 2009a). The infinite slope method (Skempton and DeLory, 1957) calculates safety factors as the ratio of resisting forces to driving forces. The infinite slope stability model as adapted by the several researchers (e.g., Montgomery and Dietrich 1994; van Westen and Terlien 1996; Acharya et al., 2006; Ray and De Smedt, 2009) is

$$FS = \frac{C_s + C_r}{\gamma_e H \sin \theta} + \left(1 - m \frac{\gamma_w}{\gamma_e} \right) \frac{\tan \phi}{\tan \theta} \quad (5-1)$$

where C_s and C_r are the effective soil and root cohesion [kN/m^2], γ_e is the effective unit soil weight [kN/m^3], H is the total depth of the soil above the failure plane [m], θ is the slope angle [$^\circ$], m is the wetness index [adimensional], ϕ is the angle of internal friction of the soil [$^\circ$], γ_w is the unit weight of water [kN/m^3]. The effective unit weight is estimated as

$$\gamma_e = \frac{q \cos \theta}{H} + (1 - m) \gamma_m + m \gamma_s \quad (5-2)$$

where q is any additional load on the soil surface [kN/m^2] and γ_m is moist unit soil weight [kN/m^3] for the unsaturated soil layer.

The wetness index model follows Ray et al. (2009a) given as

$$m = \frac{h + (H - h) * S_w}{H} \quad (5-3)$$

where h is the saturated thickness of the soil [m] above the failure plane and S_w is the degree of soil saturation [cm^3/cm^3] or vadose zone soil moisture.

The VIC-3L model (Liang et al., 1994) was used to estimate soil moisture in the unsaturated zone. VIC-3L is a macroscale land surface model that was used to simulate the water budget based on the climatic, soil and vegetation characteristics. Model details and demonstration are provided in Ray et al. (2009b)

The estimated safety factor (FS) values were categorized into stability classes using Pack et al.'s (1998) and Acharya et al.'s (2006) stability classification system. The proposed four susceptibility classes are highly susceptible ($FS \leq 1$), moderately susceptible ($1 < FS < 1.25$), slightly susceptible ($1.25 < FS < 1.5$) and not susceptible (stable) ($FS \geq 1.5$).

The critical value for slope failure, defined by the ratio of resisting force to the sliding force on a slope, is 1 (Skempton and DeLory, 1957; Westen and Terlien 1996; Burton and Bathurst, 1998; Acharya et al., 2006; Ray and De Smedt, 2009). Depending on the soil, vegetation and climatic characteristics of the region, a slope may or may not fail at this critical safety factor value. However, a slope remains unstable if the safety factor is below 1; here it is assumed that the threshold value is 1. Safety factor crossing properties are defined as the number of times a site's safety factor drops below 1 and the average duration for which the site remains unstable or equivalently time below the threshold. For unstable sites, the safety factor's intensity is defined by the difference between the threshold safety factor (1) and the estimated safety factor value.

Application

The Cleveland Corral study region in the Highway 50 corridor is located in the Sierra Nevada Mountains, California, USA (Reid et al., 2003). The study area is about 22 by 28 km or 616 km². Highway 50 is a major road located between Sacramento and South Lake Tahoe in California (Spittler and Wagner, 1998). About 600 landslides were observed along the 24 km long corridor (Spittler and Wagner, 1998; Reid et al., 2003). One major catastrophic landslide occurred in 1983 (Spittler and Wagner, 1998). Since 1996, slope movement and landslides occurred infrequently during the winter months. Mapped landslide and slope movement locations are shown in Figure 5-1a. Since 1997, the United State Geological Survey (USGS) has monitored this region using real time data acquisition systems and found that elevated pore-water pressures and wet soils enhance slope movement and landslides during the winter (rainy) season (Reid et al., 2003).

Elevations in this study area range from about 902 to 2379 m. Based on the 90 m SRTM digital elevation model (DEM), slopes in this region range from 0 to 48° with 1.27% greater than 30°. This study region has considerable variability in soil texture ranging from clay loam to sandy loam (Table 5-1). The soil is predominantly sandy loam (72%). The total soil depth ranges from 0.6 to 1.4 m. The assumed potential failure plane underneath the soil layer is bed rock. Conifer and wooded grassland are the dominant land covers, 80% and 14% of the study region, respectively. Some rock outcrops were also observed along the Highway 50 corridor during the field observation.

Weather data were obtained from the National Climatic Data Centre (NCDC) from 2003 to 2006 (Table 5-1). This region has average annual rainfall, maximum temperature and minimum temperature of 1101 mm, 19.6 °C and 5.5 °C, respectively. The majority of rainfall was observed during the winter (725 mm) in this region.

The Nepal study region has distinctly different topography, soil, vegetation and climatic characteristics. Nepal has 83% mountainous terrain and the remaining 17% is southern alluvial plains. The study area is situated in Dhading, one of the seventy-five districts of Nepal. The transnational Prithvi highway connecting Kathmandu and Pokhara runs through the southern part of the district. The road parallels the Trishuli River. Landslides occur frequently in this area during the monsoon season (June to September). Numerous major landslides have occurred along the Prithvi highway over the past decade (2000 to 2008). One of the major catastrophic landslides along the Prithvi highway at Krishna Bhir was observed in August 2003 (Fig. 5-1b).

The study area is about 25 by 14 km or 350 km². Based on the SRTM DEM, elevations range from 256 to 1918 m. Slopes in this region range from 0 to 57° with 27.8% of the study region's slopes exceeding 30°. The soils are predominantly sandy clay loam (36%) and sandy loam (22%). Woodland and cropland are the dominant land covers 50% and 29% of the study region, respectively. The total soil depth ranges from 1.0 to 1.5 m. The assumed potential failure plane underneath the soil layer is bedrock.

Rainfall, temperature and wind speed measurements were obtained from the Department of Hydrology, Nepal (Table 5-1). This region is warmer and wetter than the California study region. The monsoonal season, June to September, receives 1287 mm of 1624 mm average annual rainfall.

The soil and vegetation parameter required for the three layer variable infiltration capacity (VIC-3L) hydrologic model and the slope stability model were obtained from States Soil Geographic (STATSGO) database (NRCS, USDA), Land Data Assimilation System (LDAS; Mitchell et al., 2004) and literature values. The unit soil weight (saturated and moist) was calculated based on the soil moisture, soil porosity, and specific gravity of the soil samples using methods adapted by Ray et al. (2009a). Each land cover class was assigned a root cohesion values that was adapted from Sidle and Ochiai (2006). Each soil type was assigned soil cohesion and friction angle values that were adapted from Deoja et al. (1991) and the slope of the retention curve is from Clapp and Hornberger (1978). Similarly, soil bulk density, field capacity, wilting point and saturated hydraulic conductivity values were adapted from Miller and White (1998) and Dingman (2002).

For these study regions, the VIC-3L model was applied at a daily time-step from October 2003 to September 2006 using a 0.0083° resolution. The Cleveland Corral, California, US study region has 900, 0.7 km^2 pixels and Dhading, Nepal has 450, 0.75 km^2 pixels. The VIC-3L soil moisture values were applied to the 90 m DEM pixels using a nearest neighbour approach.

Results and Discussion

Dynamic Landslide Susceptibilities

Daily safety factors were calculated for 75,988 pixels in California and 41,800 pixels in Nepal from October 1, 2003 to September 30, 2006. Based on maximum saturated conditions, each pixel was classified as stable or highly, moderately or slightly unstable. As summarized in Table 5-2, Nepal has a much greater proportion of susceptible area than California, by class, as expected.

Figure 5-2 shows the time evolution of average FS values by category for each region. There are clearly different wet seasons in California and Nepal. However, both regions show similar safety factor variations during the wet and dry seasons. Each shares a similar time evolution across susceptibility classes. The intense rainfall events during the wet season, increasing wetness in vadose zone and raising groundwater table level, rapidly decrease safety factors. The threshold line (FS =1) shows when a typical hazard prone area becomes unstable. In California, a region is typically unstable (FS<1) for a short period of time. In Nepal, once regions become unstable they tend to stay unstable for the remainder of the monsoon season.

Annual and wet season descriptive statistics, mean, standard deviation and skew were calculated for each pixel. The results, averaged by susceptibility class, are shown in Table 5-2. The average, standard deviation (SD) and coefficient of variance (CV) of the estimated safety factors are lower during the wet season than the entire season. Those same statistical parameters are lower in Nepal than California. The SD increases with

decreasing susceptibility, but the CVs are nearly identical for all susceptible classes. The safety factor values vary less during the wet season than on an annual basis. The negative and positive skewnesses during the annual period and wet season, respectively, at each susceptibility class suggest that there are two distinct populations of safety factors.

For the highly susceptible class, the variability among susceptible locations was quantified. With the exception of skewness, the variability appears to be consistent across the wet season and the annual period as well as between locations. The variability decreases in California during the wet season, but increases in Nepal. Figure 5-3 shows the range of safety factor in each susceptible class at both study regions. Results show higher median, maximum, minimum and range of safety factors in California than Nepal.

Figures 5-4 and 5 show the spatial distribution of CV values for all susceptible classes. Relative variability differs by location and there is some spatial structure. The California study region has a higher CV throughout the study area as compared to Nepal. Due to this higher relative variability, California may have less susceptible area than Nepal. Coincidentally, both study regions have a highway and a stream passing through the center of the study region. However, CVs along the highway are completely different in each region. In Nepal, the southern region along the highway consists of steep terrain whereas the northern region consists of flat terrain including the river. Figure 5-5 shows very low CV values along the stream and highway with higher CV values along the steep terrain. In similar terrain, the California study region does not have a reduced CV along the highway and stream. This suggests that there is little influence of the stream or highway presence on stability variations if slope is not steep. The California study region

has lower CV values in the highly susceptible class (Fig. 5-4) near to the natural water body (Mapped landslide no. 1).

Susceptibility Distribution and Probability Analysis

Because landslides mainly occur during the wet season, this section further examines safety factor distributions during the wet season. The L-moment diagram, τ_3 versus τ_4 , for highly susceptible pixels does not match any of the plotted distributions (Fig. 5-6). However, the safety factor distribution in California shows three distinct populations. The two populations having a relatively high kurtosis and following a generalized pareto distribution are located near the natural water body. The remaining sections have a different, but distinct pattern with much lower kurtosis. In Nepal, kurtosis was constant and skew varied from 0.15 to 0.34. No specific distribution was identified for this region.

The cumulative distribution function (CDF) plot also shows that safety factor distributions differ by region (Fig. 5-7). Nepal has a much higher probability of highly susceptible pixels being unstable at any time in the wet season than California. Nepal's region has higher probability of being unstable than California. In Nepal, there is almost a 95% probability that the estimated safety factor will be under the FS = 1, 1.25 and 1.5 class delineations during the wet season. In contrast, California has a 70% chance of the FS being below the critical value.

Transitional (crossing properties) Characteristics of Landslide Susceptibilities

This section describes the spatiotemporal susceptibility characteristics for highly susceptible locations. For each location, the number of threshold crossings and the average duration of all crossing were determined. The crossing duration is the number of days that a pixel is unstable during a single crossing. A crossing is a transition from stable to unstable.

Figure 5-8 shows that the median duration under the threshold is less in California than Nepal whereas the median number of crossings are same in Nepal and California. 25% of Nepal's highly susceptible pixels have more than 9 numbers of crossings and less than 20 days of average duration per year. California has no pixels with more than 9 crossings in a year. 25% unstable pixels in California have sustained unstable conditions exceeding 100 days annual. This may be the primary reason why California has frequent slope movements and less slope failures and Nepal has frequent slope failures and no routine slope movements during the wet season.

Figure 5-9 shows the individual relationships among number of crossings, average duration and mapped landslide under threshold value. Both regions show a nonlinear decrease in duration with increasing crossings. Nepal's relationship is well defined ($R^2 = 0.69$) by the power law function, $y = 365x^{-0.43}$ where y is the duration and x is the number of crossings. This shows a strong correlation between duration and number of crossings for each pixel. For the equivalent number of crossings, California's locations typically have shorter durations than Nepal, but are within the Nepal range. This further explains why Nepal has frequent slope failures, while California has fewer failures and more frequent slope movements. This result is further supported by the findings of Lan et

al. (2005) who found that while some slopes can fail rapidly, others can take a long time to fail under similar saturation.

Landslide locations were mapped in each region (Figs. 5-4 and 5). Interestingly, most of these highly susceptible pixels and mapped landslides have frequent crossings and short duration unstable conditions at each study region. Of the 10 mapped landslides in California, 7 of them have short duration unstable conditions and frequent crossings. In Nepal, 11 out of the 12 slide locations have short unstable conditions and frequent crossings. The physical characteristics of the mapped landslides locations in each region are presented in previous chapter (Table 4-4a and b). A gradual decrease or increase of stress over time that causes stress relaxation can be a possible reason for slope failure with frequent crossings. This fact is further supported by the findings of Borzdyka (1974) who observed failure in material due to cyclic relaxation stress.

Crossing properties are mapped in Figures 5-10 and 11. While Nepal's region has a uniform distribution of crossing frequencies, California differs by area. Along California's highway, crossings are more frequent than in the northwest region. Physically, Nepal has no specific locations of steeper terrain whereas California has steeper terrain along the highway and in the northwest portion of the study region. These differences may be caused by different physical characteristics and distributions of the geotechnical variables and the hydrological variable distributions between regions. In California, the northwest region has longer susceptible periods, but fewer crossings than along the highway. Interestingly, frequent slope movements were observed (by USGS) along the highway, but not in the Northwest region.

Conclusion

An infinite slope stability model coupled with a hydrologic model was used to develop dynamic landslide susceptibility maps in Cleveland Corral, California, US and Dhading Nepal. The mean, standard deviation, skew and coefficient of variation of safety factors were estimated to characterize the temporal variability and distribution of safety factors. The statistical results show higher relative variability in California than Nepal. Both study regions have positive skewnesses, however, for the wet season, Nepal's safety factors are more positively skewed than California's. The results show a strong relationship between the variability in susceptibility and slope failures. The Nepal study region, which has low spatial and temporal variability in susceptibility, is more prone to failure than California.

The L-moments plot showed that there is a consistent safety factor distribution with small variations in kurtosis for Nepal. On the other hand, the California region appears to have two distinct probability distributions. One distribution clearly follows the generalized pareto distribution whereas the other distribution requires further analysis to define a distribution.

Based on the transition properties of safety factor values, both regions' median number of crossing is 5. This indicates a tendency to frequently transition between stable and unstable conditions. A strong relationship was observed between the number of crossings and the average duration, which follows a power law. Results also show that the safety factors may fluctuate around the critical threshold, but not necessary fail. This

study provides preliminary insights as to how slopes reach and sustain potential hazardous conditions not revealed by previous static spatial distribution studies.

Table 5-1: Soil, vegetation and slope characteristics of the California and Nepal study regions

	California	Nepal
	Area (%)	
Land cover		
Evergreen forest	3.3	1.0
Conifer	79.9	-
Deciduous forest	2.7	-
Woodland	-	50.3
Wooded grassland	14.1	18.2
Grassland	-	1.7
Cropland	-	28.8
Soil texture		
Loamy sand	-	16.2
Sandy loam	72.0	22.5
Loam	16.0	9.8
Sandy clay	3.0	15.0
Sandy clay loam	-	36.5
Clay loam	9.0	-
Slope (°)		
0-15	71.2	19.0
15-30	27.5	53.2
30-45	1.2	27.0
45-60	0.0	0.8
Climate		
Average Annual Rainfall (mm)	1101	1624
Average Rainfall Wet Season (mm) (Jan-May, CA and Jun-Sep, Nepal)	725	1287
Average Daily Max. Temperature (°C)	19.6	27.0
Average Daily Min. Temperature (°C)	5.5	16.6

Table 5-2: Safety factor statistics for the 2003-2006 study period and wet season (Jan to May) for California and (Jun to Sep) for Nepal. Parentheses indicate standard deviation. Classifications are based on maximum modeled susceptibility on May 8, 2005 for California and August, 18, 2004 for Nepal

Statistical Parameter	California			Nepal		
	Highly Susceptible	Moderately Susceptible	Slightly Susceptible	Highly Susceptible	Moderately Susceptible	Slightly Susceptible
Area (%)	0.49	1.67	2.87	11.59	23.30	21.12
Number of Pixels	339	1161	1993	4748	9545	8653
Annual						
Average	1.09 (0.12)	1.44	1.75	1.02 (0.13)	1.30	1.57
Std Dev	0.14 (0.03)	0.18	0.23	0.11 (0.03)	0.12	0.14
Skew	0.03 (0.23)	-0.05	-0.05	-0.09 (0.05)	-0.09	-0.09
CV	0.13 (0.02)	0.12	0.13	0.10 (0.03)	0.09	0.08
Wet Season						
Average	0.98 (0.10)	1.29	1.56	0.92 (0.11)	1.19	1.43
Std Dev	0.08 (0.02)	0.11	0.13	0.04 (0.01)	0.05	0.06
Skew	1.10 (0.19)	1.10	1.12	1.37 (0.14)	1.39	1.39
CV	0.08 (0.02)	0.09	0.09	0.05 (0.01)	0.04	0.04

* CV = Coefficient of Variance

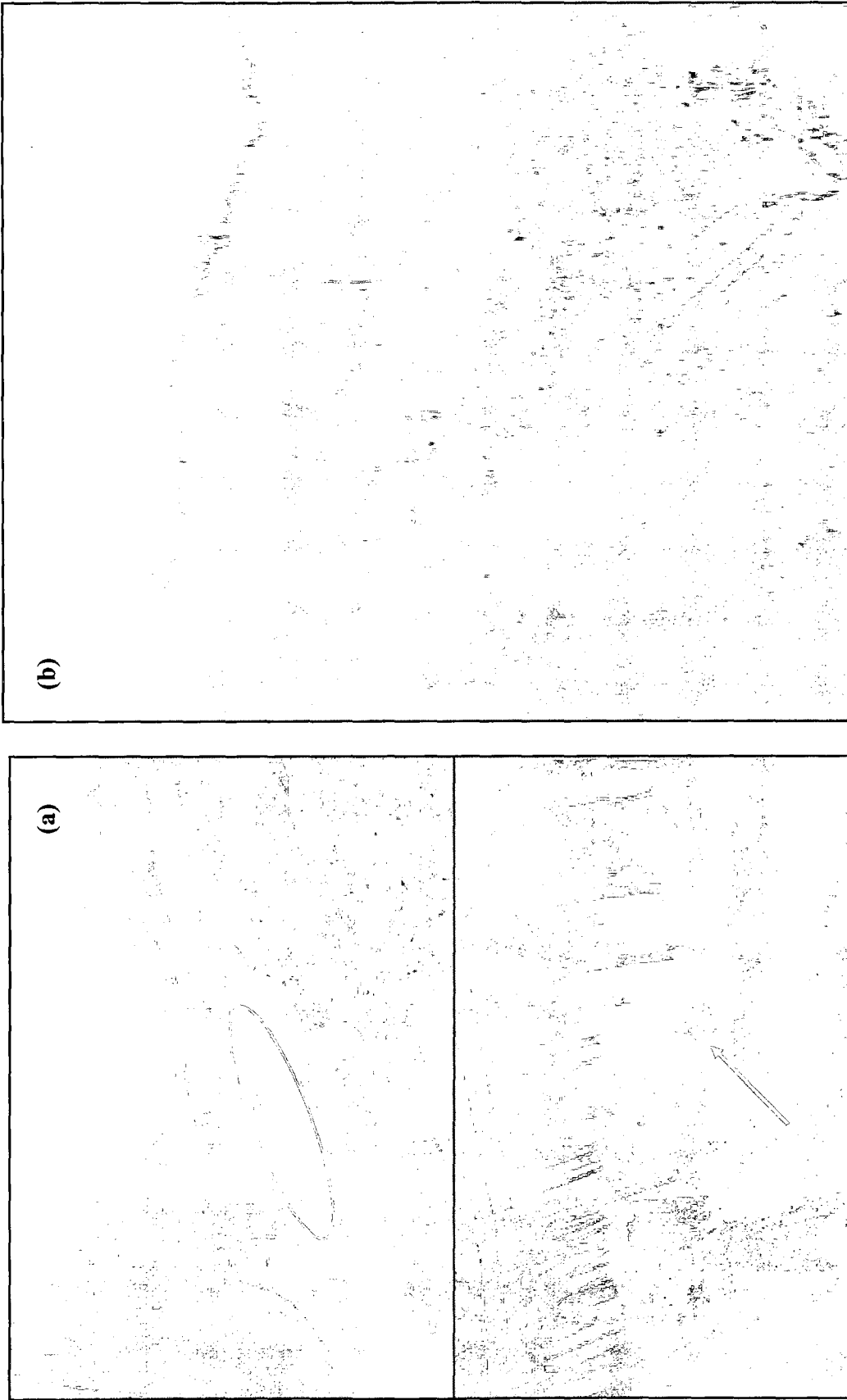


Figure 5-1: (a) Mapped landslide (top) and slope movement (bottom) locations at Cleveland Corral, California in 2006 and (b) a major catastrophic landslide along Prithvi Highway, Nepal (Picture was taken in August, 2003)

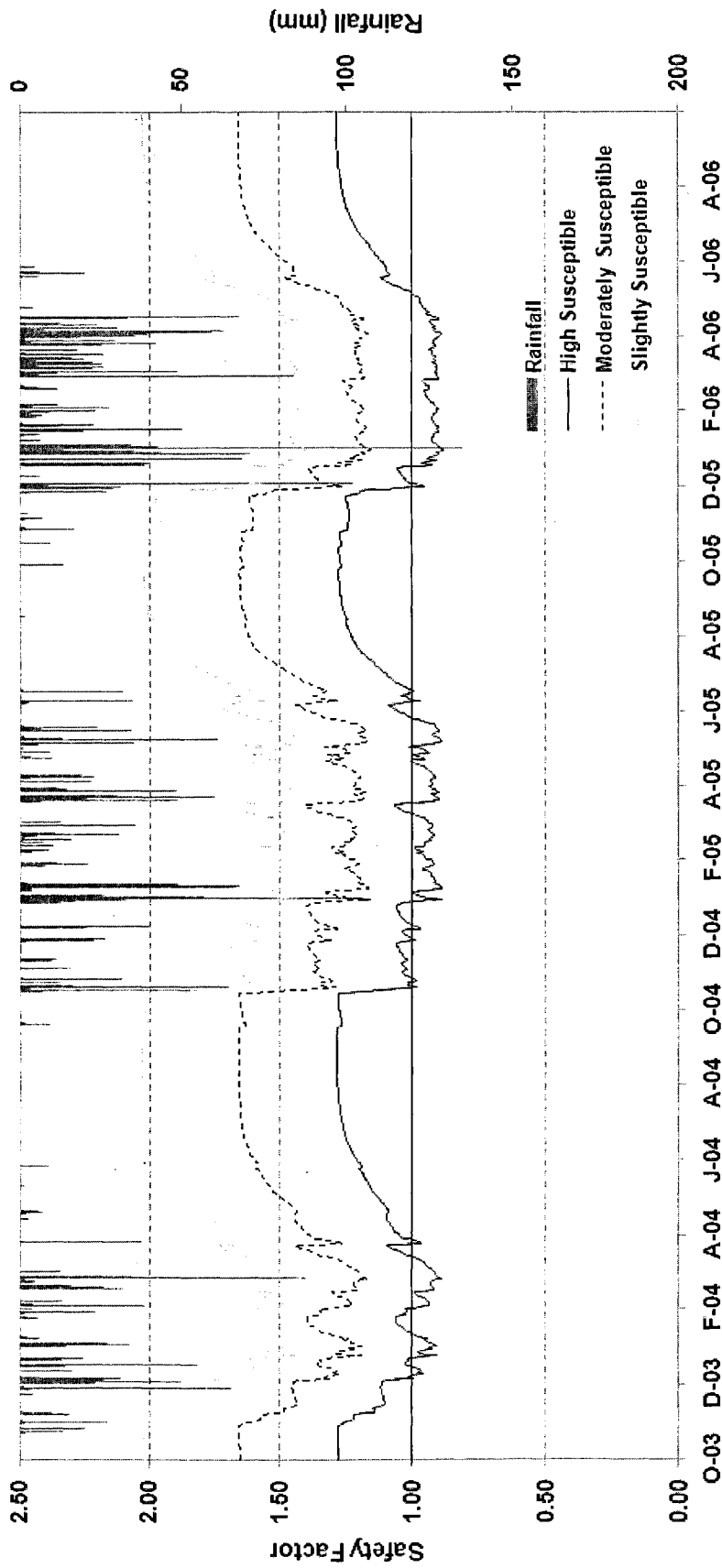


Figure 5-2a: Average safety factors and rainfall distribution by susceptibility class at the Cleveland Corral, California, US study region

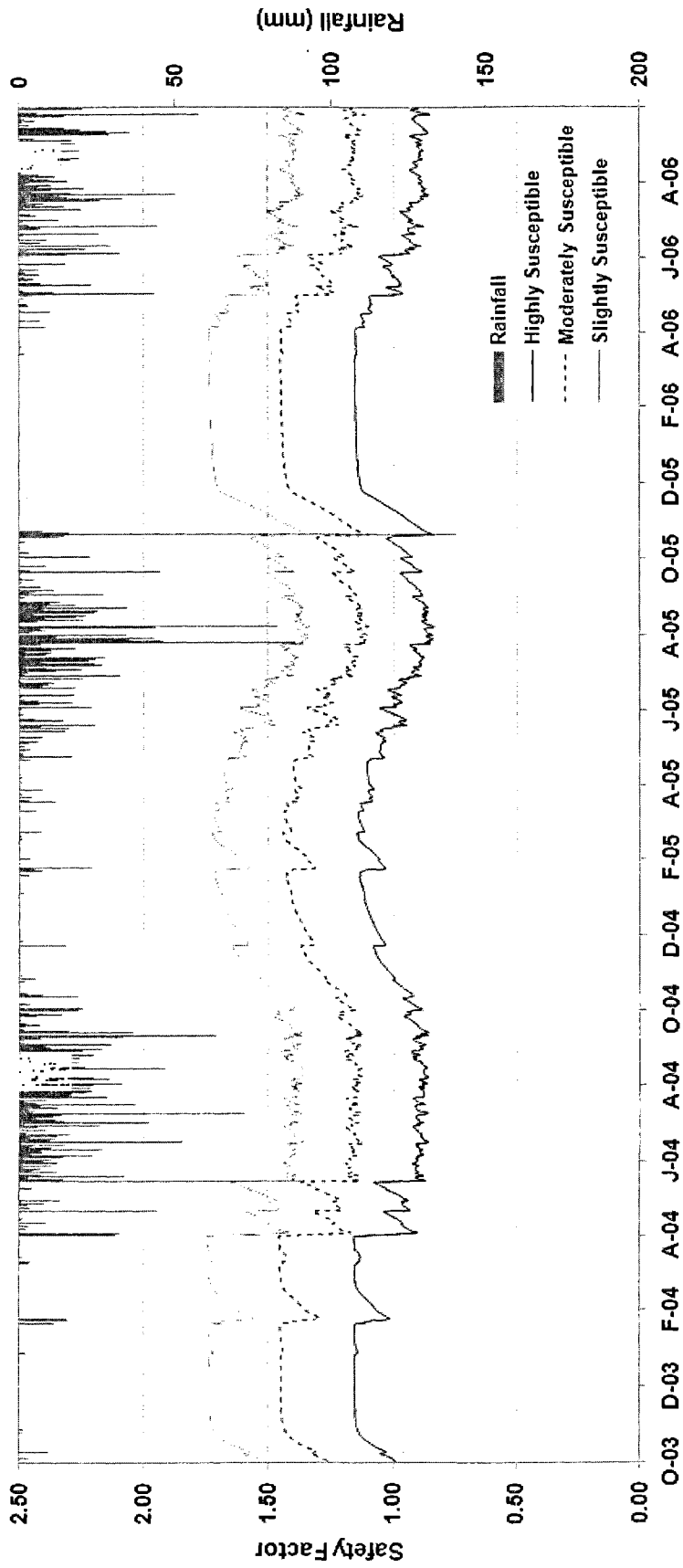


Figure 5-2b: Average safety factors and rainfall distribution by susceptibility class at the Dhading, Nepal study region

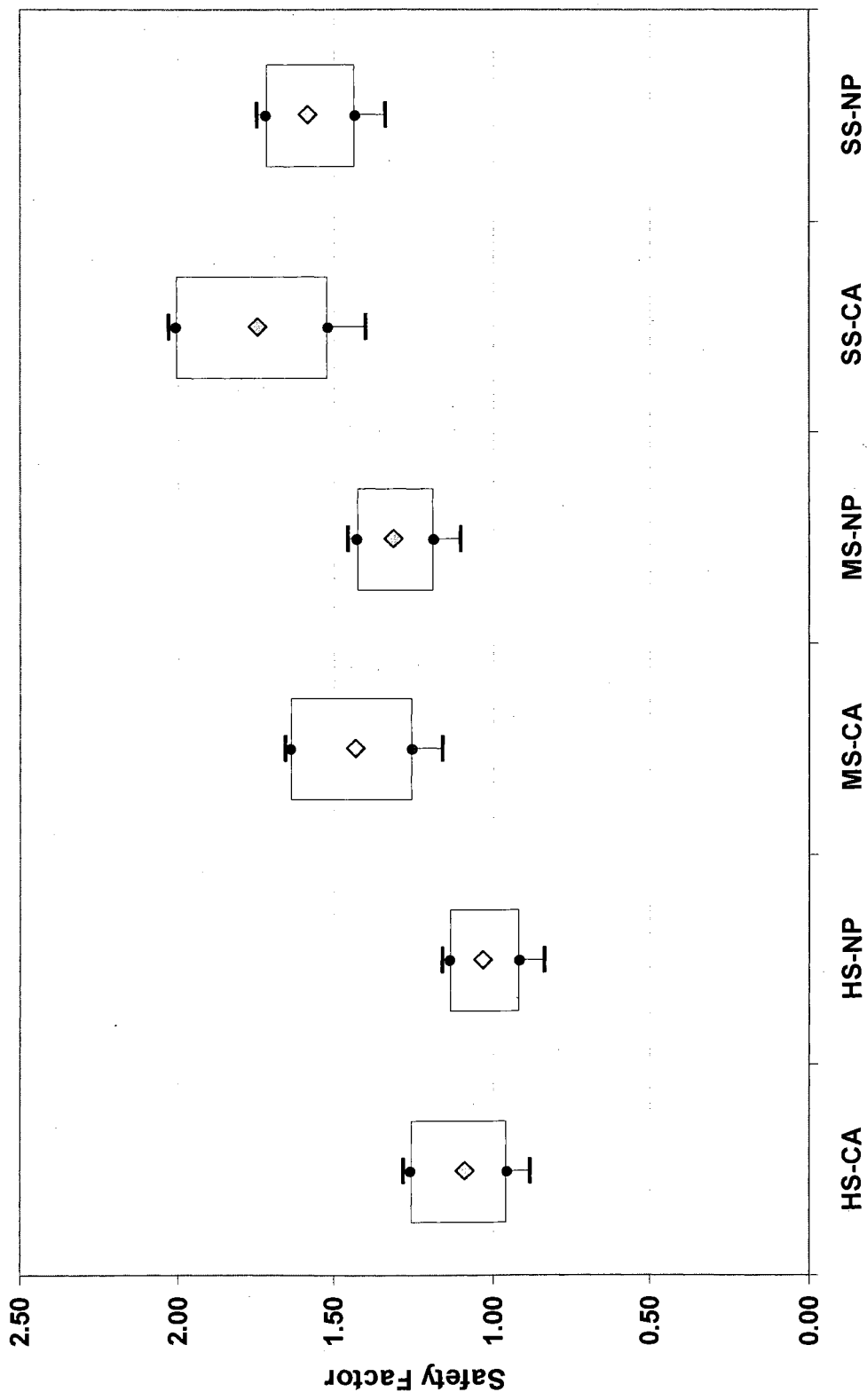


Figure 5-3: The quantile box-plots of daily annual safety factors for both study regions. HS = Highly susceptible, MS = Moderately susceptible, SS = Slightly susceptible, CA = California, NP = Nepal

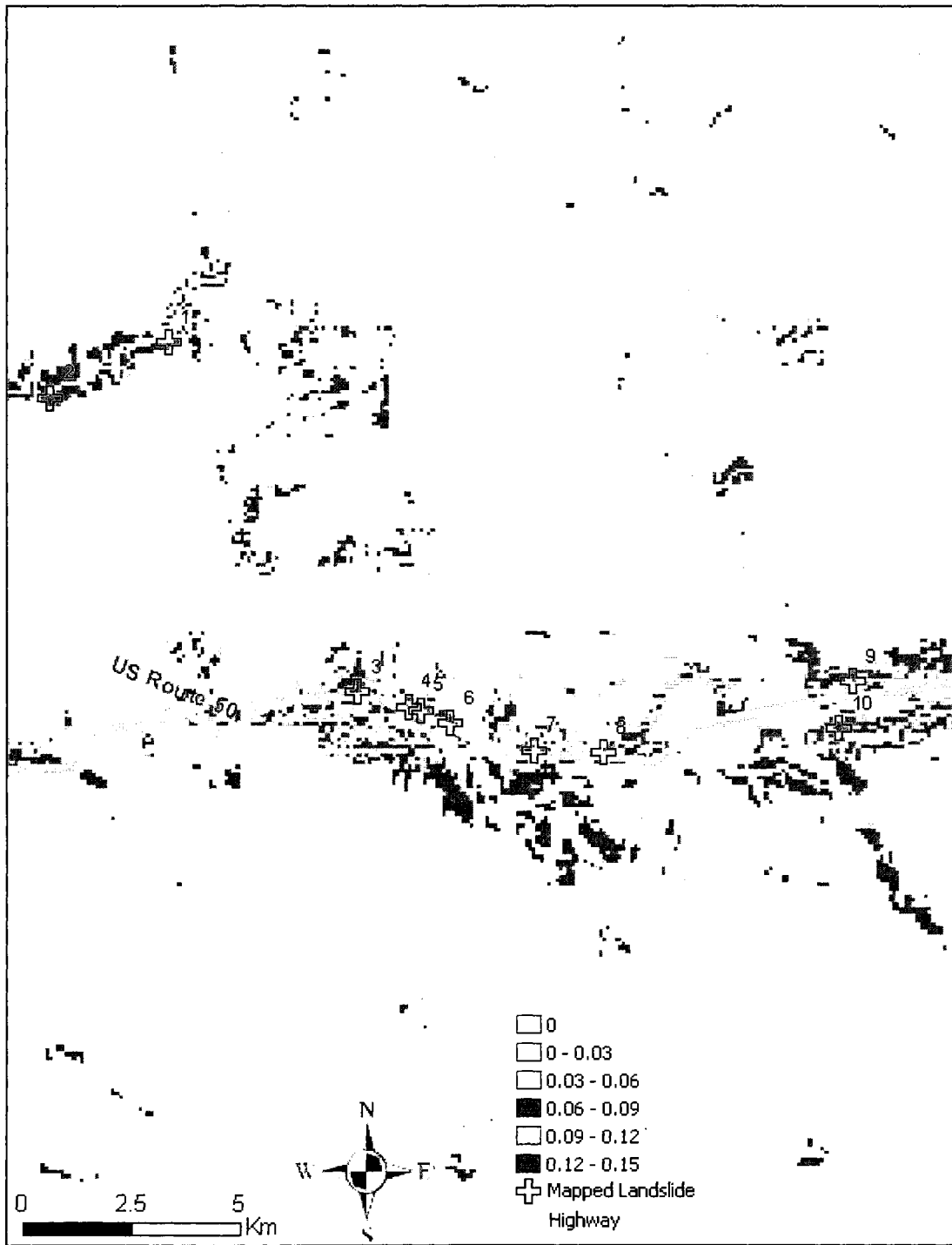


Figure 5-4: The coefficient of variance (CV) for all susceptible classes during the wet season, in Cleveland Corral, California, US. Zero represents stable class

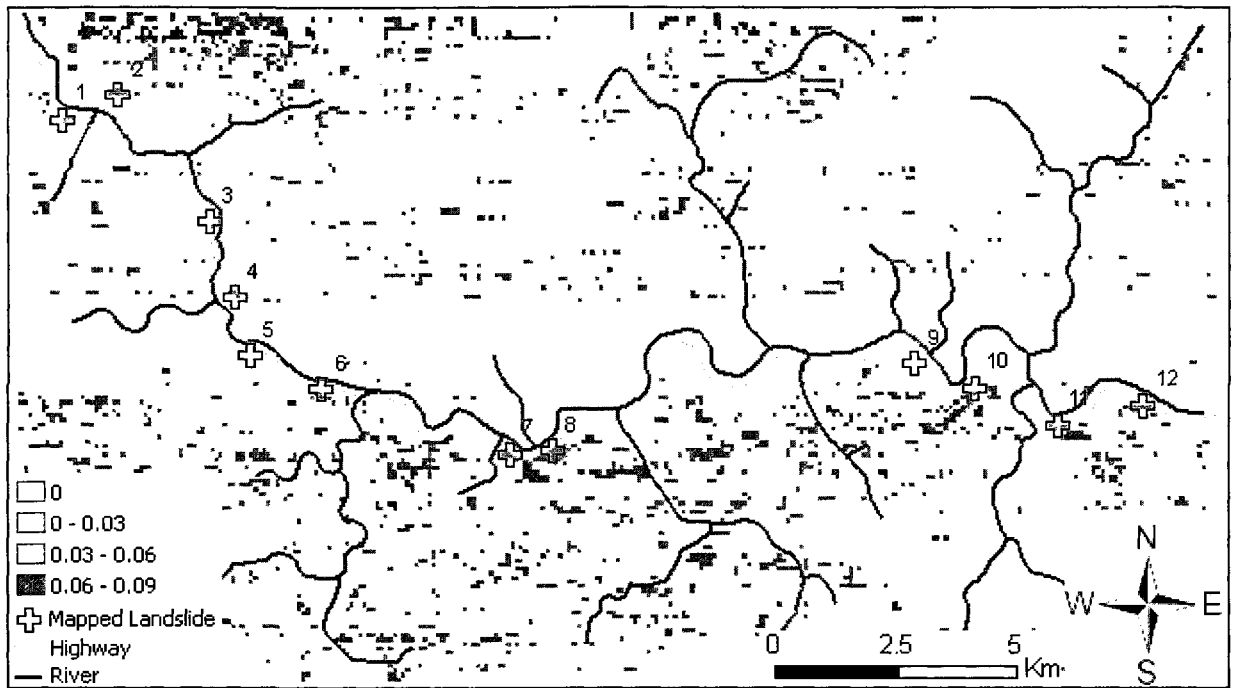


Figure 5-5: The coefficient of variance (CV) for all susceptible classes during the wet season in Dhading, Nepal. Zero represents stable class

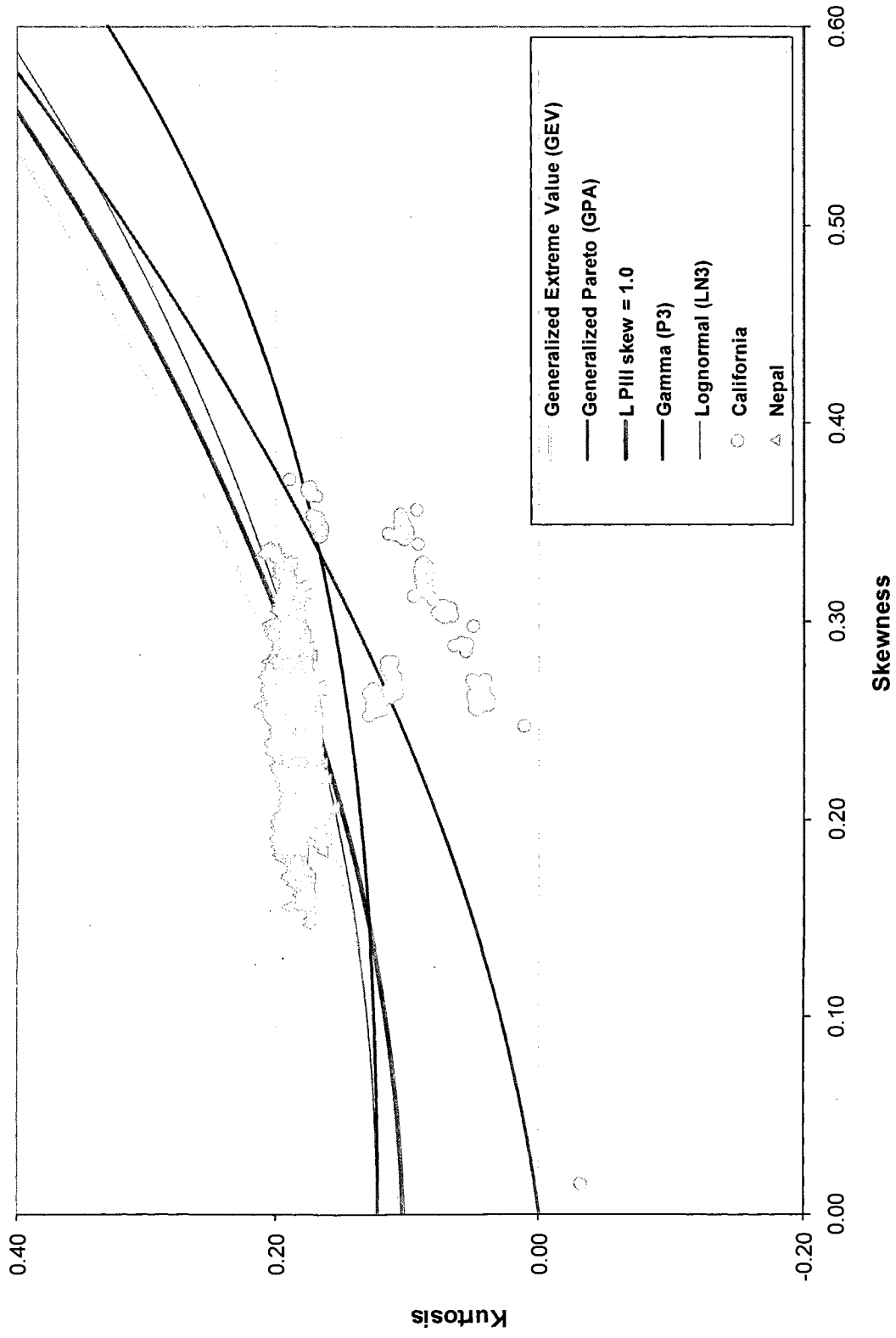


Figure 5-6: L-moment diagrams for each highly susceptible location by region and potential probability distribution functions during the wet season

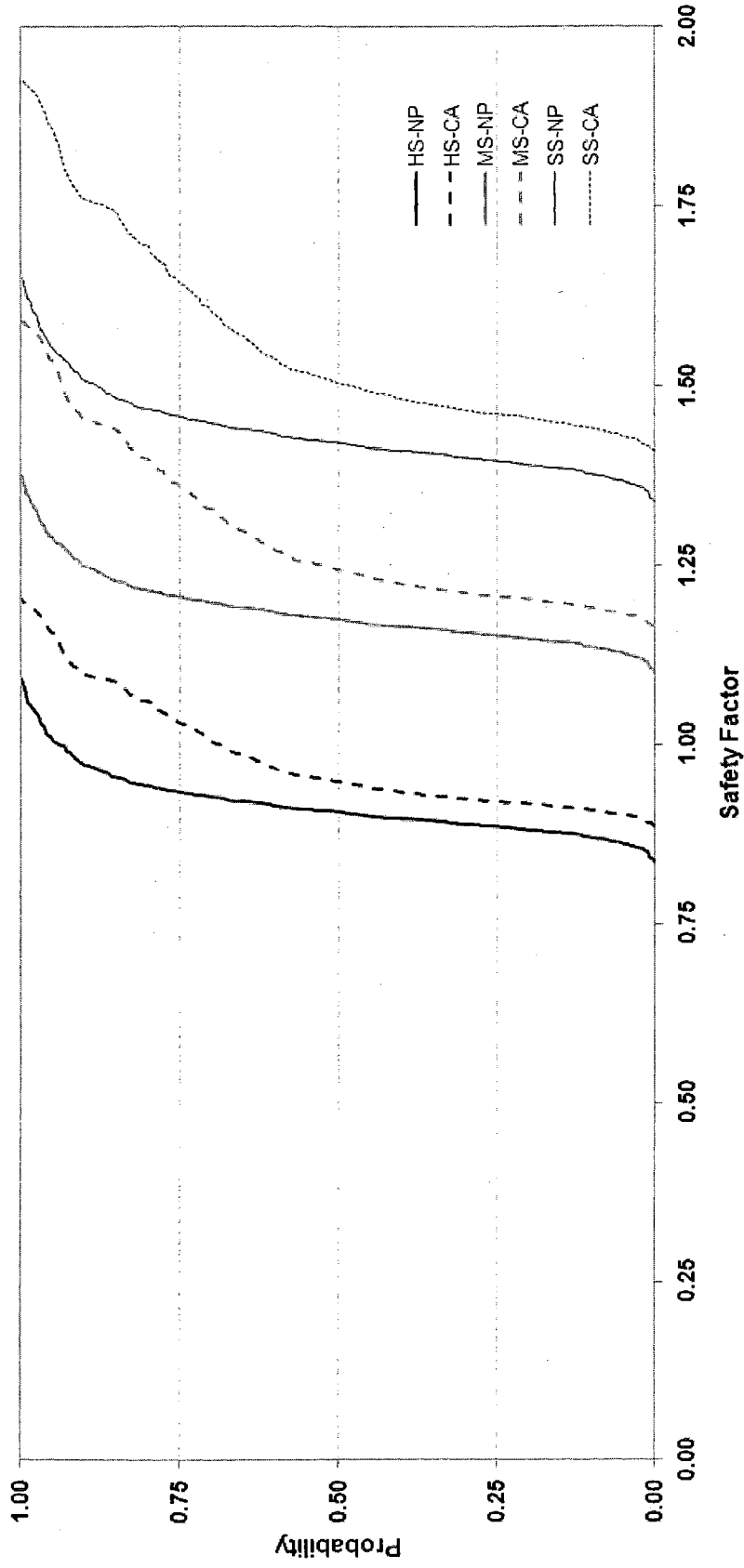


Figure 5-7: The cumulative distribution function (CDF) of daily safety factors at each region during the wet season. HS = Highly susceptible, MS = Moderately susceptible, SS = Slightly susceptible, CA = California, NP = Nepal

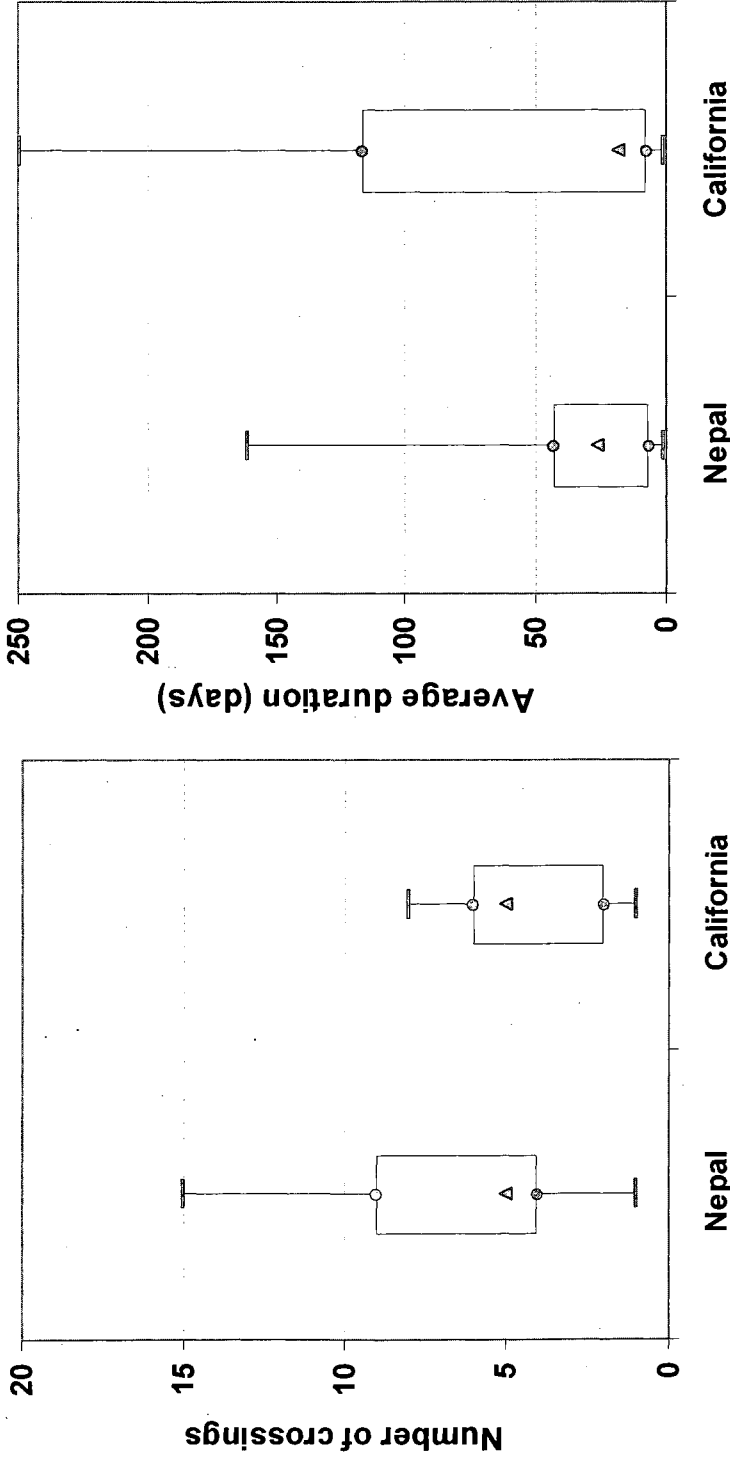


Figure 5-8: The quantile box plots of number of transitions (crossings) below the safety factor threshold value and the average duration that the safety factor stayed below by threshold at each region (Complete year)

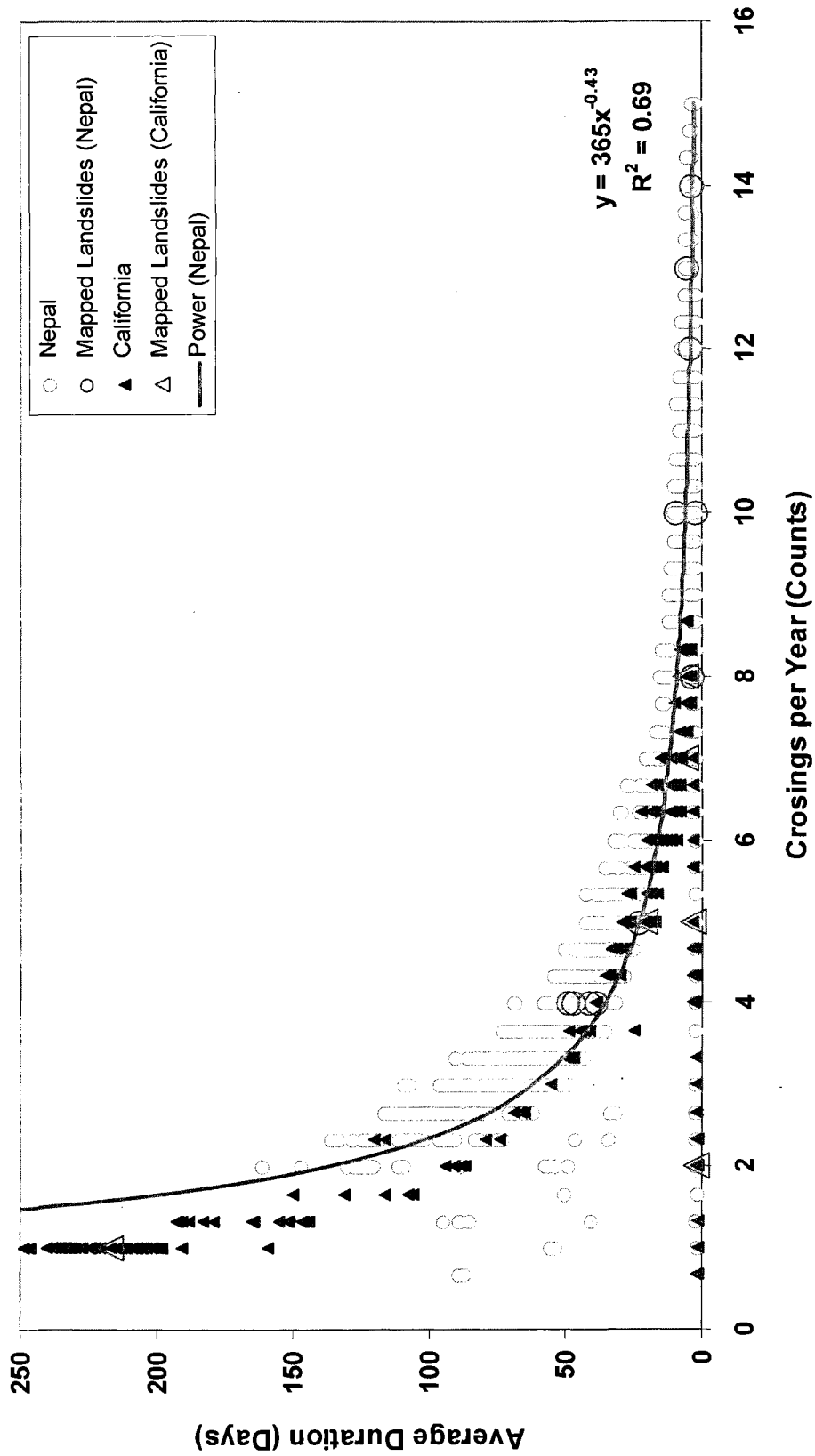
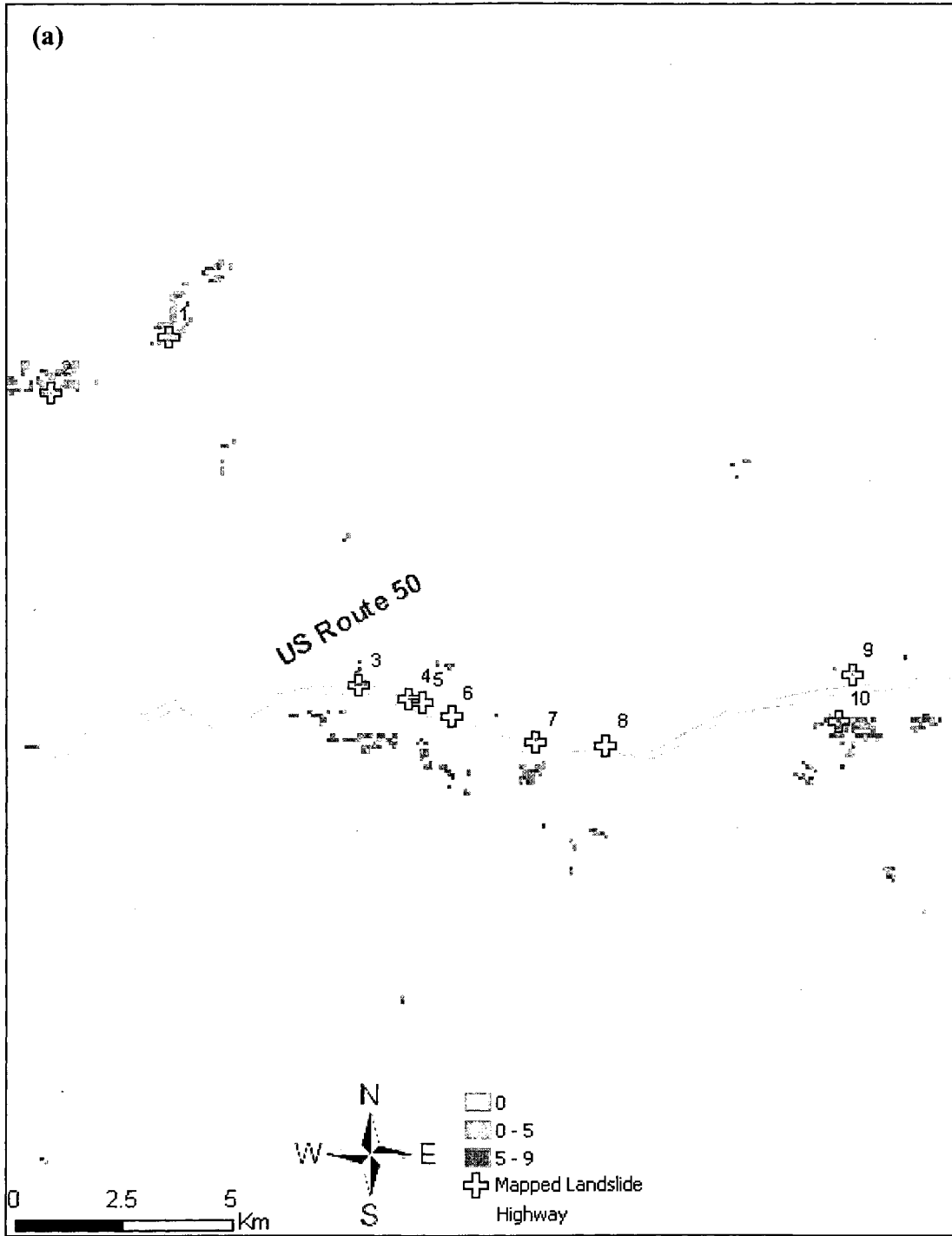


Figure 5-9: Average duration versus the number of annual crossings for each highly susceptible pixel and mapped landslides at California, US and Dhading, Nepal



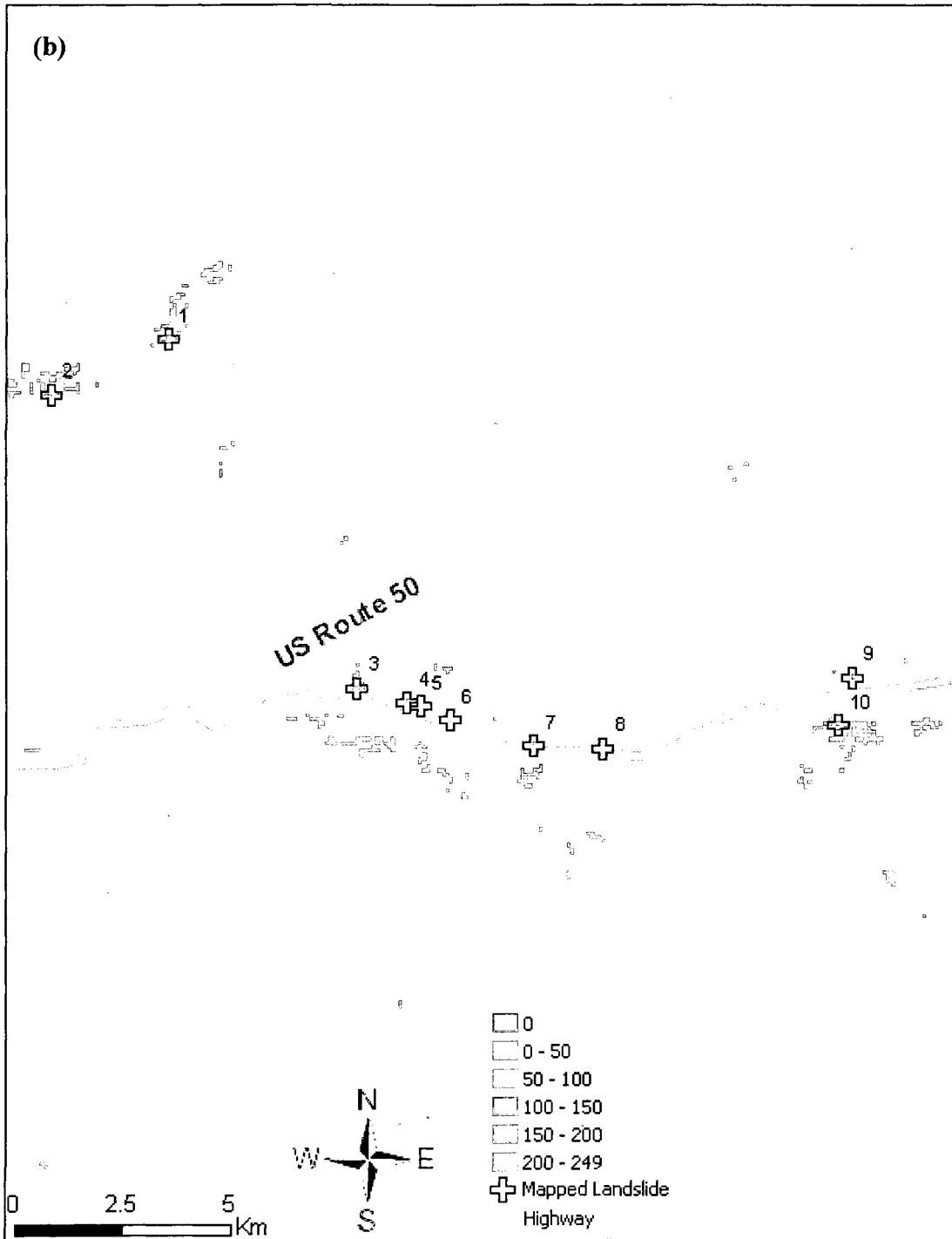


Figure 5-10: (a) Number of annual crossings below the threshold safety factor and (b) average duration (days) below threshold for highly susceptible location from Oct. 2003 to Sep. 2006 in California, US

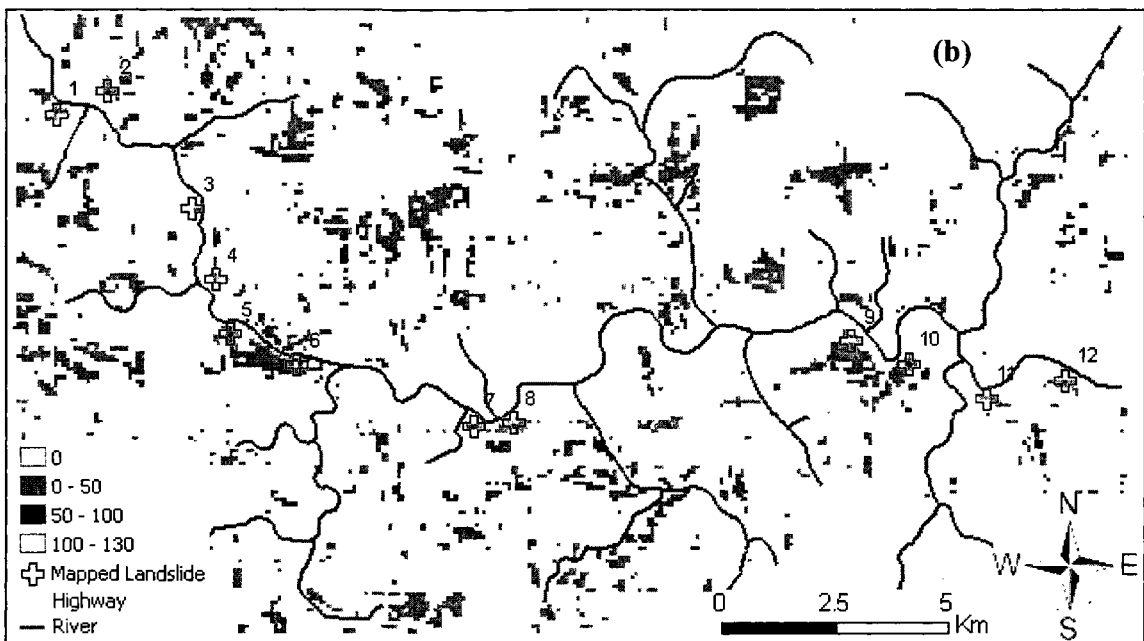
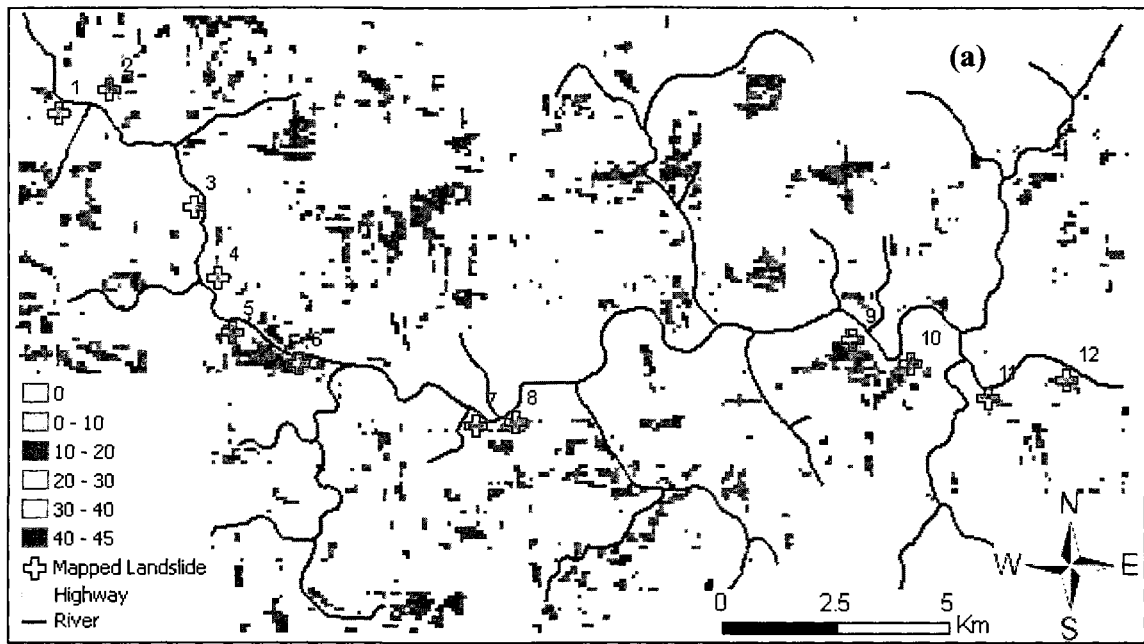


Figure 5-11: (a) Number of annual crossings below the threshold safety factor and (b) average duration (days) below threshold for highly susceptible location from Oct. 2003 to Sep. 2006 in Dhading, Nepal

CHAPTER 6.

LANDSLIDE SUSCEPTIBILITY MAPPING USING DOWNSCALED AMSR-E SOIL MOISTURE: A CASE STUDY FROM CLEVELAND CORRAL, CALIFORNIA, US

Abstract

Remotely sensed data are widely used for landslide analysis. A dynamic physically-based slope stability model that requires soil moisture can be driven by remote sensing products from multiple Earth observing platforms. This research compares slope stability maps using the advanced microwave scanning radiometer (AMSR-E) surface soil moisture with the variable infiltration capacity (VIC-3L) model's soil moisture at Cleveland Corral landslide area in California, US. Despite snow cover influences on AMSR-E surface soil moisture estimates, results show a strong relationship between AMSR-E's surface soil moisture and VIC-3L modeled soil moisture. Results match the location and extent of landslide prone regions with the two methods. Under the maximum saturation scenario, 0.40 and 0.49% of the study area was highly susceptible for AMSR-E and VIC-3L model, respectively. Preliminary results show that AMSR-E soil moisture, coupled with a slope stability model, is viable for rainfall induced slope stability analysis at a regional or global scale.

Introduction

Remote sensing and spatial analysis tools are widely used in landslide studies including landslide detection, landslide assessment, natural hazard, landslide mapping, and landslide inventories (e.g., Varnes, 1984; van Westen, 1994; Guzzetti et al., 1999; Gorsevski et al., 2003; Pradhan et al., 2006). Remote sensing data can be used to predict catastrophic events and hazardous areas (Ostir et al., 2003) and they have significant potential in landslide studies (Hong et al., 2007). Landslide inventory maps can be developed using aerial photography (Oka, 1998; Brardinoni et al., 2003; van Western and Getahun, 2003) as well as remotely sensed data with image analysis technique (Nichol and Wong, 2005; Abdallah et al., 2007). Over the past decade, the Earth Observing System (EOS) platforms have deployed a suite of instruments that monitor land conditions relevant to landslide hazard characterization such as Light Detection and Ranging (LiDAR), Interferometric Synthetic Aperture Radar (InSAR), and Differential SAR Interferometry (DInSAR) data. Multi-temporal satellite imagery is increasingly used to monitor, classify and detect landslides (Mantovani et al., 1996; Hervas et al., 2003; Cheng et al., 2004).

For landslide analyses, Landsat TM and Advanced Spaceborne Thermal Emission and Reflection Radiometer (ASTER) have been used to derive land cover in regions including the Himalayas range (Zomer et al., 2002, Saha et al., 2002; Sarkar and Kanungo, 2004). InSAR has been used to locate and characterize landslides (e.g., Canuti et al., 2004; Singhroy and Molch, 2004). Kaab (2005) showed that recent

Shuttle Radar Topography Mission (SRTM) results are promising for characterizing topography in regions having landslides.

Pelletier et al. (1997) indicated that continuous remote-sensing of soil moisture coupled with a digital elevation model is a necessary component of a successful landslide hazard mitigation program. Their work suggests the replacement of soil moisture surrogates that have been used extensively in slope stability analyses. Typically, slope stability is analyzed using wetness indices to estimate soil wetness (Montgomery and Dietrich, 1994; Van Westen and Terlien, 1996; de Vleeschauwer and De Smedt, 2002; Acharya et al., 2006). As pointed out by Rosso et al. (2006), these approaches neglect the presence of soil moisture in the upper soil layer above the groundwater table or indirectly estimate the soil moisture. Existing studies do not directly account for the temporal evolution of soil moisture prior to and during the rainfall events. Nevertheless, it is necessary to link the surface soil moisture to the subsurface layer because landslides are not triggered only by surface layer saturation; rather, it is the combined effect of surface and subsurface saturation that is critical (Ray and Jacobs, 2007). Ray et al. (2009a) enhanced wetness index model provides a means to apply vadose zone soil moisture. While they used modeled soil moisture, remotely sensed soil moisture data are a potentially viable alternative to modeled data.

Satellite remote sensing can provide surface soil moisture at national and global scales. While no landslide studies thus far have used remotely-sensed soil moisture data, the Advanced Microwave Scanning Radiometer (AMSR-E) has the potential to characterize soil moisture profiles for this purpose. Numerous studies (e.g., Njoku et al., 2003; Walker et al., 2004; Lacava et al., 2005; Njoku and Chan, 2006; Gao et al., 2006)

have shown that microwave remote sensing measurements including AMSR-E are affected by surface roughness, topographic features, dense vegetation and soil texture. This indicates that soil moisture data may have limited value on steep topography (Njoku et al., 2000). The few validation experiments, such as Soil Moisture Experiments 2004 (SMEX04) in northern Sonora, Mexico (Vivoni et al., 2008; Jackson et al., 2008), that have been conducted on such terrain show that rocky slopes can mask the moisture signal.

In addition to the aforementioned limitations, there are two other significant challenges to using AMSR-E data. The current remote sensing products can only measure the soil moisture at an upper thin surface of the Earth from 0 to 5 cm (Jackson et al., 1995; Schmugge et al., 2002). This thin layer soil moisture information may not truly represent the entire soil moisture profile underneath thick soil layer (sub surface) above the bed rock. In addition, AMSR-E processed data have a 25 km spatial resolution. This is quite coarse for landslide studies even at regional and global scales. Therefore, it may be necessary to downscale the low resolution AMSR-E soil moisture to a finer scale. A simple downscaling approach for remotely sensed soil moisture was developed by Chauhan et al. (2003) and enhanced by Yu et al. (2008). They found the significant relationship among soil moisture based on normalized vegetation index (NDVI), albedo and land surface temperature (LST) to be useful in downscaling soil moisture data.

This research tested the AMSR-E product's ability to provide the vadose zone soil moisture estimates necessary to dynamically map landslide susceptibility. The study region, Cleveland Corral, California, US, is an active hazard area. The research objectives of this paper are (1) to compare AMSR-E and variable infiltration capacity

(VIC-3L) surface soil moisture, and (2) to analyze the impacts in landslide susceptibility map using AMSR-E and VIC-3L surface soil moisture. Results consider AMSR-E 25 km pixels as well as downscaled 1 km pixels.

Theoretical Approach

Slope Stability Model

This study uses the modified infinite slope stability model (Ray et al., 2009a) to quantify landslide susceptibility including the vadose zone soil moisture and groundwater effects. The infinite slope method (Skempton and DeLory, 1957), widely applicable for shallow slope stability analysis, calculates safety factors as the ratio of resisting forces to driving forces. The infinite slope stability model as adapted by the several researchers is

$$FS = \frac{C_s + C_r}{\gamma_e H \sin \theta} + \left(1 - m \frac{\gamma_w}{\gamma_e} \right) \frac{\tan \phi}{\tan \theta} \quad (6-1)$$

where C_s and C_r are the effective soil and root cohesion [kN/m^2], γ_e is the effective unit soil weight [kN/m^3], H is the total depth of the soil above the failure plane [m], θ is the slope angle [$^\circ$], m is the wetness index [adimensional], ϕ is the angle of internal friction of the soil [$^\circ$], γ_w is the unit weight of water [kN/m^3]. The effective unit weight is estimated as

$$\gamma_e = \frac{q \cos \theta}{H} + (1 - m) \gamma_m + m \gamma_s \quad (6-2)$$

where q is any additional load on the soil surface [kN/m^2] and γ_m is moist unit soil weight [kN/m^3] for the unsaturated soil layer.

The wetness index model follows Ray et al. (2009a) given as

$$m = \frac{h + (H - h) * \frac{\theta_s}{\eta}}{H} \quad (6-3)$$

where h is the saturated thickness of the soil above the failure plane [m], θ_s is the volumetric soil moisture [cm^3/cm^3] and η is the porosity [cm^3/cm^3].

The estimated FS values were used to categorize slopes into stability classes using Pack et al. (1998) and Acharya et al.'s (2006) stability classification system. Our four susceptibility classes, used to develop landslide susceptibility map, are highly susceptible ($\text{FS} \leq 1$), moderately susceptible ($1 < \text{FS} < 1.25$), slightly susceptible ($1.25 < \text{FS} < 1.5$) and not susceptible (stable) ($\text{FS} \geq 1.5$).

Land Surface Model (VIC-3L)

This study used Ray et al.'s (2009b) VIC-3L model results for the Cleveland Corral, California study region as an independent measure of the soil moisture profile. The VIC-3L hydrologic model is a three-layer land surface model (Liang et al., 1994) that has been widely applied for surface runoff generation and soil moisture profile estimation (Liang and Xie, 2003). The model's soil column has three layers (Parada and Liang, 2004). The top, thin soil layer and the middle soil layer characterize the dynamic response of the soil to weather and rainfall events. The lowest layer captures the seasonal soil moisture behavior (Liang et al., 1996; Huang and Liang, 2006) and only responds to rainfall when the upper layer is wet. The VIC-3L model also provides a spatial representation of land cover. Each land cover has a leaf area index (LAI), minimum stomatal resistance, roughness length, displacement length and relative fraction of root

(Liang et al., 1994; Nijssen et al., 1997). Details about the VIC-3L model application are described by Ray et al. (2009b).

Downscaling

For application to the infinite slope stability model, the AMSR-E soil moisture can be used directly or downscaled. A linear or non-linear regression approach can be used to downscale the AMSR-E data from 25 to 1 km spatial resolution (Chauhan et al., 2003; Yu et al., 2008). Yu et al. (2008) found that it is possible to downscale AMSR-E soil moisture from 25 to 1 or 5 km spatial resolution using NDVI, albedo and LST. This paper uses their linear regression approach to downscale the AMSR-E soil moisture from 25 to 1 km spatial resolution.

The general downscaling approach proposed by Chauhan et al. (2003) and applied by Yu et al. (2008) is

$$\theta_s = \sum_{i=0}^{i=n} \sum_{j=0}^{j=n} \sum_{k=0}^{k=n} a_{ijk} V^i T^j A^k \quad (6-4)$$

where V is the NDVI, T is the LST and A is the albedo (1 km). The equation is applied with $n = 1$, yielding a simple linear equation with interaction terms

$$\theta_s = a_{000} + a_{001} A + a_{010} T + a_{100} V + a_{011} T A + a_{101} V A + a_{110} V T \quad (6-5)$$

The AMSR-E (25 km) values and the NDVI, LST and albedo values, aggregated to a 25 km resolution, are used to determine the regression coefficients for the linear regression model. Yu et al. (2008) aggregated the 1 km NDVI, LST and albedo products to 25 km spatial resolution by

$$V_{25} = \frac{\sum_{i=1}^n \sum_{j=1}^m V_{ij}}{mn}, \quad T_{25} = \frac{\sum_{i=1}^n \sum_{j=1}^m T_{ij}}{mn}, \quad A_{25} = \frac{\sum_{i=1}^n \sum_{j=1}^m A_{ij}}{mn} \quad (6-6)$$

where V_{25} is the 25 km average NDVI, T_{25} is the 25 km average LST, A_{25} is the 25 km average albedo and m and n are, respectively, the number of 1 km pixels in i^{th} rows and j^{th} columns in the AMSR-E pixel.

Once a regression model is established, the model is applied to estimate the 1 km soil moisture from the 1 km NDVI, LST and albedo values. The downscaled AMSR-E (1 km) can be re-aggregated to a 25 km resolution and compared with observed AMSR-E (25 km) to quantify the model error.

Remotely Sensed Data

AMSR-E Soil Moisture

The AMSR-E was developed by the National Space Development Agency of Japan (NASDA) and launched on the Aqua satellite by the National Aeronautics and Space Administration (NASA) on May 4, 2002 (Li et al., 2004). It measures radiation at six frequencies in the range 6.9-89 GHz (Njoku et al., 2003). Lower frequencies, L band (1-2 GHz), are more sensitive to soil moisture, but they are more susceptible to dense vegetation and radio frequency interference (RFI). The higher frequency C (6.9 GHz) and X (10.65 GHz) bands can be used to retrieve soil moisture (Jackson et al., 2005) because these higher frequency bands are comparatively less susceptible to RFI. The AMSR-E directly measure brightness temperature. Soil moisture retrievals use a radiative transfer (RT) model that links surface geophysical variables to the observed brightness temperature (Njoku et al., 2003). A RT model initially assumes a soil moisture value and predicts the brightness temperature based on surface parameters, vegetation parameters, and sensor parameters. If the difference between the predicted brightness temperature and the observed temperature is less than acceptable limit, then the final soil moisture value is derived. Otherwise the iteration continues with a modified initial soil moisture value. A detail description of the retrieval algorithm appears in Njoku et al. (2003).

AMSR-E level 3 products (e.g., surface soil moisture, vegetation water contents etc) are developed from the level 2B product's brightness temperature at a 25 km earth grid scale both for ascending and descending passes

(http://www.ghcc.msfc.nasa.gov/AMSR/data_products.html). This study used the AMSR-E soil moisture level 3 products for ascending values from Jan 1, 2003 to Dec 31, 2006 on a daily basis. AMSR-E level 3 products were obtained from NASA Earth Observing System Data Gateway through National Snow and Ice Data Center (NSIDC).

MODIS Data

The Moderate Resolution Imaging Spectroradiometer (MODIS) instrument developed by NASA was launched on the Terra satellite in December 1999 and on the Aqua satellite in May 2002 (Wang et al., 2006). MODIS can collect information both in the morning and in the afternoon as Terra is scheduled to pass from north to south across the equator in the morning and Aqua is scheduled to pass from south to north in the afternoon. Even though Terra and Aqua satellites pass in the morning and in the afternoon, respectively, the temporal resolution of MODIS products is only for every 1 to 2 days (Luo et al., 2008). MODIS data are available at three spatial resolutions of 250 m, 500 m, 1,000 m and coarser resolution (Luo et al., 2008).

This study required NDVI, albedo and LST at a 1 km spatial resolution. The 1 km MODIS TERRA albedo (MCD43B3), NDVI (MYD13A2) and LST (MYD11A1) products were used to downscale the AMSR-E surface soil moisture for 2005. These data are available as tiles in the Sinusoidal (SIN) projection. All these data were re-projected into geographical projection.

Study Region

The Cleveland Corral study region in Highway 50 corridor is located in the Sierra Nevada Mountains, California, USA (Reid et al., 2003). Highway 50 is a major road located between Sacramento and South Lake Tahoe in California (Spittler and Wagner, 1998). The Figure 6-1 shows observed recent landslide and location of study domain in California. The investigated area is about 28 by 22 km (616 km²) with elevations range from about 902 to 2379 m. Since 1996, slope movement and landslides occur infrequently during winter season. Additionally, one major catastrophic landslide occurred in 1983 (Spittler and Wagner, 1998). Since 1997, the United State Geological Survey (USGS) has monitored this region using real time data acquisition systems (Reid et al., 2003). They found elevated pore-water pressures and wet soils cause slope movement and landslides during the winter (rainy) season.

Table 6-1 summarizes the study region's soils, land cover and climate. The predominant soil is sandy loam (72%). The total soil depth ranges from 0.6 to 1.4 m. Underneath the soil layer, the potential failure plane is bedrock. Conifer and wooded grassland are the dominant land covers, 80% and 14% of the study region, respectively. Some rock outcrops were also observed along the Highway 50 corridor. The north-east part of the study area has limited data because of water bodies and rock outcrops. This region has an average annual rainfall of 1101 mm, with 725 mm occurring during the winter.

The soil and vegetation parameters required for the slope stability model were obtained from the States Soil Geographic (STATSGO; NRCS, USDA), Land Data Assimilation System (LDAS; Mitchell et al., 2004) as well as from the literature. Monthly LAI values were obtained from the MODIS. The MOD15A2, 8-day composite LAI values were averaged to monthly values.

Root cohesion values for each vegetation class were adapted from Sidle and Ochiai (2006). The unit soil weight (saturated and moist) was calculated based on the soil moisture, soil porosity, and specific gravity of the soil samples using methods adapted by Ray et al. (2009a). Each soil type was assigned soil cohesion and friction angle values that were adapted from Deoja et al. (1991) and the slope of the retention curve adapted from Clapp and Hornberger (1978). Similarly, soil bulk density, field capacity, wilting point and saturated hydraulic conductivity values were adapted from Miller and White (1998) and Dingman (2002).

For this region, validation data for landslide studies are difficult to obtain. The daily groundwater measurements were obtained from the USGS (Mark Reid, USGS). Previous research indicates that over 600 landslides have occurred in this the study region (Spittler and Wagner, 1998; Reid et al., 2003). In addition, field observations identified 10 locations where failures had occurred prior to December 2007. Table 6-3 gives location details and physical characteristics of the slide locations. Observations show most of the mapped landslides were located in woodland regions with sandy loam soil texture. The slopes of the mapped landslides range from 24 to 37°.

Results and Discussion

Downscaling AMSR-E Soil Moisture

AMSR-E soil moisture at Cleveland Coral, California was downscaled from 25 to 1 km using daily data from January 1 to December 31, 2005. The 1 km NDVI, LST, and albedo were aggregated to 25 km resolution using Eq. 6-6. The observed maximum LST, albedo and NDVI are, respectively, 51°C, 0.94 and 0.93. The minimum are, respectively, -20°C, 0.01 and -0.14. The AMSR-E (25 km) was regressed with aggregated NDVI, LST and albedo values (Eq. 6-5). The regression model which best fits the AMSR-E soil moisture is

$$\theta_s = -1.426 + 4.169 A + 0.006 T + 2.254 V - 0.017 TA + 0.781 VA - 0.009 VT \quad (6-7)$$

This regression model provided a good fit with an R^2 of 0.73, a root mean square error (RMSE) of 0.009 cm³/cm³ and p-values less than 0.0001 for all independent variables.

The resulting model was used to estimate the 1 km soil moisture values. These values were aggregated to 25 km and compared to the observed values (Fig. 6-2). The results show very good agreement between the observed and the downscaled AMSR-E soil moisture. However, low downscaled AMSR-E soil moisture values from January to April can be the snow cover effect to albedo and LST. A moderate correlation was observed with an R^2 of 0.58 and a small RMSE of 0.017 cm³/cm³. The results are comparable to Yu et al. (2008) R^2 values that ranged from 0.19 to 0.74 with 6 different regression techniques and Chauhan et al. (2003) RMSE of 0.016 cm³/cm³.

Both the downscaled and the observed AMSR-E capture the seasonal variations of moisture. The observed and downscaled soil moisture clearly indicate the winter wet season. However, a small time lag between the 25 km AMSR-E values and the downscaled soil moisture is evident during the wet season. The time lag is about a week. This time lag may be due to two types of errors (Chauhan et al., 2003). The first error is due to regression analysis and the second error is associated with input data. They found regression error in analysis and precision error in NDVI, albedo and LST. Overall, the results suggest that reasonable downscaled AMSR-E soil moisture can be produced using 1 km MODIS LST, albedo and NDVI values.

Comparison between Observed AMSR-E and VIC-3L Soil Moisture

Figure 6-3 shows the observed AMSR-E soil moisture, the VIC-3L model's 1st and 2nd layers soil moisture, in situ groundwater measurements and snow accumulation at an active landslide pixel. The VIC-3L's first and second soil layer thicknesses were 0.05 and 0.35 m, respectively. Both VIC-3L and AMSR-E estimate higher surface soil moisture during the rainy season and lower soil moisture values during the dry season. The results show minimal differences between the first and second layer's soil moisture estimated by the VIC-3L model. This suggests that the surface moisture provides an indicator of the vadose zone soil moisture profile for this region. For a shallow slope stability analysis, the unsaturated soil layer is often a comparatively thin layer.

Since no in situ soil moisture measurements were available, modeled soil moisture and AMSR-E soil moisture values were compared with groundwater

measurements. Although groundwater, AMSR-E and modeled soil moistures have different measuring units, results show similar groundwater, AMSR-E and modeled soil moisture variations during the wet season.

As shown in Figure 6-3, snow occurs regularly from December to March. AMSR-E does not completely capture the soil moisture variability when there is snow. When snow is present on the ground, the surface temperature is below 0°C. At this freezing temperature, dielectric constant is very small and AMSR-E soil moisture retrievals are not possible (Hallikainen et al., 1985; Wang et al., 2009). For this region, lower or no soil moisture is indicated by AMSR-E in early winter. Thus, operational in-situ or remotely sensed snow monitoring is very important to use in combination with AMSR-E soil moisture for landslide studies in snowy regions.

Another challenge is that the AMSR-E soil moisture measurements are lower during the wet season as compared to the VIC-3L measurements and have much lower variability overall. Some of this difference may be caused by the layer thicknesses. AMSR-E's 0-2 cm thin soil layer may dry faster than the VIC-3L's 5 cm soil layer. Previous research shows that the AMSR-E has lower estimations in comparison to land surface models and measured values (Choi et al., 2008; Sahoo et al., 2008; Gruhier et al., 2008). These limitations are particularly apparent for dense vegetation and steep terrain.

Overall, the AMSE-E soil moisture measurements can capture the timing of the modeled soil moisture wetting. However, the degree of wetness is considerably different and further complicated by snow.

Scaling (AMSR-E)

Reichle et al. (2004) suggest that satellite soil moisture should be rescaled to use with land surface modeled soil moisture. Choi and Jacobs (2008) found that the AMSR-E soil moisture can be scaled to match with in situ as well as land surface model's wetness. To address the low variability of the AMSR-E surface soil moisture, the observed AMSR-E values were scaled, then compared to the VIC-3L surface soil moisture.

AMSR-E soil moisture was scaled to minimum and maximum values using a simple interpolation approach. These scaled soil moisture values are appropriate for this study region's soil. The minimum and maximum observed AMSR-E soil moisture values were 0.09 and 0.33 cm^3/cm^3 in 2005, respectively. For the sandy loam soils in Cleveland Corral, California, Rawls et al. (1982) suggested a residual saturation of 0.05 and an upper bound equal to the 0.48 soil porosity. AMSR-E soil moisture values were scaled from 0.05 to 0.48 cm^3/cm^3 .

Figure 6-4 shows promising agreement between the VIC-3L soil moisture and the scaled AMSR-E soil moisture. With the scaling, AMSR-E has a soil wetness similar to that estimated by the VIC-3L model during the dry and wet season. While the snow challenges are still evident, soil moisture values are still consistent during the critical failure period, late spring.

Soil Moisture Variability

Soil wetness defined by groundwater and vadose zone soil moisture plays a critical role in slope instability. During the rainy season, rainfall increases soil moisture

and groundwater table. With the constant slope and geotechnical parameters, soil saturation is the dynamic factor that causes slopes to become unstable because instability increases with increasing soil saturation. A slope becomes unstable when its soil saturation results in its safety factor falling below 1.

For the 3-year study period, the maximum saturation occurred on May 8, 2005. The maximum modeled saturation is the wettest day and had a GW table close to the surface and high vadose zone SM. Figures 6-5 and 6 show AMSR-E (1 km) and VIC-3L (1 km) soil moisture distributions, respectively, on May 8, 2005. The VIC-3L soil moisture values are higher than the AMSR-E values. The VIC-3L soil moisture values range from 0.25 to 0.52 whereas the AMSR-E soil moisture values range from 0.09 to 0.33 (cm^3/cm^3).

Both AMSR-E and the VIC-3L model reveal similar soil moisture distribution patterns in the north-west and south-east corners as well as along Highway 50. The VIC-3L and AMSR-E show a low soil moisture values along the highway because the physical characteristics of the ground such as paved highway, numerous retaining and revetment walls, built up area and stream affect the quality of AMSR-E and VIC-3L modeled soil moisture. Differences in the soil moisture distribution were observed at the north-east and south-west corners of the study region. The north-east region has a number of physical features that appear to challenge the satellite soil moisture retrieval and the disaggregation approach. The observed brightness temperature is used to retrieve AMSR-E soil moisture. High albedo values were found in the north-east region (Fig. 6-7a). Thus, a lower brightness temperature and higher albedo caused by snow or bright exposed surface such as sand or bare rock may influence disaggregation. AMSR-E measurements

are comparatively low in the southwestern corner of the study region. This area has the densest vegetation cover as evidenced by the high NDVI values (Fig. 6-7b). AMSR-E can not provide reasonable measurements with dense vegetation (McCabe et al., 2005; Njoku and Chan, 2006) because of the sensitivity of the C- and X-bands to dense vegetation. Accurate brightness temperature measurements are not possible over dense vegetation.

On May 8, 2005, the observed AMSR-E soil moisture value was $0.17 \text{ cm}^3/\text{cm}^3$ at the native 25 km scale. This $0.17 \text{ cm}^3/\text{cm}^3$ SM value matches the average of the 1 km pixels in the study region. The simple downscaling model is promising. It captures much of the soil moisture variability in the study region with values ranging from 0.09 to $0.33 \text{ cm}^3/\text{cm}^3$ instead of the single $0.17 \text{ cm}^3/\text{cm}^3$ SM value for the entire study region. In the future, higher resolution sensors and better downscaling approaches may improve soil moisture estimation for landslide prone regions.

Susceptibility Analysis

AMSR-E soil moisture values at the 25 and 1 km scale were used to calculate safety factors. These results were compared to previous estimated safety factors using VIC-3L soil moisture (Ray et al., 2009b). This section presents regional landslide susceptibility results using AMSR-E soil moistures. Three wetness scenarios were considered. The half saturation condition occurred on May 23, 2005. On this date, the vadose zone SM varies spatially and the GW table was located at the middle of the soil. The maximum saturation, May 8, 2005, was discussed in the previous section. The full

saturation scenario was not observed, but is presented to provide an upper bound to landslide susceptibility based on an assumed completely saturated profile

Table 6-2 presents the predicted susceptible and stable areas using the AMSR-E soil moisture (25 and 1 km) and the VIC-3L soil moisture for the three scenarios. As expected, the predicted susceptible areas for all saturation scenarios were below the fully saturated condition for both AMSR-E and VIC-3L soil moisture. Under the half and maximum modeled saturation scenarios, the predicted susceptible area with the VIC-3L soil moisture was slightly higher than that using AMSR-E soil moisture. This reflects the wetter VIC-3L vadose zone compared to the AMSR-E surface soil moisture under maximum saturation scenario. The results show that 0.39 and 0.49% of the area is highly susceptible using AMSR-E (25 km) and VIC-3L model (1 km) soil moisture, respectively.

A small prediction difference was observed with AMSR-E (25 km) and downscaled (1 km) soil moisture under half and maximum modeled saturation scenarios. This shows it can also be appropriate to use AMSR-E observed soil moisture in slope stability analysis if downscaling is not possible or desirable. However, in comparison to the observed AMSR-E (25 km), the downscaled AMSR-E (1 km) may be more appropriate to use in slope stability analysis because the higher resolution datasets are consistently recommended for landslide mapping.

Figures 6-8 and 9 show susceptibility distributions by class for VIC-3L and AMSR-E soil moisture, respectively under the maximum modeled saturation scenario. Qualitatively, both VIC-3L and AMSR-E vadose zone soil moisture identified the same hazard zones as highly, moderately and slightly susceptible. However, small differences occur in the predicted susceptible areas (Fig. 6-10). 83.2% of highly susceptible locations

predicted using VIC-3L vadose zone soil moisture were also identified as highly susceptible by AMSR-E. Most of those not successfully identified were adjacent to areas correctly predicted.

Susceptibility maps were compared with the landslide inventory data. For the May 8, 2005 saturation conditions, six of the mapped landslide locations would have been considered highly unstable. On May 8, 2005, four of the mapped landslides were identified as moderately susceptible. Since, the exact dates of mapped landslides are unknown; it is possible that some of the landslides occurred when soil moisture was higher than maximum modeled soil moisture on May 8, 2005. Moreover, moderately susceptible areas are not stable zones. External forces such as of vibrations caused by an Earthquake, large tree shaking (due to wind) and heavy highway traffic can trigger a slope to fail in a moderately susceptible area. Interestingly, the four mapped landslides are located along the Highway 50 and any external forces that are not included in slope stability model can cause slope failure in moderately susceptible area.

Overall, the results show good potential to use the AMSR-E soil moisture for vadose zone in landslide susceptibility mapping.

Conclusion

This work has downscaled AMSR-E soil moisture measurements to use in a slope stability model for landslide susceptibility mappings. The AMSR-E surface soil moisture can be used for vadose zone moisture in landslide susceptibility mapping at regional or global scale. For a shallow slope stability analysis or landslide mapping, AMSR-E soil moisture can play an important role at regional and global scales. Susceptibility maps for this study region were compared and validated with landslides inventory data and show promising agreement. The satellite-based products can provide an efficient means to develop landslide susceptibility maps based on antecedent soil moisture conditions.

While AMSR-E can provide surface soil moisture, there are still challenges. Since, AMSR-E has much lower soil moisture and less variability than would be expected, it is necessary to scale the AMSR-E soil moisture. In addition, the spatial scale of observed AMSR-E is much greater than the typical landslide scale. While downscaling provides some improvement, better methods are needed. Moreover, AMSR-E can not produce reasonable soil moisture when there is snow on the surface. Finally, the lack of in-situ soil moisture on landslides prone slopes as well as observed slope failures coincident with soil moisture observations is a significant obstacle to validating results and enhancing hazard mitigation.

The ability to capture the evolution of soil moisture will allow us to anticipate critical hazard periods on an ongoing, real time basis. For developed nations, EOS measurements can complement existing physical databases by characterizing changing

terrestrial systems and hydrologic stores. For less data rich regions, EOS measurements provide high resolution characterization of the Earth's surface. Although, this approach can produce promising results at regional and global scales, this approach is not appropriate for local scale slope stability analysis because of remotely sensed soil moisture's coarse scale.

Table 6-1: Soil, vegetation, slope and climate characteristics for the Cleveland Corral, California, US study area

California	
Land cover	Area (%)
Evergreen forest	3.3
Conifer	79.9
Deciduous forest	2.7
Wooded grassland	14.1
Soil texture	
Sandy loam	72.0
Loam	16.0
Sandy clay	3.0
Clay loam	9.0
Slope (°)	
0-15	71.2
15-30	27.5
30-45	1.2
45-60	0.0
Climate	
Average Annual Rainfall (mm)	1101.0
Average Rainfall Wet Season (mm, Jan-May)	725.0
Average Maximum Temperature (°C)	19.6
Average Minimum Temperature (°C)	5.5

Table 6-2: The portion of the study area (%) for each landslide susceptibility classification using VIC-3L, AMSR-E 25 km and downscaled soil moisture at Cleveland Corral, California, US. Three wetness scenarios are presented

Scenario	Highly Susceptible	Moderately Susceptible	Slightly Susceptible	Stable
Full Saturation	0.58	1.90	3.01	94.51
Half Saturation ¹				
VIC-3L (1 km)	0.26	1.01	2.12	96.60
AMSR-E (25 km)	0.23	0.91	1.98	96.87
AMSR-E (1 km)	0.21	0.96	2.07	96.76
Maximum Modeled Saturation ²				
VIC-3L (1 km)	0.49	1.67	2.87	94.96
AMSR-E (25 km)	0.39	1.39	2.54	95.67
AMSR-E (1 km)	0.40	1.46	2.66	95.47

¹Half saturation - Groundwater position table at half of the soil layer (May 23, 2005)

²Maximum modeled saturation - The day having the groundwater was closest to the surface and wettest vadose zone (May 8, 2005).

Table 6-3: Physical characteristics and estimated safety factor (FS) of the mapped landslide's region. FS values were calculated under maximum modeled saturation conditions (May 8, 2005) and full saturation

S.N.	Longitude	Latitude	Slope (°)	Land cover	Soil types	FS: Full saturation	FS: VIC-3L (1 km)	FS: AMSR-E (1 km)	FS: AMSR-E (25 km)
1	-120° 27' 26"	38° 51' 03"	27.4	Evergreen	Loam	0.753	0.770	0.797	0.799
2	-120° 29' 18"	38° 50' 23"	28.6	Evergreen	Loam	0.875	0.896	0.933	0.931
3	-120° 24' 22"	38° 46' 46"	32.5	Woodland	Sandy loam	0.815	0.838	0.861	0.864
4	-120° 23' 34"	38° 46' 37"	27.4	Woodland	Sandy loam	0.987	1.016	1.040	1.047
5	-120° 23' 23"	38° 46' 33"	24.1	Woodland	Sandy loam	0.997	1.026	1.050	1.058
6	-120° 22' 53"	38° 46' 23"	36.1	Woodland	Sandy loam	0.988	1.012	1.040	1.040
7	-120° 21' 34"	38° 46' 05"	31.1	Woodland	Sandy loam	0.856	0.881	0.905	0.908
8	-120° 20' 28"	38° 46' 04"	29.6	Woodland	Sandy loam	0.939	0.965	0.994	0.992
9	-120° 16' 33"	38° 46' 58"	36.6	Woodland	Sandy loam	0.988	1.014	1.025	1.040
10	-120° 16' 47"	38° 46' 20"	34.9	Woodland	Sandy loam	0.751	0.775	0.802	0.796

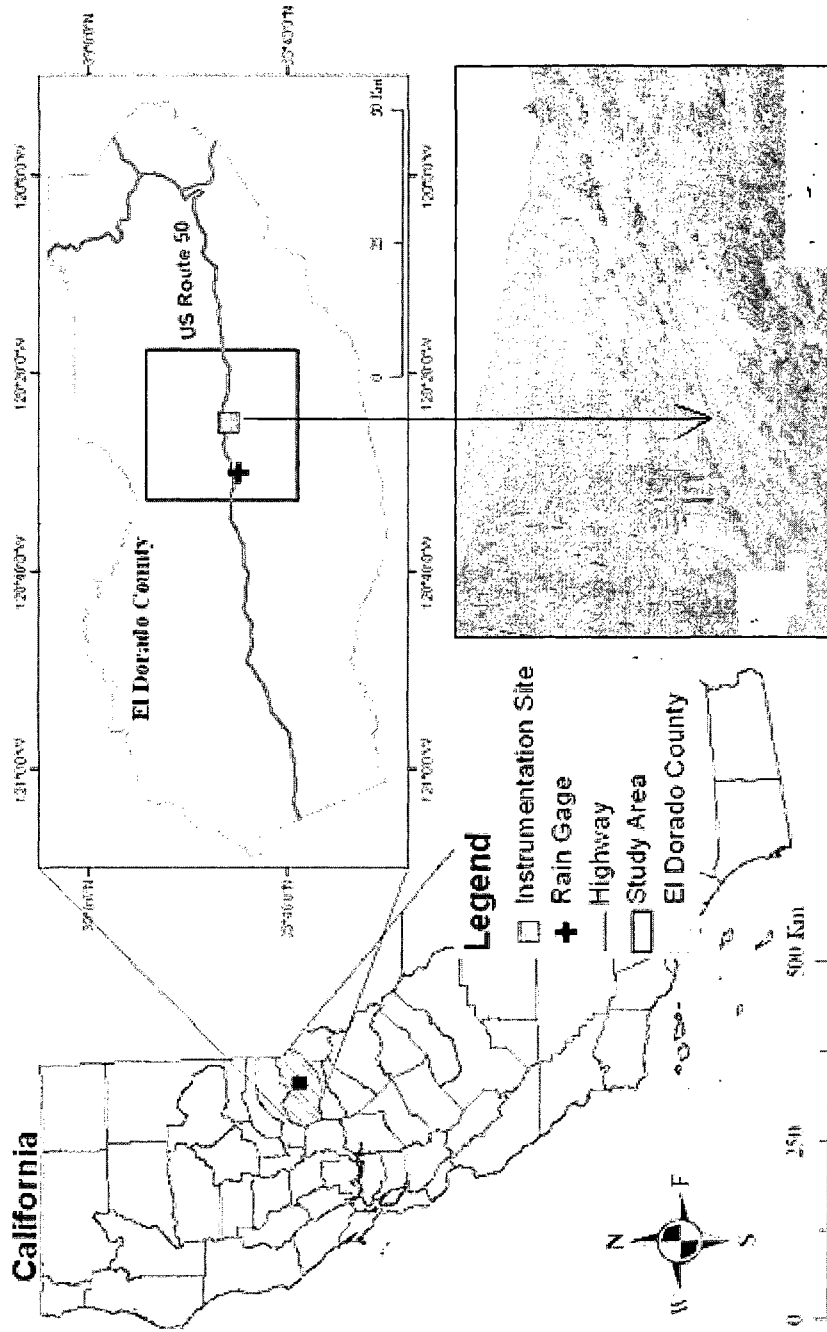


Figure 6-1: The study region in El Dorado County in California with the mapped landslide

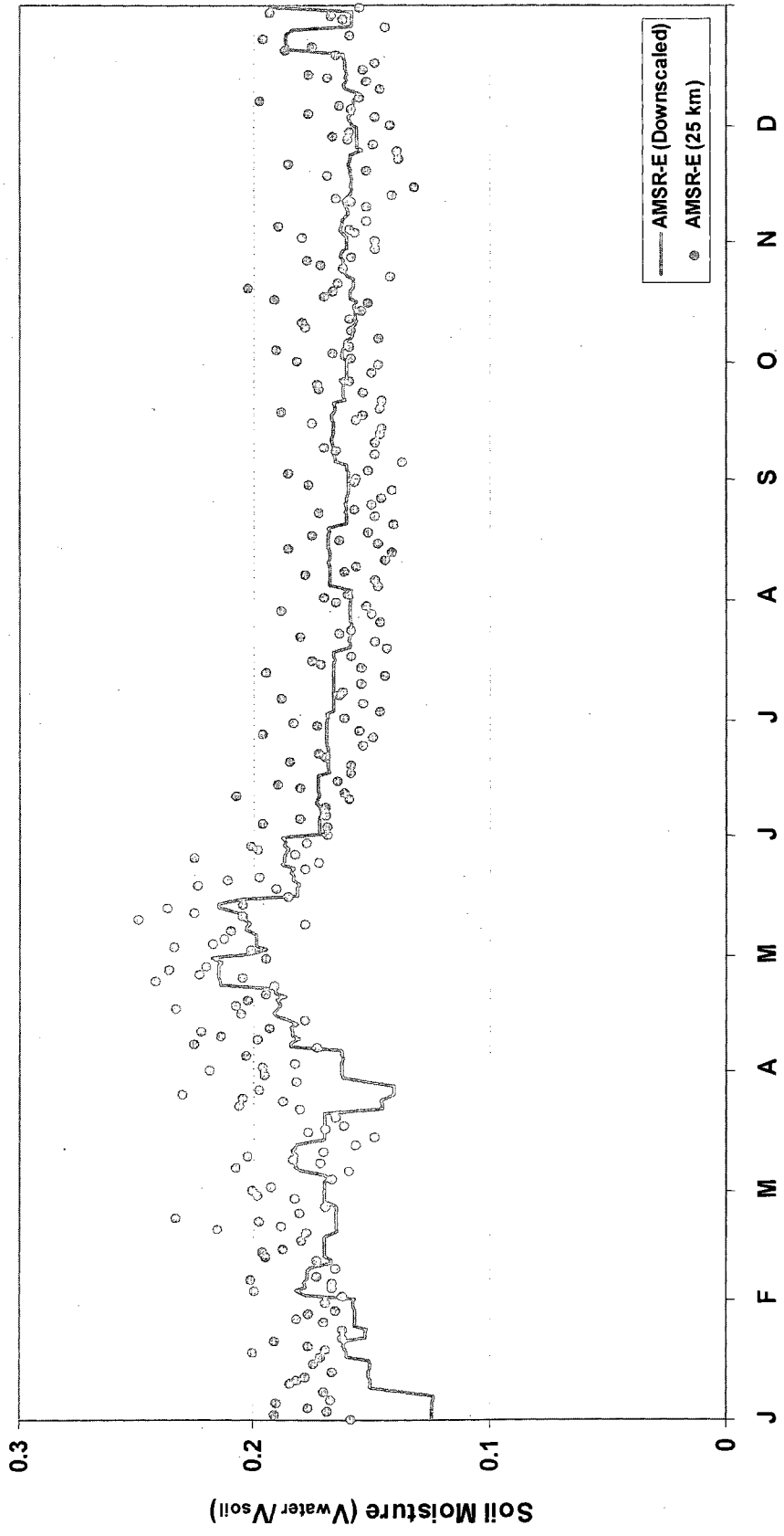


Figure 6-2: Daily observed AMSR-E (25 km spatial resolution) and downscaled AMSR-E 1 km spatial resolution aggregated to 25 km spatial resolution in 2005 at Cleveland Corral, California, US. $R^2 = 0.58$, $RMSE = 0.017 \text{ cm}^3/\text{cm}^3$

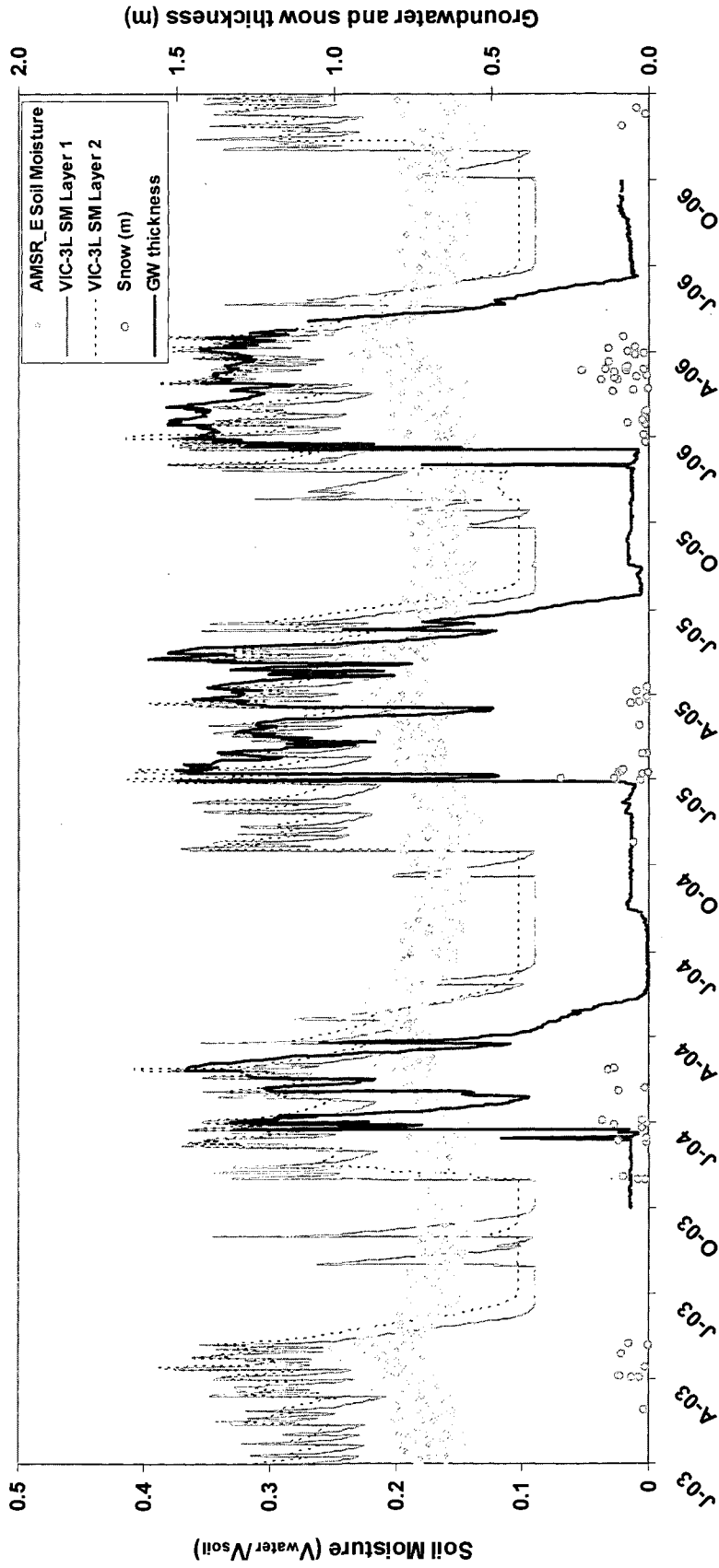


Figure 6-3: Observed AMSR-E soil moisture, VIC-3L soil moisture layer (1 and 2), snow and groundwater measurements at Cleveland Corral, California, US. Groundwater thickness is measured from the bottom of piezometer installed at 1.82 m below the surface

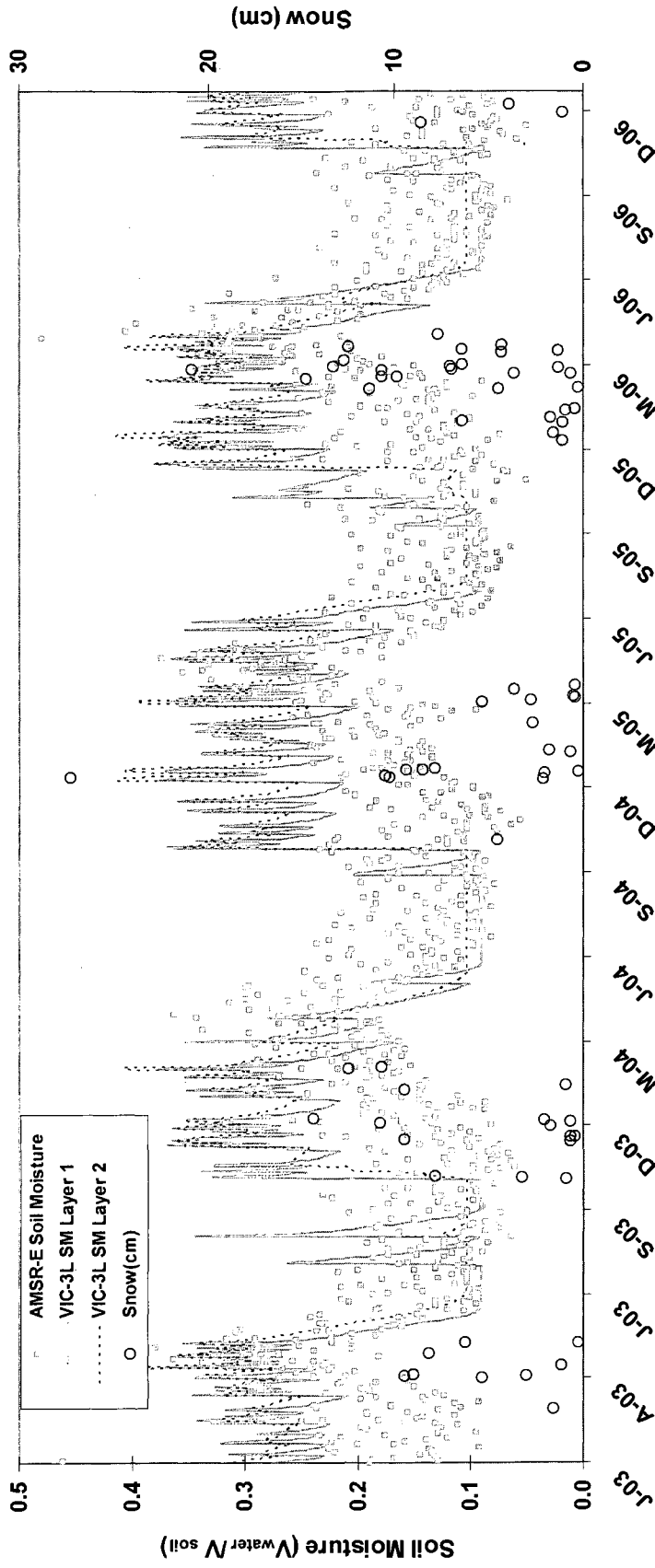


Figure 6-4: Observed scaled (0.05-0.48 cm³/cm³) AMSR-E soil moisture, VIC-3L soil moisture layer (1 and 2) and snow values at Cleveland Corral, California, US

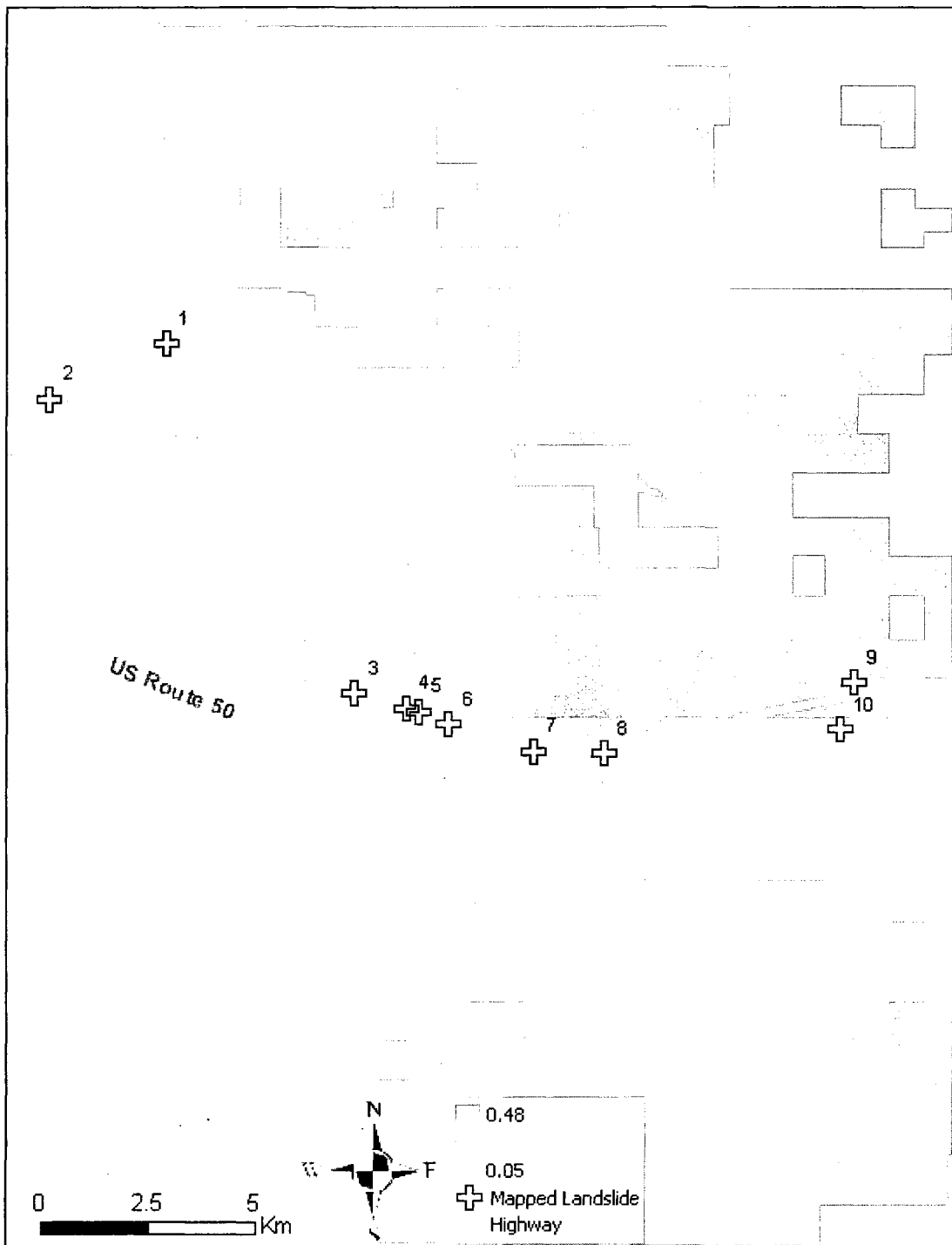


Figure 6-5: AMSR-E (1 km) soil moisture on maximum modeled soil moisture day (May 8, 2005)

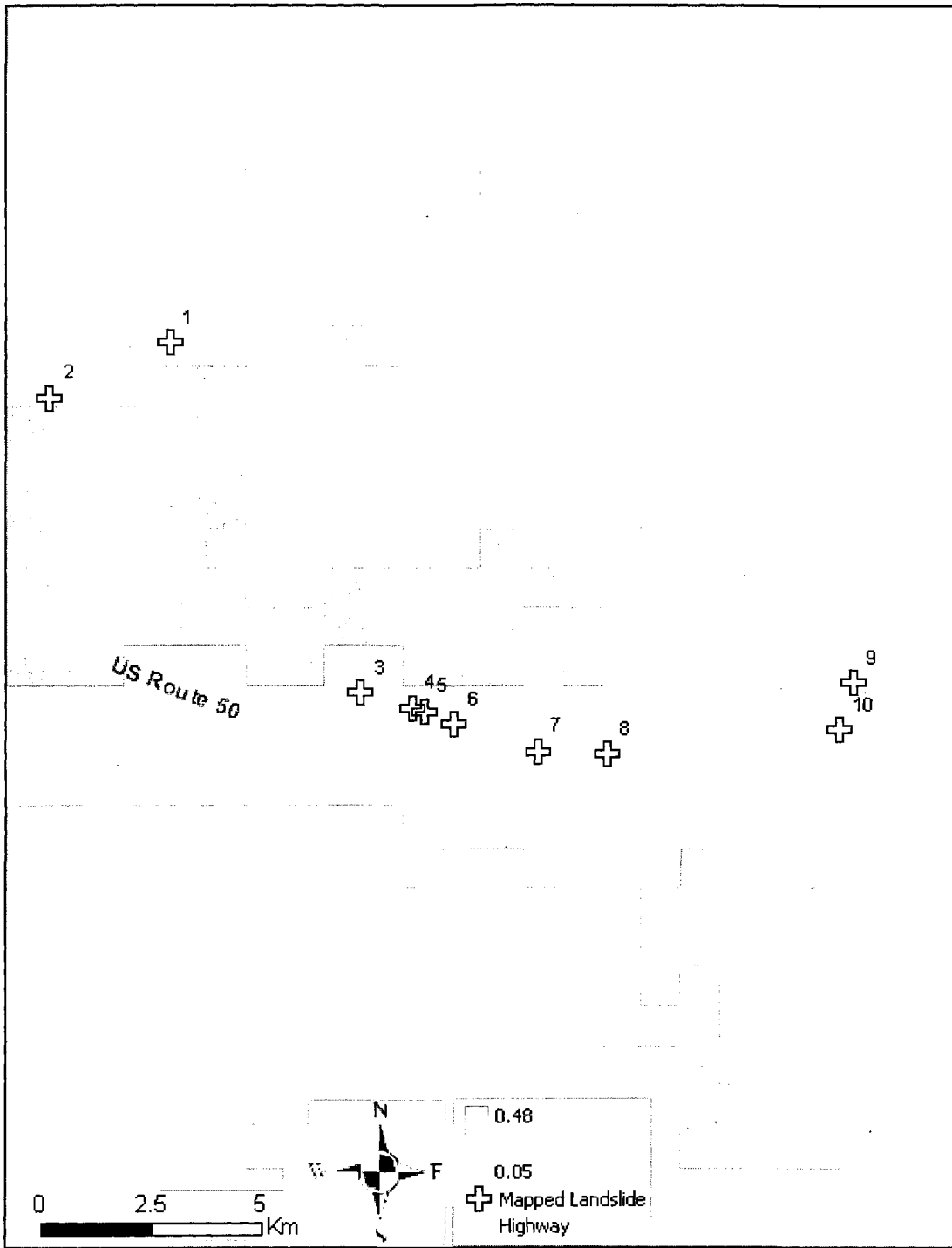


Figure 6-6: VIC-3L (1 km) soil moisture on maximum modeled soil moisture day (May 8, 2005)

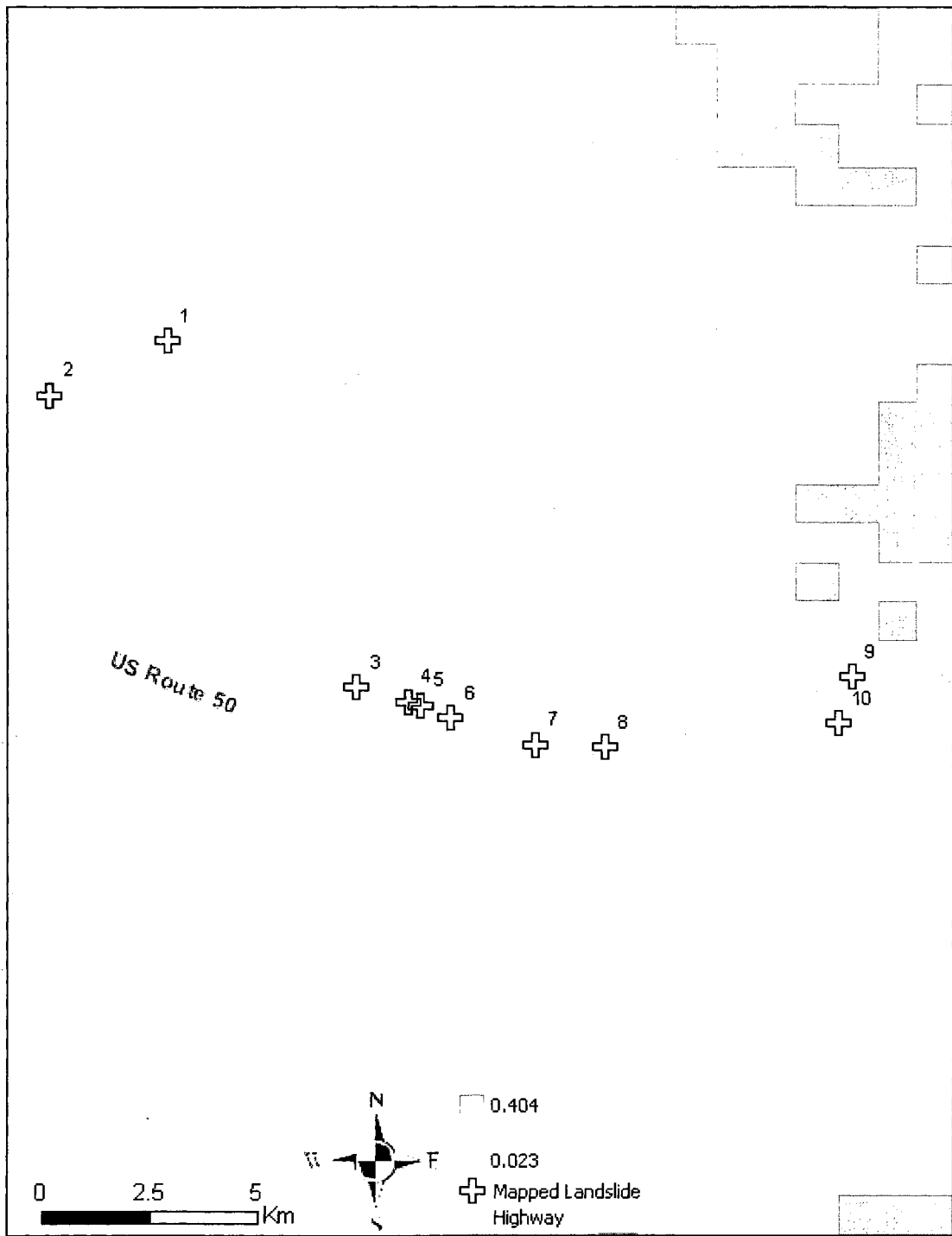


Figure 6-7a: The observed albedo (1 km) on maximum modeled soil moisture day (May 8, 2005)

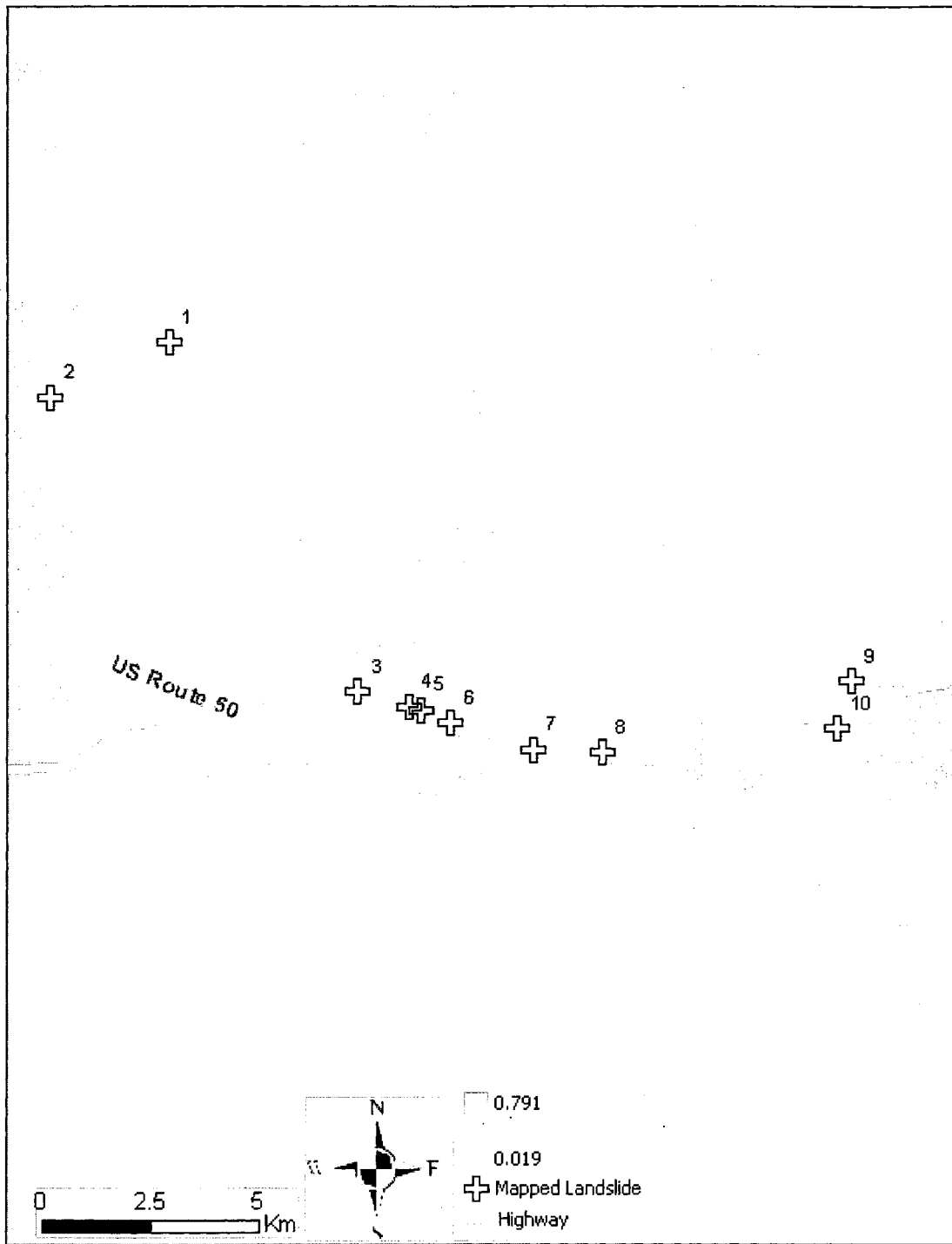


Figure 6-7b: The observed NDVI (1 km) on maximum modeled soil moisture day (May 8, 2005)

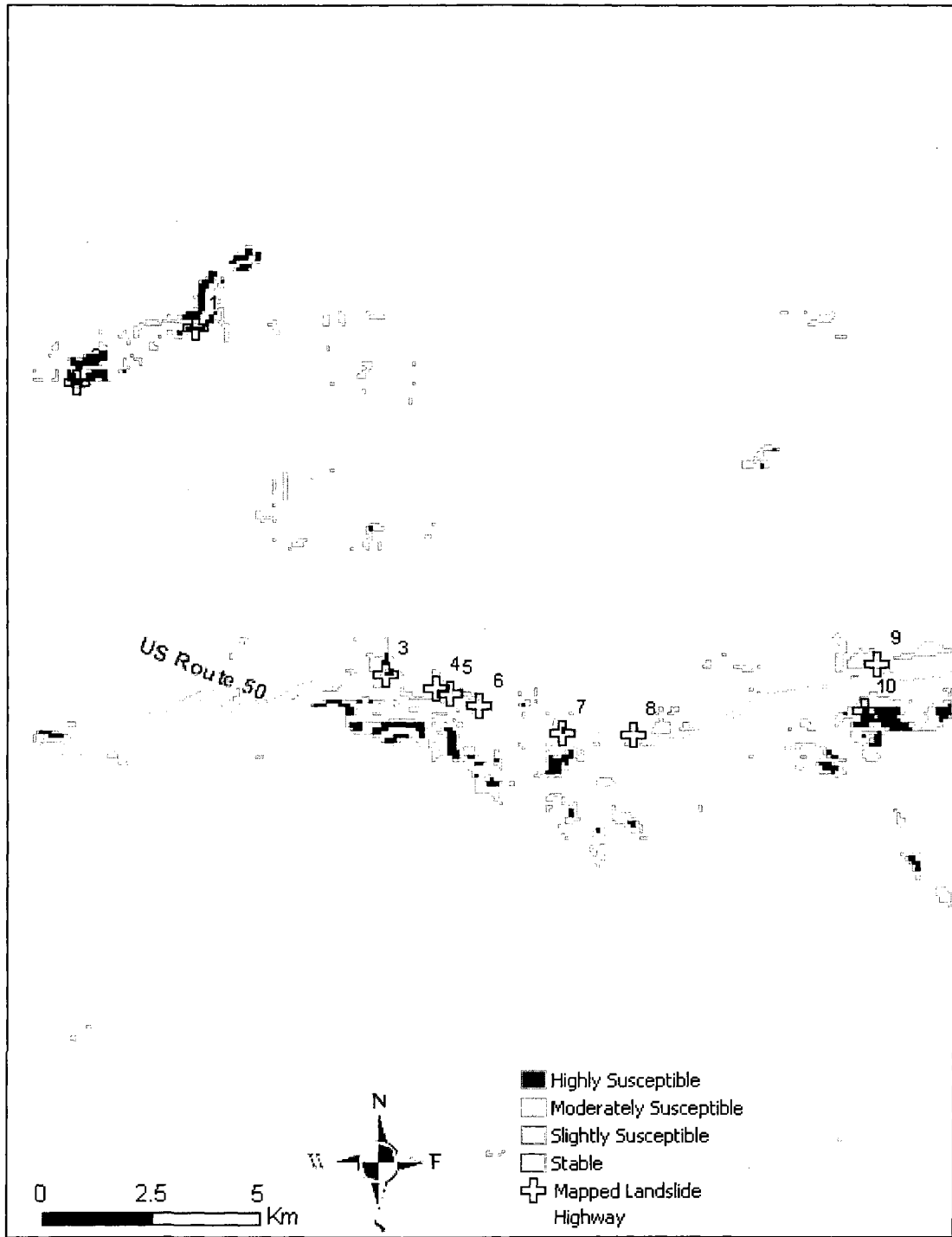


Figure 6-8: Landslide susceptibility map for maximum modeled saturation day (May 8, 2005) using VIC-3L soil moisture

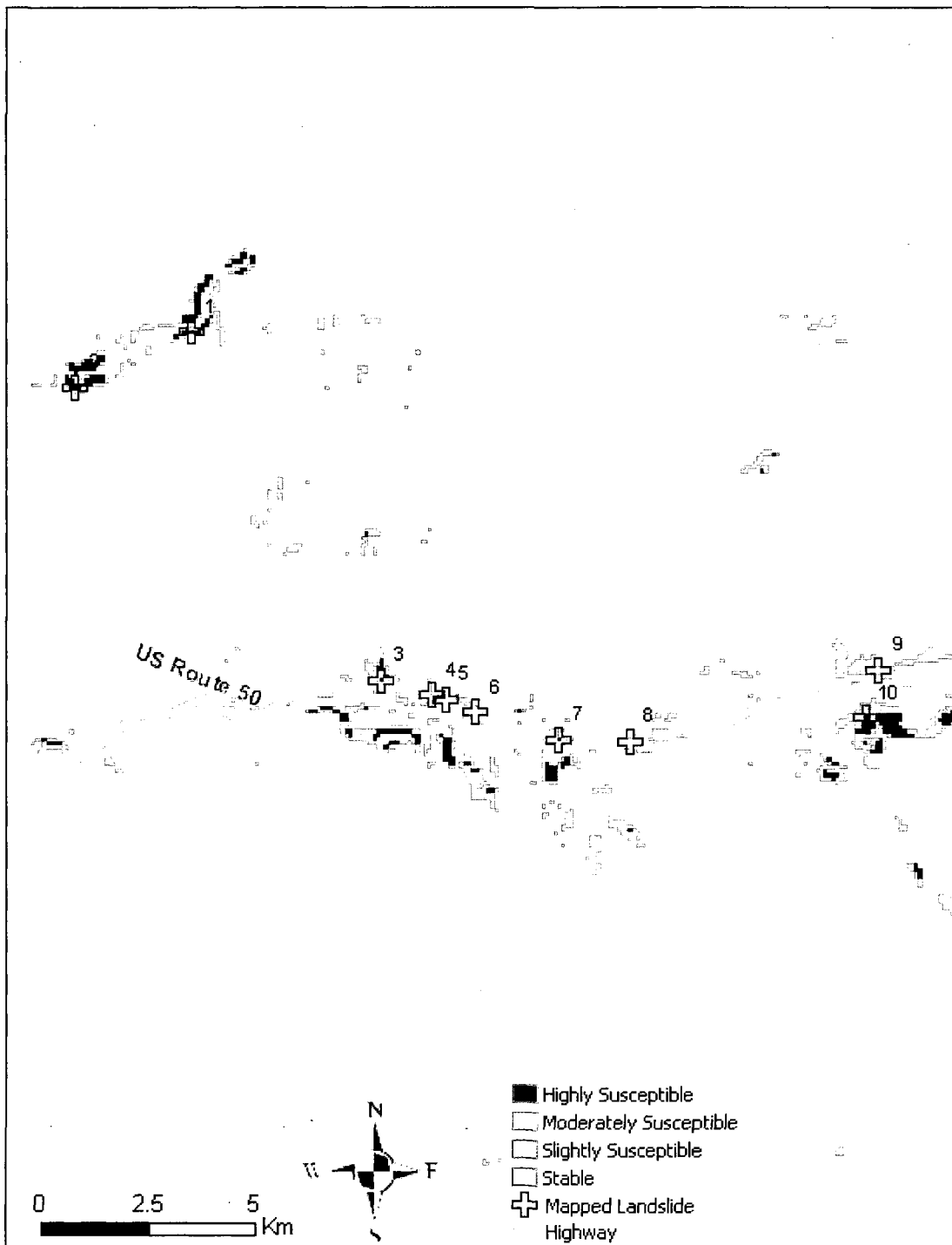


Figure 6-9: Landslide susceptibility map for maximum modeled saturation day (May 8, 2005) using downscaled AMSR-E soil moisture

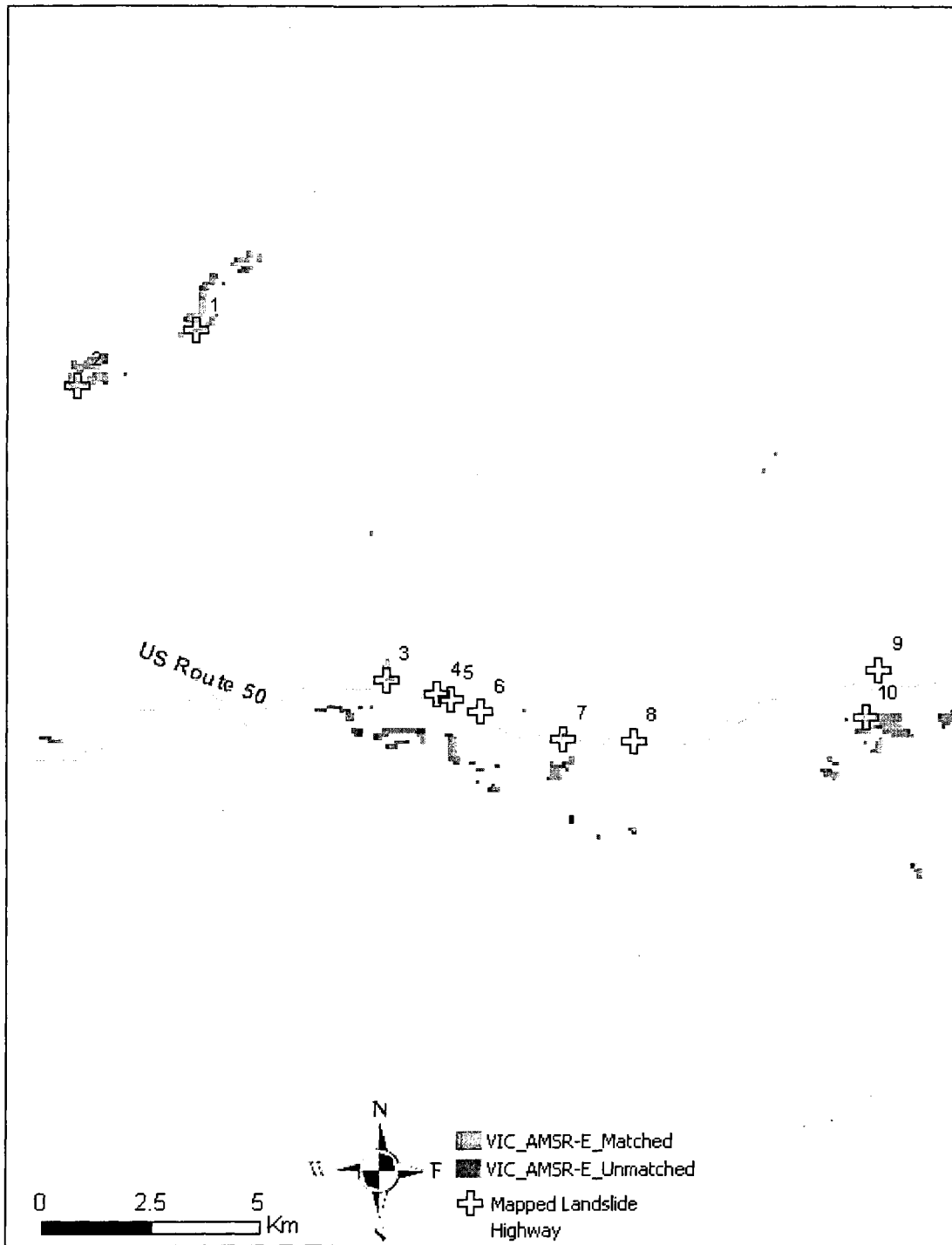


Figure 6-10: Comparison of highly susceptible area predicted using VIC-3L and AMSR-E on maximum modeled soil moisture day (May 8, 2005). Green square indicates identical predictions. Red squares are location identified by VIC-3L highly susceptible, but not by AMSR-E

CHAPTER 7.

CONCLUSION

This study modified infinite slope stability model that directly includes vadose zone soil moisture and groundwater depth using variable infiltration capacity (VIC-3L) as a modeled soil moisture and Advanced Microwave Scanning Radiometer (AMSR-E) satellite soil moisture. This model was applied in California, US and Dhading, Nepal to develop dynamic landslide susceptibility maps at a regional scale. The major findings of this study are summarized in four categories.

1. Linking remotely sensed data with landslide disasters:

- There was a strong relationship among landslide disaster, AMSR-E soil moisture and
- Tropical rainfall Measuring Mission (TRMM) rainfall data.
- AMSR-E soil moisture has potential to be used for landslide studies.

2. Impact of vadose zone soil moisture in slope stability analysis

- The traditional infinite slope stability model was modified to include the impact of vadose zone soil moisture for shallow landslide analysis at regional or global scale.
- Landslides are not triggered only due to surface layer saturation; rather, it is the combined effect of surface and subsurface saturation that is critical.

- A significant impact of vadose zone soil moisture was found for shallow landslides whereas it was less significant for deep landslides.
- The susceptibility to slope failure increases non linearly with an increase of vadose zone soil moisture as well as groundwater position.

3. Modeling landslides using dynamic soil moisture

- A simple wetness based model can be used to predict groundwater table during the wet season
- Modeled vadose zone soil moisture enhance quasi-dynamic landslide studies

4. Spatiotemporal distribution of susceptibility

- A strong relationship was observed between the relative variability of susceptibility and slope failure.
- A strong relationship was observed between the number of crossings and the average duration
- Results showed it is not necessary a slope must fail when the safety factor is less than 1 as it is traditionally assumed, rather, it may stay longer under unstable condition before the failure took place.
- The spatiotemporal distribution of susceptibility is necessary to predict the possible timing of slope failure

An improved infinite slope stability model can produce reasonable susceptibility maps in landslide studies enhances susceptibility prediction by showing susceptibility evolution over time. Moreover, previous spatial distribution studies are not sufficient to predict possible timing of slope failure.

The Nepal study region is more vulnerable to landslides than the California. More frequent landslides occur in Nepal and more frequent slope movements in California. These regions have significant climate and hydrogeological differences. California region receives less rainfall than Nepal. In addition, Nepal has steeper terrain than the California. Soil texture and vegetation cover differs by region. As a result, the statistical properties differ somewhat between regions. However, there are many similarities as well.

For a less data rich region, the applied model and approach will be very useful for slope stability analysis using remotely sensed data. This study used many remotely sensed data including AMSR-E for soil moisture, TRMM for rainfall, SRTM for DEM, MODIS for leaf area index, vegetation index, surface albedo, and land surface temperature. Hence, this study somewhat reduced the dependency of landslide studies on in-situ data that is necessary to study economically at regional and global scales.

This model can be used from local scale to global scales. However, it is not possible to use remotely sensed soil moisture for landslide studies at local scale.

FUTURE STUDY

The approach used in this study can be very useful to develop landslide susceptibility mapping by using modeled and or remotely sensed soil moisture at regional and global scales. Relationships between remotely sensed data and landslides, the role of vadose zone soil moisture in instability, statistical analysis of susceptibility and the use of remotely sensed soil moisture in landslide susceptibility will be very helpful to explore the variability of landslide prone regions. It will further help to forecast landslides from local to global scale. However, the coarse scale remotely sensed and hydrologic modeled data, lack of in-situ soil moisture and groundwater data in landslide prone regions and the limited landslide inventory data are important issues that needed to be addressed in future for landslide susceptibility mapping and landslide forecast.

Major future work is to (1) enhance the experimental datasets that are necessary to calibrate and validate models, 2) to improve the understanding of Digital Elevation Model (DEM) scaling effects on instability prediction and (3) to develop better downscaling approach to use remotely sensed soil moisture at hillslope scales.

For the experimental work, a mountainous region needs to be instrumented to measure in-situ soil moisture, groundwater and required climatic parameters for the infinite slope stability model. Since very few validation experiments have been carried out on a slope, this work will be critical to validate the land surface hydrologic models as well as AMSR-E satellite soil moisture, TRMM precipitation on slopes.

For DEM scaling effects on instability prediction, in-situ as well as remotely sensed DEM needs to be compared and used to develop susceptibility maps from regional to global scales. The LIDAR datasets can be used as a higher resolution DEM to quantify errors in instability prediction using lower resolution DEM (in-situ and SRTM).

Landslide inventory maps need to be developed using digital image processing and photogrammetric technique (possibly stereoscopic viewing) based on satellite images or aerial photographs depending on the scope and availability of required imagery. For this purpose, Landsat images and/or Lidar, InSAR and DInSAR data can be used. This will enhance methods used for landslide inventory mapping as well as in validating and characterizing landslides at regional and global scales. It will also refine our understanding of which tools provide the best information given the required prediction scale.

These future works will help to develop global landslide forecasting models as well as provide better validation datasets for landslide studies.

LIST OF REFERENCES

- Abella, E.A.C., and Van Westen, C.J., 2008. Qualitative landslide susceptibility assessment by multicriterian analysis: A case study from San Antonio del Sur, Guantanamo, Cuba. *Geomorphology*, 94: 453-466.
- Abdallah, C., Chowrowicz, J., Bouheir, R., and Dhont, D., 2007. Comparative use of processed satellite images in remote sensing of mass movements: Lebanon as a case study. *International Journal of Remote Sensing*, 28 (19): 4409-4427.
- Abramson, L.W., Lee T.S., Sharma, S., and Boyce, G.M., 1996. *Slope Stability and Stabilization Methods*. A Wiley-Interscience Publication, John Wiley & Sons, inc., NY.
- Acharya, G., De Smedt, F., and Long, N. T., 2006. Assessing landslide hazard in GIS: a case study from Rasuwa, Nepal. *Bulletin of Engineering Geology and the Environment*, 65(1): 99-107.
- Adler, R., Hong, Y., and Huffman, G.J., 2006. An experimental global prediction system for rainfall-triggered landslides. *Proceedings, the International Symposium on Landslide Risk Analysis and Sustainable Disaster Management (IPL 2007)*, 21-25 jan 2007, United Nations University, Tokyo.
- Anderson, S.A., and Sitar, N., 1995. Analysis of rainfall induced debris flows. *Journal of Geotechnical Engineering*, 121(7): 544-552.
- Arya, L.M, Richter, J.C., and Paris, J.F., 1983. Estimating profile water storage from surface zone soil moisture measurements under bare field conditions. *Water Resources Research*, 19(2): 403-412.
- Au, S.W.C., 1998. Rain-induced slope instability in Hong Kong. *Engineering Geology* 51, 1-36.
- Ayalew, L., and Yamagishi, H., 2005. The application of GIS-based logistic regression for landslide susceptibility mapping in the Kakuda-Yahiko Mountains, central Japan. *Geomorphology*, 65: 15-31.
- Barros, A.P., Kim, G., Williams, E., and Nesbitt, S.W., 2004 Probing orographic controls in the Himalayas during the monsoon using satellite imagery. *Natural Hazards and Earth System Sciences*, 4: 29-51.

- Barros, A.P., and Lang, T.J., 2003. Monitoring the monsoon in the Himalayas: Observations in central Nepal, June 2001. *Monthly water review*, 131(7): 1408-1427.
- Barling, R.D., Moore, I.D., Grayson R.B., 1994. A quasi-dynamic wetness index for characterizing the spatial distribution of zones of surface saturation and soil water content. *Water Resources Research* 30 (4), 1029-1044.
- Beven, K.J., Kirkby, M.J., 1979. A physically based variable contributing area model of basin hydrology. *Hydrological Science Bulletin* 24(1), 43-69.
- Borga, M., Dalla Fontana, G., Da Ros, D., Marchi, L., 1998. Shallow landslide hazard assessment using physically based model and digital elevation data. *Environmental Geology* 35(2-3), 81-88.
- Borga, M., Tonelli, F., Dalla Fontana, G., Cazorzi, F., 2005. Evaluating the influence of forest roads on shallow landsliding. *Ecological Modelling* 187, 89-98.
- Borzdyka, A.M., 1974. Failure of austenitic steel under conditions of cyclic stress relaxation at 750°C. *Strength of Materials*, 6 (1): 47-50.
- Brarddinoni, F., Slaymaker, O., and Hassan, M.A., 2003. Landslide inventory in rugged forested watershed: a comparison between air-photo and field survey data. *Geomorphology*, 54: 179-196.
- Brooks, R.H., Corey, A.T., 1988. Hydraulic properties of porous media. *Hydrol. Pap. Colorado State University*, 3.
- Burton, A., and Bathurst, J.C., 1998. Physically based modeling of shallow landslide sediment yield at a catchment scale. *Environmental Geology*, 35(2-3): 89-99.
- Caine, N., 1980. The rainfall intensity-duration control of shallow landslides and debris flows. *Gegrafiska Annaler Series A-Physical Geography*, 62(1-2): 23-27.
- Canuti, P., Casagli, N., Ermini, L., Fanti, R; and Farina, P., 2004. Landslide activity as a geoinicator in Italy: Significance and new perspectives from remote sensing. *Environmental Geology*, 45(7): 907-919.
- Cashion, J., Lakshmi, V., Bosch, D., and Jackson, T.J., 2005. Microwave remote sensing of soil moisture: evaluation of the TRMM microwave imager (TMI) satellite for little river watershed Tifton, Georgia. *Journal of Hydrology*, 307: 242-253.
- Cernica, J.N., 1982. *Geotechnical engineering*. Holt, Rinehart and Winston, New York. 488 pp.

- Chauhan, N.S., Miler, S., and Aradny, P., 2003. Spaceborn soil moisture estimation at high resolution: a microwave-optical/IR synergistic approach. *International Journal of Remote Sensing*, 24(22): 4599-4622.
- Cheng, K.S., Wei, C., and Chang, S.C., 2004. Locating landslides using multi-temporal satellite images. *Advances in Space Research*, 33: 296-301.
- Cherkauer, K.A., and Lettenmaier, D.P., 1999. Hydrologic effect of frozen soils in the upper Mississippi river basin. *Journal of Geophysical Research-Atmospheres*, 104 (D16): 19599-19610.
- Chiang, S.H., Chang, K.T., 2009. Application of radar data to modeling rainfall-induced landslides. *Geomorphology* 103, 299-309.
- Cho, S.E., and Lee, S.R.L., 2002. Evaluation of surficial stability for homogeneous slopes considering rainfall characteristics. *Journal of Geotechnical and Geoenvironmental Engineering*, 128(9), 756-763.
- Choi, M, and Jacobs, J.M., (2007). Soil moisture variability of root zone profiles within SMEX02 remote sensing footprints. *Advances in Water Resources*, 30(4): 883-896.
- Choi, M., Jacobs, J.M., and Bosch, D.D., 2008. Remote sensing observatory validation of surface soil moisture using Advanced Microwave Scanning Radiometer E, Common Land Model, and ground based data: Case study in SMEX03 Little River Region, Georgia, U.S. *Water Resources Research*, 44 W08421, doi:10.1029/2006WR005578.
- Choi, M., and Jacobs, J.M., 2008. Temporal variability corrections for Advanced Microwave Scanning Radiometer E (AMSR-E) surface soil moisture: Case study in Little River Region, Georgia, U.S. *Sensors*, 8: 2617-2627.
- Clapp, R.B., and Hornberger, G.M., 1978. Empirical equations for some soil hydrologic properties. *Water resources Research*, 14(4): 601-604.
- Collins, B.D., and Znidarcic D., 2004. Stability analysis of rainfall induced landslides. *Journal of Geotechnical and Geoenvironmental Engineering*, 130(4): 362-372.
- Dahal, R.K., Hasegawa, S., Nonomura, A., and Yamanaka, M., 2008. Predictive modelling of rainfall-induced landslide hazard in the Lesser Himalaya of Nepal based on weights-of-evidence. *Geomorphology*, 102: 496-510.
- Dai, F.C., and Lee, C.F., 2002. Landslide characteristics and slope instability modeling using GIS, Lantau Island, Hong Kong. *Geomorphology*, 42:213-238.

- Dai, Y.J., Zeng, X.B., Dickinson, R.E., Baker, I., Bonan, G.B., Bosilovich, M.G., Denning, A.S., Dirmeyer, P.A., Houser, P.R., Niu, G.Y., Oleson, K.W., Schlosser, C.A., Yang, Z.L., 2003. The common land model, *Bulletin of the American Meteorological Society*, 84 (8), 1013-+
- Dickinson, R.E., Henderson-Sellers, A., Kennedy, P.J., Wilson, M.F., 1986. Biosphere-atmosphere transfer scheme (BATS) for the NCAR community climate model, NCAR tech note, Natl. Cent. For Atmos. Res. Boulder, Colo., 69 pp.
- Dietrich, W.E., Wilson, C.J., Montgomery, D.R., McKean, J., 1993. Analysis of erosion thresholds, channel networks, and landscape morphology using a digital terrain model. *The Journal of Geology* 101, 259-278.
- Dingman, S.L., 2002. *Physical Hydrology*. Prentice Hall, Upper Saddle River, New Jersey. 646 pp.
- Denghong, Z., and Wanchang, Z., 2005. Rainfall-runoff simulation using the VIC-3L model over the Heihe River mountainous basin, China. *IEEE*, 0-7803-9050-4/05, 4391-4394.
- Deoja, B. B., Dhital, M., Thapa, B., and Wagner, A., 1991. *Mountain risk engineering handbook*. International Centre for Integrated Mountain Development (ICIMOD), Kathmandu: 875 pp.
- De Smedt, F., 2006. Two- and three dimensional flow of groundwater. In Delleur JW (ed) *The Handbook of Groundwater Engineering - second edition*, CRC Press:4.1-4.36
- De Vleeschauwer, C., and De Smedt, F., 2002. Modeling slope stability using GIS on a regional scale, *Proceedings of the first Geological Belgica International Meeting*, Leuven, 11-15 September 2002. *Aardkundige Mededelingen*, 12: 253-256.
- D' Odorico P., Fagherazzi S., 2003. A probabilistic model of rainfall-triggered shallow landslides in hollows: A long-term analysis. *Water Resources Research* 39(9), 1262, doi:10.1029/2002WR001595.
- D' Odorico P., Fagherazzi S., Rigon, R., 2005. Potential for landsliding: Dependence on topographic characteristics. *Journal of Geophysical Research* 110, F01007, doi: 10.1029/2004JF000127.
- de Rosney, P., Calvet, J.C., Kerr, Y., Wigneron, F.L., Lemaitre, F., Escorihuela, M.J., Sabater, J.M., Saleh, K., Barrie, J., Bouhours, G., Coret, L., Cherel, G., Dedieu, G., Durbe, R., Fritz, N.E.D., Froissard F., Hoedjes, J., Kruszewski, A., Lavenu, F., Suquia, D., and Waldteufel, P., 2006. SMOSREX: A long term field campaign experiment for soil moisture and land surface processes remote sensing. *Remote Sensing of Environment*, 102: 377-389.

- de Vleeschauwer, C., and De Smedt, F., 2002. Modeling slope stability using GIS on a regional scale, Proceedings of the first Geological Belgica International Meeting, Leuven, 11-15 September 2002. *Aardkundige Mededelingen*, 12: 253-256.
- Drinkwater, M., Kerr, Y., Font, J., and Berger, M., 2009. Exploring the water cycle of the 'Blue Planet': The Soil Moisture and Ocean Salinity (SMOS) mission. *European Space Agency Bulletin*, 137: 7-15.
- Ermini, L. Catani, F., and Casagli, N., 2005. Artificial neural networks applied to landslide susceptibility assessment. *Geomorphology*, 66: 327-343.
- Francini, M., Pacciani, M., 1991. Comparative analysis of several conceptual rainfall-runoff models, *J. Hydrol.*, 122, 161-219.
- Gabet, E.J., Burbank, D.W., Putkonen, J.K., Pratt-Sitaula, B.A., Ojha, T., 2004. Rainfall thresholds for landsliding in the Himalayas of Nepal. *Geomorphology* 63, 131-143.
- Guzzetti, F., Carrara, A., Cardinali, M., and Reichenbach, P., 1999. Landslide hazard evaluation: a review of current techniques and their application in a multi-scale study, Central Italy. *Geomorphology* 31(1-4):181-216.
- Gao, H., Wood, E.F., Jackson, T.J., Drusch, M., and Bindlish, R., 2006. Using TRMM/TMI to retrieve surface soil moisture over the southern United States from 1998 to 2002. *Journal of Hydrometeorology*, 7: 23-38.
- Gorsevski, P.V., Gessler, P.E., and Jankowski, P., 2003. Integrating a fuzzy k-means classification and a Bayesian approach for spatial prediction of landslide hazard. *Journal of Geographical Systems*, 5(3):223-251.
- Gorsevski, P.V., Jankowski, P., and Gessler, P.E., 2006. An heuristic approach for mapping landslide hazard by integrating fuzzy logic with analytic hierarchy process. *Control and Cybernetics*, 35(1): 121-146.
- Gorsevski, P.V., Gessler, P.E., Boll, J., Elliot, W.J., and Foltz, R.B., 2006. Spatially and temporally distributed modelling of landslide susceptibility. *Geomorphology*, 80: 178-198. I
- Gruhler, C., de Rosnay, P., Kerr, Y., Mougin, E., Ceschia, E., and Calvet, J.C., 2008. Evaluation of AMSR-E soil moisture product based on ground measurements over temperate and semi-arid regions. *Geophysical Research letters*, 35: L10405: doi: 10.1029/2008GL033330.

- Gull, G., Antronico, L., Iaquina, P., and Terranova, O., 2008. Susceptibility and triggering scenarios at a regional scale for shallow landslides. *Geomorphology*, 99: 39-58.
- Hallikainen, M.T., Ulaby, F.T., Dobson, M.C., El-rayes, M.A., and Wu, L., 1985. Microwave dielectric behavior of wet soil-part I: Empirical models and experimental observations. *IEEE Transactions on Geoscience and Remote Sensing*, GE-23 (1): 25-34.
- Hansen, M.C., DeFries, R.S., Townshend, J.R.G., Sohlberg, R., 2000. Global land cover classification at 1 km spatial resolution using a classification tree approach. *International Journal of Remote Sensing* 21 (6 & 7), 1331-1364.
- Hervas, J., Barredo, J.I., Rosin, P.L., Pasuto, A., Mantovani, F., and Silvano, S., 2003. Monitoring landslides from optical remotely sensed imagery: the case history of Tessina landslide, Italy. *Geomorphology*, 54: 63-75.
- Hoffmann, J., 2005. The future of satellite remote sensing in hydrogeology. *Hydrogeology Journal*, 13:247-250, doi: 10.1007/s10040-004-0409-2.
- Hong, Y., Adler, R., and Huffman, G., 2007. Use of satellite remote sensing data in the mapping of global landslide susceptibility. *Natural hazards*, 43:245-256.
- Huang, M., Liang, X., 2006. On the assessment of the impact of reducing parameters and identification of parameter uncertainties for a hydrologic model with applications to ungauged basins. *Journal of Hydrology* 320, 37-61.
- Iverson, R.M., and Major, J.J., 1987. Rainfall, ground-water flow, and seasonal movement at Minor Creek landslide, northwestern California: Physical interpretation of empirical relations. *Geological Society of America Bulletin*, 99: 579-594.
- Iverson, R.M., 2000. Landslide triggering by rain infiltration. *Water Resources Research*, 36(7): 1897-1910.
- Jackson, T.J., 1980. Profile soil moisture from surface measurements. *Journal of the Irrigation and Drainage Division, American Society of Civil Engineers*, 106(IR2): 81-92.
- Jackson, T.J., 1982. Passive microwave sensing of soil moisture under vegetation canopies. *Water Resources Research*, 18 (4): 1137-1142.
- Jackson, T.J., 1993. III Measuring surface soil moisture using passive microwave remote sensing. *Hydrological processes*, 7: 139-152.

- Jackson, T. J., D. M. Le Vine, C. T. Swift, T. J. Schmugge, and F. R. Schiebe (1995), Large area mapping of soil moisture using the ESTAR passive microwave radiometer in Washita'92, *Remote Sens. Environ.*, 53, 27–37.
- Jackson, T.J., and Hsu, A.Y., 2001. Soil moisture and TRMM microwave imager relationships in the Southern Great Plains 1999 (SGP99) experiment. *IEEE Transactions on Geoscience and Remote Sensing*, 39(8): 1632-1642.
- Jackson, T.J., 2002. Remote sensing of soil moisture: implications for groundwater recharge. *Hydrogeology Journal*, 10: 40-51.
- Jackson, T.J., Bindlish, R., Gasiewski, A.J., Stankov B., Njoku, E.G., Bosch, D., Coleman, T.L., Laymon, C.A., and Starks, P., 2005. Polarimetric scanning radiometer C- and X-band microwave observations during SMEX03. *IEEE Transactions on Geoscience and Remote Sensing*, 43(11): 2418-2430.
- Jackson, T.J., Moran, M.S., and O'Neill, P.E., 2008. Introduction to soil moisture experiments 2004 (SMEX04) special issue. *Remote Sensing of Environment*, 112: 301-303.
- Joshi, J., Majtan, S., Morita, K., and Omura, H., 2000. Landslide hazard mapping in the Nallu Khola watershed, Central Nepal. *Journal of the Nepal Geological Society* 21: 21-28.
- Kaab, A., 2005. Combination of SRTM3 and repeat ASTER data for deriving alpine glacier flow velocities in the Bhutan Himalaya. *Remote Sensing of Environment*, 94: 463-474.
- Kerr, Y.H., Waldteufel, P., Wigneron, J.P., Martinuzzi, J.M., Font J., and Berger, M., 2001. Soil moisture retrieval from space: The Soil Moisture and Ocean Salinity (SMOS) mission. *IEEE Transactions on Geoscience and Remote Sensing*, 30(8): 1729-1735.
- Kjekstad, O., 2002. Assessment of high-risk disaster hotspots. Review Workshop, Lamont Doherty Earth Observatory (LDEO), 6-8 November.
- Kummerow, C., Barnes, W., Koju, T., Shiue, j., and Simpson, J., 1998. The Tropical Rainfall Measuring Mission (TRMM) sensor package. *Journal of Atmospheric and Oceanic Technology*, 15: 809-817.
- Lacava, T., Greco, M., Di Leo, E.V., Martino, G., Pergola, N., Sannazzaro, F., and Tramutoli, V., 2005. Monitoring soil wetness variations by means of satellite passive microwave observations: the HYDROPTIMET study cases. *Natural Hazardous and Earth System Sciences*, 5: 583-592.

- Lagmay, A.M.A., Ong, J.B.T., Fernandez, D.F.D., Lapus, M.R., Rodolfo, R.S., Tengonciang, M.P., Soria, J.L.A., Baliatan, E.G., Quimba, Z.L., Uichanco, C.L., Paguican, M.R., Remedio, A.R.C., Lorenzo, G.R.H., Valdivia, W., and Avila, F.B., 2006. Scientists investigate recent Philippine Landslide, EOS Transaction, American Geophysical Union, 87(12).
- Lan, H.X., Zhou, C.H., and Martin, C.D., 2005. Dynamic characteristics analysis of shallow landslides in response to rainfall event using GIS. *Environmental geology*, 47: 254-267.
- Li, L., Njoku, E.G., Chang, P.S., and Germain, K.S., 2004. A preliminary survey of radio-frequency interference over the U.S. in Aqua AMSR-E Data. *IEEE Transactions on Geoscience and Remote Sensing*, 42 (2): 380-390.
- Lee, S., 2005. Application of logistic regression model and its validation for landslide susceptibility mapping using GIS and remote sensing data. *International Journal of remote Sensing*, 26(7): 1477-1491.
- Lee, S., 2004. Application of likelihood ratio and logistic regression models to landslide susceptibility mapping using GIS. *Environmental Management*, 34(2): 223-232.
- Liang, X., Wood, E.F., and Lettenmaier, D.P., 1996. Surface soil moisture parameterization of the VIC-2L model: Evaluation and modifications. *Global Planet. Change*, 13: 195-206.
- Liang, X., Lettenmaier, D.P., Wood, E.F., and Burges, S.J., 1994. A simple hydrologically based model of land surface water and energy fluxes for GSMs. *Journal of Geophysical Research* 99 (D7), 14415-14428.
- Liang, X., Wood, E.F., and Lettenmaier, D.P., 1999. Modeling ground heat flux in land surface parameterization schemes. *Journal of Geophysical Research*, 104 (D8), 9581-9600.
- Liang, X., and Xie, Z., 2003. Important factors in land-atmosphere interactions: surface runoff generations and interactions between surface and groundwater. *Global and Planetary Change*, 38: 101-114.
- Loew, A., Ludwig, R., and Mauser, W., 2006. Derivation of surface soil moisture from ENVISAT ASAR wide swath and image mode data in agricultural areas. *IEEE Transactions on Geoscience and Remote Sensing*, 44(4): 889-899.
- Lohmann, D., Raschke, E., Nijssen, P, and Lettenmaier, D.P., 1998. Regional scale hydrology: I. Formulation of the VIC-2L model coupled to a routing model. *Hydrological Sciences Journal*, 43(1): 131-141.

- Lu, N., Godt, J., 2008. Infinite slope stability under steady unsaturated seepage conditions. *Water Resources Research* 44, W11404, doi: 10.1029/2008WR006976.
- Luo, Y., Trishchenko, A.P., and Khlopenkov, K.V., 2008. Developing clear-sky, cloud shadow mask for producing clear-sky composites at 250-meter spatial resolution for the seven MODIS land bands over Canada and North America. *Remote Sensing of Environment*, 112: 4167-4185.
- McCabe, M.F., Gao, H., and Wood, E.F., 2005. Evaluation of AMSR-E derived soil moisture retrievals using ground-based and PSR airborne data during SMEX02. *Journal of Hydrometeorology-Special Edition*, 6: 864-877.
- Mantovani, F., Soeters, R., and Van Western, C.J., 1996. Remote sensing techniques for landslide studies and hazard zonation in Europe. *Geomorphology*, 15: 213-225.
- Maurer, E.P., Wood, A.W., Adam, J.C., Lettenmaier, D.P., Nijssen, B., 2002. A long-term hydrologically based dataset of land surface fluxes and states for the conterminous United States. *Journal of Climate* 15, 3237-3251.
- Meisina, C., Scarabelli, S., 2007. A comparative analysis of terrain stability models for predicting shallow landslides in colluvial soils. *Geomorphology* 87, 207-223.
- Metternicht, G., Hurni, L., and Gogu, R., 2005. Remote sensing of landslides: An analysis of the potential contribution to geo-spatial systems for hazard assessment in mountainous environments. *Remote Sensing of Environment* 98: 284-303.
- Miller, D.A. and R.A. White, 1998: A Conterminous United States Multi-Layer Soil Characteristics Data Set for Regional Climate and Hydrology Modeling. *Earth Interactions*, 2. [Available on-line at <http://EarthInteractions.org>]
- Mitchell, K.E., Lohman D., Houser, P.R., Wood, E.F., Schaake, J.C., Robock, A., Cosgrove, B.A., Sheffield, J., Duan Q., Luo, L., Higgins, R.W., Pinker, R.T., Tarpley, J.D., Lettenmaier, D.P., Marshall, C.H., Entin, J.K., Pan M., Shi W., Koren, V., Meng J., Ramsay B.H., and Bailey A.A., 2004. The multi-institution North American Land Data Assimilation System (NLDAS): Utilizing multiple GCIP products and parameters in a continental distributed hydrological modeling system. *J. Geophysics. Res.*, 109, Do7S90, doi:1029/2003JD003823.
- Montgomery, D.R., and Dietrich, W.E., 1994. A physically based model for the topographic control on shallow landsliding. *Water Resources Research*, 30(4): 1153-1171.
- Moran, M.S., Peters-Lidard, C.D., Watts, J.M., and McElroy, S., 2004. Estimating soil moisture at the watershed scale with satellite-based radar and land surface models. *Canadian Journal of Remote sensing*, 30(5): 808-826.

- Muntohar, A.S., Liao, H.J., 2009. Analysis of rainfall-induced infinite slope failure during typhoon using a hydrological-geotechnical model. *Environmental Geology* 56, 1145-1159.
- Nichol, J., and Wong, M.S., 2005. Satellite remote sensing for detailed landslide inventories using change detection and image fusion. *International Journal of Remote Sensing*, 26(9): 1913-1926.
- Nijssen, B., Lettenmaier, D.P., Liang, X., Wetzel, S.W., and wood, E.F., 1997. Streamflow simulation for continental-scale river basins. *Water resources Research*, 33(4): 711-724.
- Nijssen, B., Schnur, R., and Lettenmaier, D.P., 2001. Global retrospective estimation of soil moisture using the variable infiltration capacity land surface model, 1980-93. *Journal of Climate*, 14: 1790-1808.
- Njoku, E.G., Jackson, T.J., and Koike T., 2000. AMSR-E Science Data Validation Plan, version 2, 7/00. 76 pp.
- Njoku, E.G., Jackson, T.J., Lakshmi, V., Chan T.K., and Nghiem, S.V., 2003. Soil Moisture Retrieval From AMSR-E. *IEEE Transactions on Geoscience and Remote Sensing*, 41(2): 215-229.
- Njoku, E.G., and Chan, S.K., 2006. Vegetation and surface roughness effects on AMSR-E land observations. *Remote Sensing of Environment*, 100: 190-199.
- O'Loughlin, E.M., 1986. Prediction of surface saturation zones in natural catchments by topographic analysis. *Water Resources Research*, 22: 794-804.
- Oka, N., 1998. Application of photogrammetry to the field observation of failed slopes. *Engineering Geology*, 50: 85-100.
- Onda, Y., Tsujimura, M., Tabuchi, H., 2004. The role of subsurface water flow paths on hillslope hydrological processes, landslides and landform development in steep mountains of Japan. *Hydrological Processes* 18, 637-650.
- Ostir, K., Veljanovski, T., Podobanikar, T., and Stancic, Z., 2003. Application of satellite remote sensing in natural hazard management: the Mount Mangart landslide case study. *International Journal of Remote Sensing*, 24 (20): 3983-4002.
- Pack, R.T., Tarboton, D.G., Goodwin, C.N., 1998. The SINMAP approach to terrain stability mapping. In: Moore DP, Hungr O (eds) *Proceedings—international congress of the International Association for Engineering Geology and the Environment* 8, v. 2, A.A. Balkema, Rotterdam, Netherlands, 1157–1165.

- Petley, D. N., Hearn, G. J., and Hart, A., 2004. Towards the development of a landslide risk assessment for rural roads in Nepal. In: Glade, T. and Crozier, M. J. (eds), *Landslide Hazard and Risk*. J. Wiley and Sons Ltd., London: 597-679.
- Pelletier, J.D., Malamud, B.D., Blodgett, T., and Turcotte, D.L., 1997. Scale-invariance of soil moisture variability and its implications for the frequency-size distribution of landslides. *Engineering Geology*, 48(3-4): 255-268.
- Parada, L.M., Liang, X., 2004. Optimal multiscale Kalman filter for assimilation for near-surface soil moisture into land surface models. *Journal of Geophysical Research* 109, D24109, doi: 10.1029/2004JD004745.
- Pradhan, B., Singh, R.P., and Buchroithner, M.F., 2006. Estimation of stress and its use in evaluation of landslide prone regions using remote sensing data. *Advances in Space research*, 37 698-709.
- Ray, R.L., and De Smedt, F., 2009. Slope Stability Analysis using GIS on a Regional Scale: A case study from Dhading, Nepal. *Environmental Geology*, 57 (7): 1603-1611.
- Ray, R. L., 2004. Slope Stability Analysis using GIS on a Regional Scale: a case study from Dhading, Nepal. MSc. thesis in Physical Land Resources, Vrije Universiteit Brussel, 98 pp.
- Ray, R.L., and Jacobs, J.M., 2007. Relationships among remotely sensed soil moisture, precipitation and landslide events. *Natural Hazards*, 43(2):211-222.
- Ray, R.L., Jacobs, J.M., and de Alba, P. Impact of vadose zone soil moisture and groundwater in slope instability, anticipated submission, July 2009.
- Ray, R.L., Jacobs, J.M., and Douglas, E.M. Modeling landslide susceptibility using dynamic soil moisture profiles, anticipated submission, July 2009.
- Rahardjo, H., 2000. Rainfall-induced slope failures. Research Rep. No. NSTB 17/6/16, Nanyang Technological University, Singapore.
- Rahardjo H, Ong, T.H., Rezaur, R.B., Leong, E.C., 2007. Factors controlling instability of homogeneous soil slopes under rainfall. *Journal of Geotechnical and Geoenvironmental Engineering*, 133(12), 1532-1543.
- Reid, M.E., Brien, D.L., LaHusen, R.G., Roering, J.J., de la Fuente, J., and Ellen, S.D., 2003. Debris-flow initiation from large, slow-moving landslides. *Debris-Flow Hazards Mitigation: Mechanics, Prediction, and Assessment*, Rickenmann and Chen (eds). Millpress, Rotterdam, ISBN 90 77017 78X.

- Reid, M.E., 2006. Personal communication. USGS.
<http://landslides.usgs.gov/monitoring/hwy50/>
- Reichle, R.H., Koster, R.D., Dong, J., and Berg, A.A., 2004. Global soil moisture from satellite observations, Land Surface Models, and ground data: Implications for data assimilation. *Journal of Hydrometeorology*, 5: 430-442.
- Reutov, E.A., and Shutko A.M., 1991. Estimation of the water table using remote microwave radiometer measurements. *Soviet Journal of Remote Sensing*, 9(2): 315-327.
- Reutov, E.A., and Shutko A.M., 1992. Estimation of the depth to a shallow water table using microwave radiometry. *International Journal of Remote Sensing*, 13: 2223-2232.
- Rosso, R., Rulli, M.C., Vannucchi, G., 2006. A physically based model for the hydrologic control on shallow landsliding. *Water Resources Research* 42, W06410, doi:10.1029/2005WR004369.
- Ruff , M., and Czurda, K., 2008. Landslide susceptibility analysis with a heuristic approach in the Eastern Alps (Vorarlberg Austria). *Geomorphology*, 94: 314-324.
- Saha, A.K., Gupta, R.P., and Arora, M.K., 2002. GIS-based Landslide Hazard Zonation in the Bhagirathi (Ganga) Valley, Himalayas. *International Journal of Remote Sensing*, 23(2): 357-369.
- Saha, A.K., Gupta, R.P., Arora, M.K., and Csaplovics, E., 2005. An approach for GIS-based statistical landslide susceptibility zonation-with a case study in the Himalayas. *Landslides*, 2(1): 61-69.
- Sahoo, A.K., Houser, P.R., Ferguson, C., Wood, E.F., Dirmeyer, P.A., and Kafatos, M., 2008. Evaluation of AMSR-E soil moisture results using the in-situ data over the Little River experimental Watershed, Georgia. *Remote Sensing of Environment*, 112: 3142-3152.
- Saldivar-Sali, A., and Einstein, H.H., 2007. A landslide risk rating system for Baguio, Philippines. *Engineering geology*, 91(2-4), 85-99.
- Sarkar, S., and Kanungo, D.P., 2004. An integrated approach for landslide susceptibility mapping using remote sensing and GIS. *Photogrammetric Engineering and Remote Sensing*, 70(5): 617-625.
- Schmugge, T., and Jackson, T.J., 1994. Mapping surface soil moisture with microwave radiometers. *Meteorology and Atmospheric Physics*, 54: 213-223.

- Schmugge, T. J., W. P. Kustas, J. Ritchie, T. J. Jackson, and A. Rango (2002), Remote sensing in hydrology, *Adv. Water Resour.*, 25, 1367–1385.
- Scipal, K., Scheffler, C., and Wagner, W., 2005. Soil moisture runoff relation at the catchment scale as observed with coarse resolution microwave remote sensing. *Hydrology and Earth System Sciences*, 9: 173-183.
- Sellers, P.J., Mintz, Y., Sud, Y.C., Dalcher. A., 1986. A simple biosphere model (SiB) for use within general circulation models, *J. Atmos. Sci.*, 43(6), 505-531.
- Sidle, R.C., and Ochiai, H., 2006. *Landslides: Processes, Prediction, and Land Use*. American Geophysical Union, Water Resources Monograph, 18, 312pp.
- Sidle, R.C., Taylor, D., Lu, X.X., Adger, W.N., Lowe, D.J., de Lang, W.P., Newnham, R.M., and Dodson, J.R., 2004. Interactions of natural hazards and society in Austral-Asia: Evidence in past and recent records. *Quaternary International*, 118-19: 181-203.
- Singhroy, V., and Molch K., 2004. Characterizing and monitoring rockslides from SAR techniques. *Advances in Space Research*, 33: 290-295.
- Skempton, A.W., DeLory F.A., 1957. Stability of natural slopes in London clay. In: *Proceedings 4th international conference on Soil Mechanics and Foundation Engineering London 2*, 378–381.
- Skirikar, S. M., Rimal, L. N., and Jäger, S., 1998. Landslide hazard mapping of Phewa Lake catchment area, Pokhara, Central West Nepal. *Journal of the Nepal Geological Society* 18: 335-345.
- Spittler, T.E., and Wagner, D.L., 1998. Geology and slope stability along highway 50. *California Geology*, 51(3): 3-14.
- Soil Survey Staff, Natural Resources Conservation Service, United States Department of Agriculture. U.S. General Soil Map (STATSGO) for CA, Jan 4, 2008 <http://soildatamart.nrcs.usda.gov>
- Soeters, R., and Van Westen, C.J., 1996. Slope instability. Recognition, analysis and zonation. In: Turner, A.K., Schuster, R.L. (Eds.), *Landslide: Investigations and Mitigation*. Special Report, 247: Transportation Research Board, National Research Council, National Academic Press, Wasington, D.C., 129-177 pp.
- Suzen, M.L., and Doyuran, V., 2004. A comparison of the GIS based landslide susceptibility assessment methods: multivariate vrsus bivariate. *Environmental Geology*, 45(5): 665-679.

- Teng, W.L., Wang, J.R., and Doraiswamy, P.C., 1993. Relationship between microwave radiometric data, antecedent precipitation index, and regional soil moisture. *International Journal of Remote sensing*, 14(13): 2483-2500.
- Vanacker, V., Vanderschaeghe, M., Govers, G., Willems, E., Poesen, J., Deckers, J., De Bievre, B., 2003. Linking hydrological, infinite slope stability and land-use change models through GIS for assessing the impact of deforestation on slope stability in high Andean watersheds. *Geomorphology* 52, 299-315.
- Van Westen, C.J., 1994. GIS in landslide hazard zonation: A review, with examples from the Andes of Colombia. In: Price MF, Heywood DI (eds) *Mountain Environments and Geographic Information Systems*, Taylor and Francis Publishers:135-165
- Van Westen, C.J., and Trelim, T.J., 1996. An approach towards deterministic landslide hazard analysis in GIS: A case study from Manizales (Colombia). *Earth Surf. Process. Landforms*, 21: 853-868.
- Van Western, C.J., and Getahun, F.L., 2003. Analyzing the evolution of the Tessina landslide using aerial photographs and digital elevation models. *Geomorphology*, 54: 77-89.
- Varnes, D.J., 1984. *Landslide Hazard Zonation: A Review of Principles and Practice*. Commission on the Landslides of the IAEG, UNESCO, Natural Hazard 3:66pp.
- Vivoni, E.R., Gabremichael, M., Watts, C.J., Bindlish, R., and Jackson, T.J., 2008. Comparison of ground-based and remotely-sensed surface soil moisture estimates over complex terrain during SMEX04. *Remote Sensing of Environment*, 112: 314-325.
- Walker, J.P., Houser, P.R., and Willgoose G.R., 2004. Active microwave remote sensing for soil moisture measurement: a field evaluation using ERS-2. *Hydrological Processes*, 18: 1975-1997.
- Wang, L., Wen, J., Zhang, T., Zhao, Y., Tian, H., Shi, X., Wang, X., Liu, R., Zhang, J., and Lu, S., 2009. Surface soil moisture estimates from AMSR-E observations over an arid area, Northwest China. *Hydrology and earth System Sciences Discussion*, 6: 1056-1087.
- Whitfield, B., Jacobs, J.M., and Judge, J., 2006. Intercomparison study of the land surface process model and the common model for a Prairie wetland, Florida. *Journal of Hydrometeorology*, 7: 1247-1258.
- Wood E.F., Lettenmaier, D.P., and Zartarain, V.G., 1992. A land-surface hydrology parameterization with subgrid variability for general circulation models. *Journal of Geophysical Research* 97 (D3), 2717-2728.

- Wu, W. and Sidle, R.C., 2005. A distributed slope stability model for steep forested basins. *Water Resource Research*, 31 (8): 2097-2110.
- Yu, G., Di, L., and Yang, W., 2008. Downscaling of global soil moisture using auxiliary data. *IEEE*, 978-1-4244-2808-3/08, I-304-307.
- Yuan, f., Xie, Z., Liu, Q., Yang, H., Su, F., Liang, X., and Ren, L., 2004. An application of the VIC-3L land surface model and remote sensing data simulating streamflow for the Hanjiang River basin. *Canadian Journal of Remote Sensing*, 30 (5): 680-690.
- Yulin, C, Zhifeng, G., and Li, Y., 2008. A macro hydrologic model simulation based on remote sensing data. 2008 International Workshop on Earth Observation and Remote sensing Applications, *IEEE*, 1-4244-2394-1/08. 4 pp.
- Zhou, S.Q., Liang, X., Chen, J., and Gong, P., 2004. An assessment of the VIC-3L hydrological model for the Yangtze River basin based on remote sensing: A case study of the Baohe River basin. *Canadian Journal of Remote Sensing*, 30(5): 840-853.
- Zomer, R., Ustin S., and Ives J., 2002. Using satellite remote sensing for DEM extraction in complex mountainous terrains: landscape analysis of the Makalu Barun National park of eastern Nepal. *Int. J. Remote Sensing*, 23(1): 125-143.

APPENDIX A
Physical Properties of Soil

Physical Properties of Soil

Soil Type	Group Symbol	Cohesion Range (t/m ²)		Frictional Angle (°)
		Maximum	Minimum	
Well Graded Gravel	GW	0	0	>38
Poorly Graded Gravel	GP	0	0	>37
Gravel with Silts	GM	-	-	>34
Gravel with Clay	GC	-	-	>31
Well Graded Sand	SW	0	0	38
Poorly Graded Sand	SP	0	0	37
Sand with Silts	SM	5	2	34
Sand with Clay	SC	7.5	1	31
Mixture of SM-SC	SM-SC	0.5	0.15	33
Inorganic Silts	ML	7	1	32
Inorganic Clay	CL	9	1.5	28
Mixture of CL-ML	CL-ML	6.5	2	32
Organic Silts	OL	-	-	-
Inorganic Silts	MH	7.5	2.1	25
Inorganic Clay	CH	10	1	19

(Source: Mountain Risk Engineering Handbook, Deoja, 1991)

APPENDIX B
List of Published and Potential Papers

List of Published and Potential Papers

1. Ray, R.L., and Jacobs, J.M., 2007. Relationships among remotely sensed soil moisture, precipitation and landslide events. *Natural Hazards*, 43(2):211-222.
2. Ray, R.L., Jacobs, J.M., and de Alba, P. Impact of vadose zone soil moisture and groundwater in slope instability, anticipated submission, July 2009.
3. Ray, R.L., Jacobs, J.M., and Douglas, E.M. Modeling landslide susceptibility using dynamic soil moisture profiles, anticipated submission, July 2009.
4. Ray, R.L., Jacobs, J.M., and Ballesterro, T.P. Regional landslide susceptibility statistical distribution in space and time, anticipated submission, August 2009.
5. Ray, R.L., Jacobs, J.M., and Cosh, M. Landslide susceptibility mapping using downscaled AMSR-E soil moisture: A case study from California, US, anticipated submission, August 2009.

Conference Proceedings Papers

1. Ray, R.L., and Jacobs, J.M., 2008. Landslide susceptibility mapping using remotely sensed soil moisture. Proceedings: IEEE International Geosciences and Remote Sensing Symposium (IGARSS), Boston, USA, pp. III-47-50, ISBN:978-1-4244-2808-3.
2. Ray, R.L., and Jacobs, J.M., 2007. Linking landslides with remotely sensed soil moisture and satellite derived rainfall at Cleveland Corral, El Dorado County in California. 1st North American Landslide Conference, June 3-8, 2007, Vail, CO (USA), AEG S.P. No. 23, pp. 376- 386, ISBN: 978-0-975-4295-3-2.